Compressive Failure of Fiber Composites

N. A. FLECK

Cambridge University Engineering Department,
Cambridge, England

I. Introduction

Compression failure is a design-limiting feature of aligned, continuous fiber composite materials. For example, the compressive strengths of unidirectional carbon fiber-epoxy laminates are often less than 60% of

ADVANCES IN APPLIED MECHANICS, VOL. 33

0065-2165/97 $25.00

Vol. 33, eds. J.W. Hutchinson & T.Y. Wu

their tensile strengths. A number of competing failure modes result in compressive failure: the operative mode is particularly sensitive to the shear properties of the matrix and to the degree of imperfection of the composite (typically, fiber waviness). For example, polymer matrix and carbon matrix composites have low shear strengths and failure is usually localized compressive buckling of the fibers in a cooperative manner. We shall refer to this failure process by the term **microbuckling**; this is the main topic of the current article.

The broad outline of this review is as follows: In Section II, the main mechanisms of compressive failure of composites are summarized, and operative mechanisms for various classes of material are displayed in the form of failure maps. In Section III, recent results are summarized for the initiation of microbuckling in unidirectional composites. The propagation of a microbuckle is addressed for unidirectional composites in Section IV and for multi-directional notched laminates in Section V. The article concludes with some suggestions for future research.

II. Competing Failure Mechanisms in Composites

Long fiber composites are usually designed to possess a high-axial stiffness and strength. Accordingly, the fibers are made from a strong and stiff material such as graphite or silica glass; the matrix has a much higher toughness and lower strength than the fibers in order to endow the composite with adequate in-plane strength and ductility. The axial compressive strength of the composite is usually relatively low, as most of the individual mechanisms of compressive failure are dictated by matrix properties. The main competing mechanisms of compressive failure are sketched in Figure 1 and may be listed as:

(A) *Elastic microbuckling*. This is a shear buckling instability and the matrix deforms in simple shear;
(B) *Plastic microbuckling*. Again, this is a shear instability, which occurs at sufficiently large strains for the matrix to deform in a non-linear manner;
(C) *Fiber crushing*. Failure occurs at the fiber level of scale due to a shear instability such as buckling within the fiber. It is often associated with the fact that the fibers themselves are microcomposites comprising wavy fibers embedded in a soft matrix;

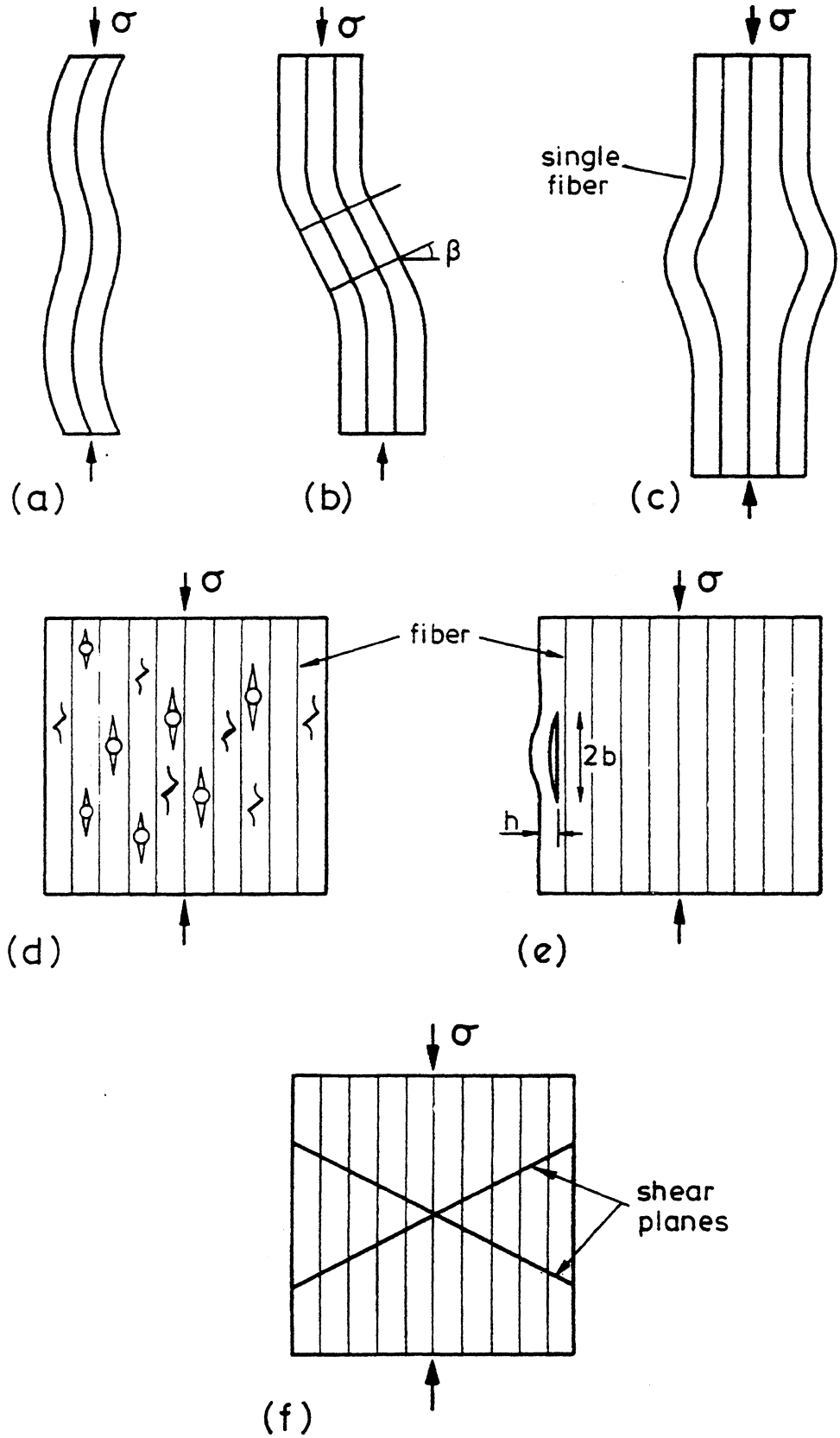

FIG. 1. The main competing failure modes of composites. (a) Elastic microbuckling, (b) Plastic microbuckling, (c) Fiber crushing, (d) Splitting of the matrix, (e) Buckle delamination of a surface layer, (f) Shear band formation.

(D) *Splitting*. The matrix cracks parallel to the main axial fiber direction. It is associated with a low toughness of the matrix;
(E) *Buckle delamination*. This occurs by the buckling of a surface layer from a sub-surface debond. It is observed in both ceramic matrix and polymer matrix composites. Post-impact compressive strength is often a concern in the use of composites, as the impact event leads to a large debond. Subsequent compressive loading can induce buckle-delamination growth. Buckle delamination is associated with a low matrix toughness and the presence of a large subsurface flaw.
(F) *Shear band formation*. Matrix yield and fracture occur in a band, oriented at about 45° with respect to the loading axis.

Each of the above mechanisms of compressive failure is now reviewed, and practical examples are given of material systems which fail by each mechanism.

A. Elastic Microbuckling

Several attempts have been made to model microbuckling by assuming elastic bending of the fibers and elastic shear of the matrix (Hahn and Williams, 1986; Johnson and Ellen, 1974, 1975a,b, 1976). In general, they add little to the pioneering analysis of Rosen (1965), who assumed that elastic bifurcation occurs in two possible modes:

(i) a *transverse buckling mode*, whereby the matrix undergoes extensional straining transverse to the fiber direction, and
(ii) a *shear buckling mode*, where the matrix shears parallel to the fibers (see Figure 1a).

In practical fiber composites, containing a significant fiber volume fraction $c > 0.3$, the shear mode gives lower failure loads. Rosen assumed that the fibers are initially perfectly aligned and calculated the elastic bifurcation load at which the fibers deflect into a sinusoidal shape. Rosen found that the composite compressive strength σ_c due to shear buckling is

$$\sigma_c = G + \frac{\pi^2}{3}\left(\frac{d}{\lambda}\right)^2 E \tag{2.1}$$

where G and E are the in-plane shear and axial moduli of the composite, respectively, d is the fiber diameter, and λ is the buckling wavelength.

Note that the wavelength, λ, is not specified by the analysis: the lowest predicted strength is $\sigma_c = G$ at $\lambda = \infty$. This corresponds to the case of straight fibers which undergo a uniform rotation ϕ. The term G on the right-hand side of (2.1) is the contribution to the compressive strength from matrix shear, and the remaining term

$$\frac{\pi^2}{3}\left(\frac{d}{\lambda}\right)^2 E$$

is the contribution to compressive strength associated with the finite-bending resistance of the fibers. It is clear from Rosen's analysis that the lowest strength is obtained in the long-wavelength limit, wherein the role of fiber bending is negligible. The same conclusion holds true in the more typical case of a non-linear matrix response: we may neglect the role of fiber bending in estimating the compressive strength. The *kinking theory* outlined in subsequent sections makes this approximation.

1. *Experimental Support for Elastic Microbuckling*

In order to test Rosen's elastic microbuckling theory for the case where the matrix behaves in a linear elastic manner, Jelf and Fleck (1992) fabricated model composite materials made from baked wheat flour (spaghetti) rods in a silicon elastomer matrix. Flat-plate specimens were compressed in a direction parallel to the fiber direction, and held between transparent anti-buckling guides to prevent out-of-plane Euler macrobuckling. Compressive failure was by in-plane microbuckling with a wavelength λ equal to twice the specimen height h. The compressive strength given by (2.1) is in good agreement with the observed compressive strength, as shown in Figure 2. As h increases, the compressive strength σ_c decreases to the asymptotic value of $G = 1.5$ MPa, in support of (2.1). We conclude that the Rosen theory is accurate when the matrix behaves in a linear elastic manner.

More typically, polymer, ceramic, and metal matrices of long-fiber composites display a non-linear behavior and the observed compressive strengths of the composites are about $\sigma_c = G/4$, due to *imperfection-sensitive plastic microbuckling*. The compressive strength is knocked down by imperfections in the form of pre-existing fiber waviness. Early attempts to fit the Rosen model to experimental data have involved empirical correlation factors (Lager and June 1969): in effect, an empirical knock-down factor was used for the shear modulus, G.

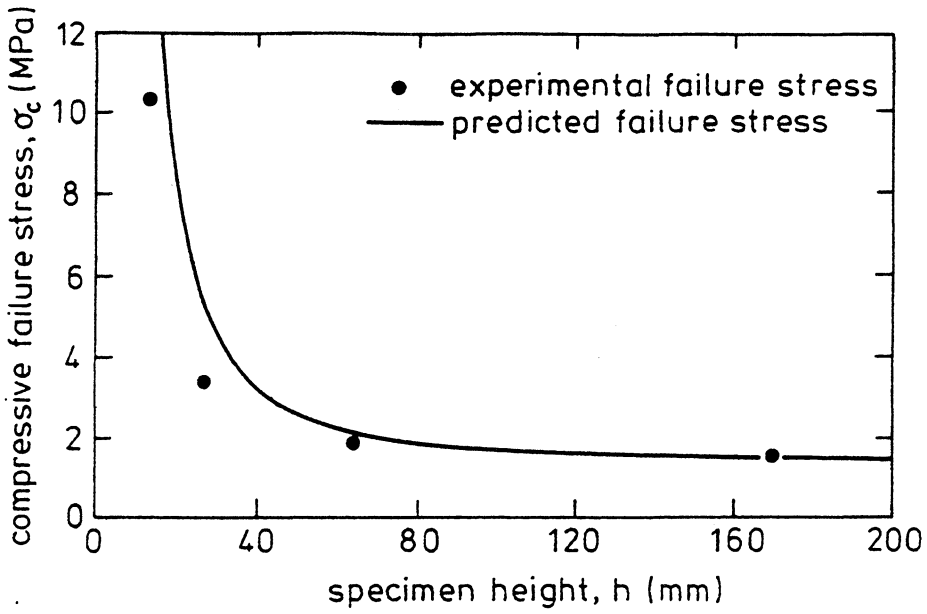

FIG. 2. Elastic microbuckling of a silicon rubber matrix reinforced with 31% volume fraction of spaghetti fibers, of diameter 2 mm.

B. PLASTIC MICROBUCKLING

Evidence is accruing that the dominant mechanism of compressive failure in polymer-matrix composites is *plastic microbuckling*: the compressive strength is controlled by fiber misalignment together with plastic shear deformation in the matrix (Argon, 1972; Budiansky and Fleck, 1993). These composites possess a compressive strength of less than 60% of their tensile strengths. The role played by plastic microbuckling in the compressive failure of metal matrix and ceramic matrix composites is less clear, though microbuckling has been observed in aluminum alloy matrix composites (Schulte and Minoshima (1991)) and in carbon–carbon composites (Evans and Adler, 1978). Plastic microbuckling is also an important failure mechanism in woods (Grossman and Wold, 1971; Dinwoodie, 1981).

Argon (1972) and Budiansky (1983) identified the shear yield strength k of the composite and the initial fiber misalignment angle $\bar{\phi}$ of the fibers as the main factors controlling compressive strength. In their analyses, the bending resistance of the fibers is neglected and it is assumed that fibers within a band of infinite length and finite width w suffer an initial uniform misalignment $\bar{\phi}$. The unit normal to the band of imperfection is rotated through an angle β with respect to the fiber direction as shown in Figure 3. Argon (1972) considered kinking within a $\beta = 0$ band for a rigid-perfectly plastic composite having yield stress k in longitudinal shear.

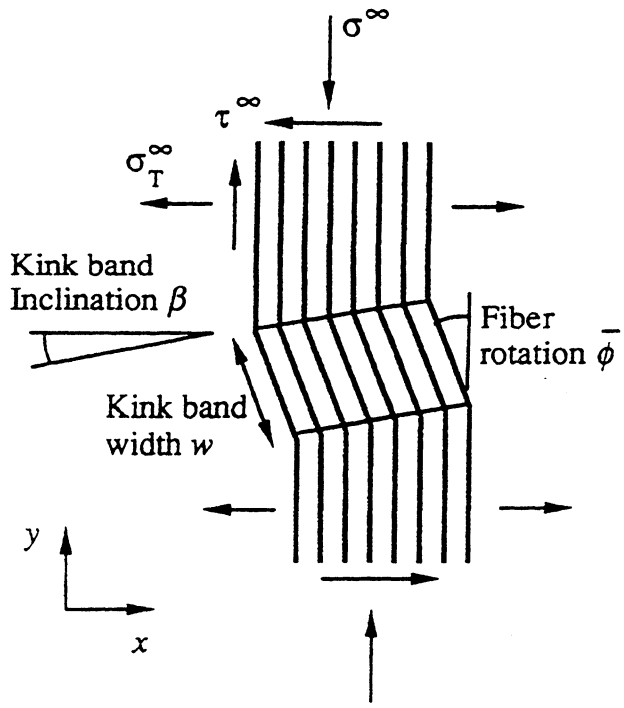

FIG. 3. Plastic kinking of a band of width w, inclined at an angle β to the remote fiber direction. Fibers within the band have an initial misalignment of $\bar{\phi}$, and rotate through an additional angle ϕ under the remote load.

He showed that an additional rotation ϕ cannot develop until the critical compressive stress

$$\sigma_c = \frac{k}{\bar{\phi}} \tag{2.2}$$

is applied. The compressive stress decreases with increasing ϕ in accordance with $\sigma = k/(\bar{\phi} + \phi)$.

The Argon formula (2.2) for the plastic kinking stress was extended by Budiansky (1983) to an *elastic*-perfectly plastic composite, with yield strain $\gamma_Y = k/G$ in longitudinal shear, for which the kinking stress is

$$\sigma_c = \frac{k}{\gamma_Y + \bar{\phi}} = \frac{G}{1 + \bar{\phi}/\gamma_Y} \tag{2.3}$$

This result (still for $\beta = 0$) is uniformly valid for all $\bar{\phi}$, giving the long-wavelength Rosen bifurcation stress $\sigma_c = G$ for $\bar{\phi} = 0$, and is asymptotically equivalent to the Argon result (2.2) for large $\bar{\phi}$.

Available experimental evidence for polymer matrix composites supports the hypothesis that microbuckling is a plastic rather than an elastic event. Test data from a variety of sources for the axial compressive strength σ_c of

aligned-fiber polymer matrix composites are plotted against G in Figure 4. The elastic kinking stress is given by the heavy line (corresponding to $\bar{\phi}/\gamma_Y = 0$) and the other slanted straight lines are plots of (2.3) for several values of $\bar{\phi}/\gamma_Y > 0$. The simplifying assumptions (e.g., $\beta = 0$, ideal plasticity) used in the derivation of (2.3) limit its direct applicability; more realistic analyses taking into account strain-hardening as well as $\beta > 0$, will be made below. We note, nevertheless, that most of the data in Figure 4 fall well below the elastic buckling line, and are consistent with (2.3) for a range of values of $\bar{\phi}/\gamma_Y$ near 4. If we set γ_Y equal to some nominal magnitude—say 1%—this gives values of $\bar{\phi}$ scattered about a mean value in the vicinity of 2°. As we shall see later, this rough estimate for typical values of $\bar{\phi}$ may change somewhat in the light of more refined calculations, but it is in good agreement with measured values of the misalignment of fiber bundles when a laminate was sectioned and examined under a light microscope by Yurgatis (1987). Yurgatis found that most of the fibers in a carbon fiber-PEEK unidirectional composite were oriented within ±3° of the mean fiber direction, and the standard deviation of the distribution was 1.9°.

Indirect evidence to support eq. (2.3) comes from compression tests on woven carbon fiber cloth by Wilkinson *et al.* (1986). They found that the

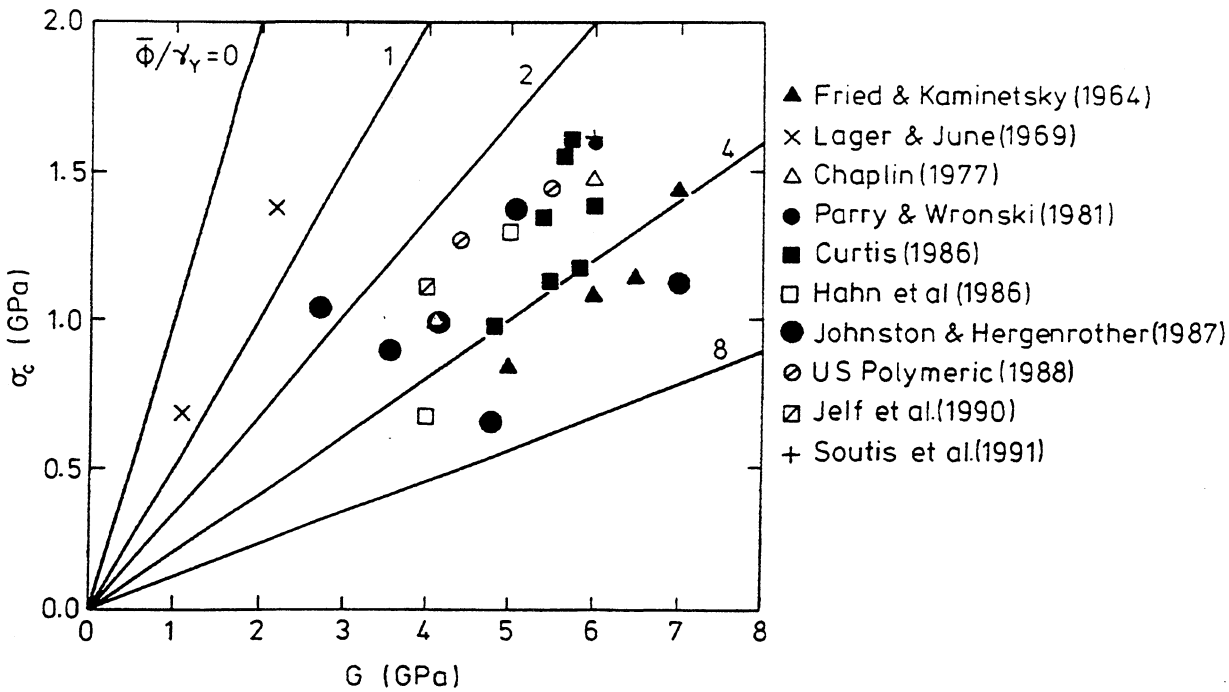

FIG. 4. Compressive strength data and predictions of microbuckling strength, based on Budiansky's (1983) formula for elastic-perfectly plastic behavior. The data suggests $\bar{\phi}/\gamma_Y = 4$, where $\bar{\phi}$ is the fiber misalignment angle and γ_Y is the shear yield strain of the composite.

compressive strength of T300/914 carbon-epoxy cloth ($G \approx 6$ GPa) decreased from about 1 GPa to 200 MPa when they inserted brass wires into the cloth normal to the fiber direction in order to increase the waviness. From these strength measurements the inferred value of $\bar{\phi}/\gamma_Y$ increases from 5 to 29 via (2.3). With $\gamma_Y \approx 0.01$ (0.57°) this corresponds to an increase of $\bar{\phi}$ from 3° to 17°. These theoretical values agree well with our measurements of the maximum fiber bundle waviness from the micrographs published by Wilkinson *et al.* (1986), which show increases from approximately 3° to approximately 20°.

The compressive strength of composites shows a large degree of scatter, with nominally identical specimens often varying in strength by 25%. This is consistent with plastic microbuckling, for which the analytic prediction (2.3) shows high imperfection sensitivity, with strength strongly dependent on the misalignment angle. In contrast, the *elastic* microbuckling collapse load is fairly insensitive to imperfections (Budiansky, 1979), and would not show much scatter.

In an illuminating set of tests (Piggott and Harris, 1980; Piggott, 1981), the modulus of a polyester resin matrix was varied by partial curing, and it was found that the matrix yield strength varied proportionally. With reinforcing fibers of either glass or Kevlar, and the fiber volume fraction $c = 0.31$, a nominal, uniform value of $\gamma_Y \approx 0.024$ (1.4°) for the composites can be estimated from their data. Figure 5 shows the measured composite strengths on a plot of σ_c versus G. Again, we infer a value $\bar{\phi} \approx 2°$ for both the glass and Kevlar fibers from the initial, nearly linear ranges of the data, presumed to reflect plastic kinking. Above transitional values of the composite stiffness G, the failure-stress levels, shown by the arrows in Figure 5, become more-or-less independent of G (or of $\tau_Y = G\gamma_Y$). Piggott and Harris surmise that in this range, failure was due to *fiber crushing*. This mechanism of compressive failure is outlined below.

Microbuckling in carbon–carbon composites has been observed by Evans and Adler (1978), Chatterjee and McLaughlin (1979), and Gupta *et al.* (1994). The latter found compressive strengths as low as 1/20 of the elastic-kinking stress (2.1), and suggested plastic kinking as the operative failure mechanism. The plasticity of the carbon matrix is probably due primarily to microcracking. Similar non-linear stress-strain behavior due to matrix microcracking and consequent kinking mechanisms might also be expected in some ceramic-matrix composites. Although little experimental evidence is available, Lankford (1989) did observe kinking in a pyroceramic matrix reinforced with silicon carbide fibers. His measured compressive

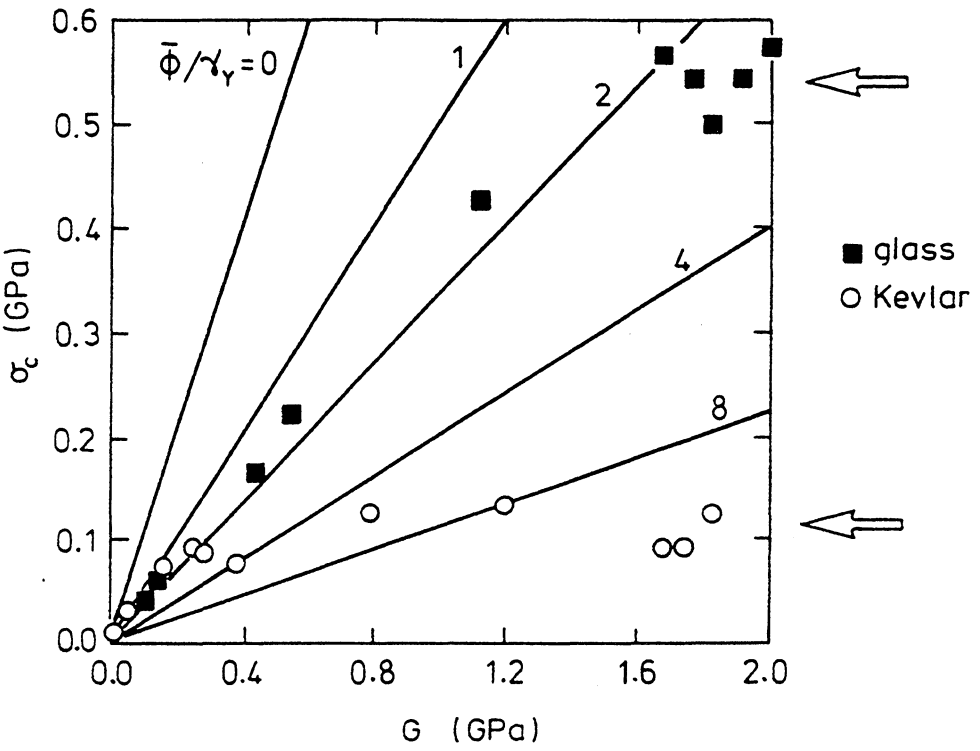

FIG. 5. Measured compressive strength of glass and Kevlar fiber reinforced, partially cured resins. The arrows indicate presumed stress levels at the transition from microbuckling to fiber crushing. Data taken from Piggott and Harris (1980) and Piggott (1981).

strengths of $\sigma_c \approx 1500$ MPa, and our roughly estimated values of $\tau_Y \approx 115$ MPa and $\gamma_Y \approx 0.01$, when substituted into the plastic kinking formula (2.3), give $\bar{\phi} \approx 4°$ for the fiber misalignment. Lankford (1989) also investigated the effect of applied strain rate on compressive strength by performing tests using a split Hopkinson pressure bar. He found a significant enhancement in microbuckling strength when the axial strain rate exceeds about 10^3 s^{-1}: this strength evaluation is partly due to the micro-inertia of rotating fibers within the microbuckle band, and partly due to the strain rate sensitivity of matrix strength.

Compressive failure in metal-matrix fiber composites has received little study, and the importance of kinking as a failure mode in such composites has not been established. A preliminary study has been conducted by Schulte and Minoshima (1991) on alumina fibers in an aluminium-2.5% lithium matrix. They observed microbuckling at a compressive strength of $\sigma_c = 1500$ MPa, compared to a tensile strength of $\sigma_t = 600$ MPa. A fiber misalignment angle of $\bar{\phi} = 3.6°$ is inferred from (2.2) on assuming a shear yield strength for the composite of $k = 100$ MPa; such a value for $\bar{\phi}$ is plausible.

There is accumulating evidence that the dominant mechanism of compressive failure in polymer matrix woven composites is fiber microbuckling. Microbuckles form at many of the cross-over points of neighboring tows (Cox *et al.*, 1994; Fleck *et al.*, 1995a). A typical scanning electron micrograph of this distributed form of damage development is shown in Figure 6, for a two-dimensional $\pm\theta$ braid of glass fibers in an epoxy matrix (Harte and Fleck, 1996).

C. Fiber Crushing

When the matrix is sufficiently stiff and strong, alternative failure modes such as fiber crushing intervene. Fiber crushing occurs when the uniaxial strain in the composite equals the intrinsic crushing strain ε_{fc} of the fibers. A variety of mechanisms may be associated with fiber crushing. In the case of steel fibers, local crushing is due to *plastic yielding* (Moncunill de Ferran and Harris, 1970; Piggott and Wilde, 1980). Glass fibers tend to fail in compression by *longitudinal splitting*. In the case of carbon, Kevlar, and wood fibers, *microscopic microbuckling* or kinking occurs *within* each fiber, and kink bands are observed within the fibers of width less than the fiber radius (Greszczuk, 1972, 1975; Prandy and Hahn, 1990; Young and Young, 1990; Piggott and Harris, 1980; Gibson and Ashby, 1988). Pitch-

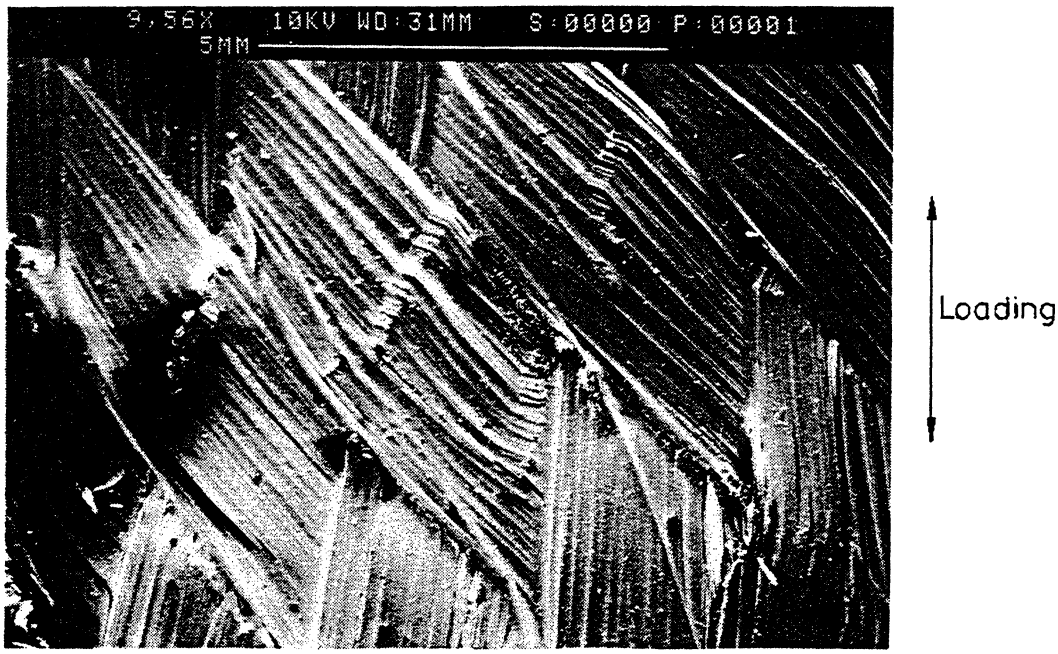

FIG. 6. Microbuckling failure of a two-dimensional braid of glass fibers in an epoxy matrix (Harte and Fleck, 1996).

based carbon fibers have a very well-aligned longitudinal microstructure, and they fail in compression by a combination of internal buckling and longitudinal splitting. Typical values of crushing strain are $\varepsilon_{fc} = 0.5\%$ for Kevlar and pitch-based carbon fibers, and $\varepsilon_{fc} = 2.5\%$ for PAN-based carbon fibers. When *microscopic microbuckling* occurs, the compressive strength of the fiber, σ_{fc}, is of the order $G/4$, where G is the longitudinal shear modulus of the fiber (deTeresa *et al.*, 1988; Kumar *et al.*, 1988). This supports the hypothesis that buckling loads are knocked down by wavy micro-fibrils within each fiber and the intervening matrix deforms non-linearly in shear: plastic microbuckling occurs at the micro-fibril level.

The fiber-crushing strength for glass fibers and for Kevlar fibers may be estimated from the compressive strength data of Piggott and Harris (1980) in Figure 5. The average axial stress in the composite at which fiber crushing occurs is given approximately by the rule-of mixtures formula, $\sigma_{crush} = [cE_f + (1 - c)E_m]\varepsilon_{fc}$, where E_f is the Young's modulus of the fibers and c is the fiber volume fraction. In the Piggott-Harris tests, $E_m/E_f \ll 1$, and so the fiber crushing strength $\sigma_{fc} = E_f\varepsilon_{fc}$ can be estimated as $\sigma_{fc} \approx \sigma_c/c$ from the upper-shelf values of σ_c. This gives fiber crushing strengths of about 1.7 GPa and 0.4 GPa for the glass and Kevlar, respectively; these values are plausible.

Early carbon fiber-epoxy matrix systems were manufactured from carbon fibers of low-crushing strength and epoxies of high-yield strength. These materials failed by fiber crushing at test temperatures below approximately 100°C (Ewins and Potter, 1980). At higher temperatures, the yield strength of the early epoxies drops sufficiently for the failure mechanism to switch to plastic microbuckling. More modern carbon fiber-epoxy systems possess carbon fibers of higher crushing strength, and a tougher, lower-yield strength matrix. The transition temperature from fiber crushing to plastic microbuckling is shifted from 100°C to −40°C, and modern carbon fiber-epoxy laminates fail by plastic microbuckling at both ambient and elevated temperatures (Barker and Balasundaram, 1987).

D. Splitting

Ceramic–ceramic composites such as SiC—SiC fail in compression by a splitting mode (Kaute *et al.*, 1996), see Figures 1 and 7. The failure mode is one of tensile mode I cracking along the fiber direction; the cracks develop from inhomongeneities such as voids or inclined flaws within the compos-

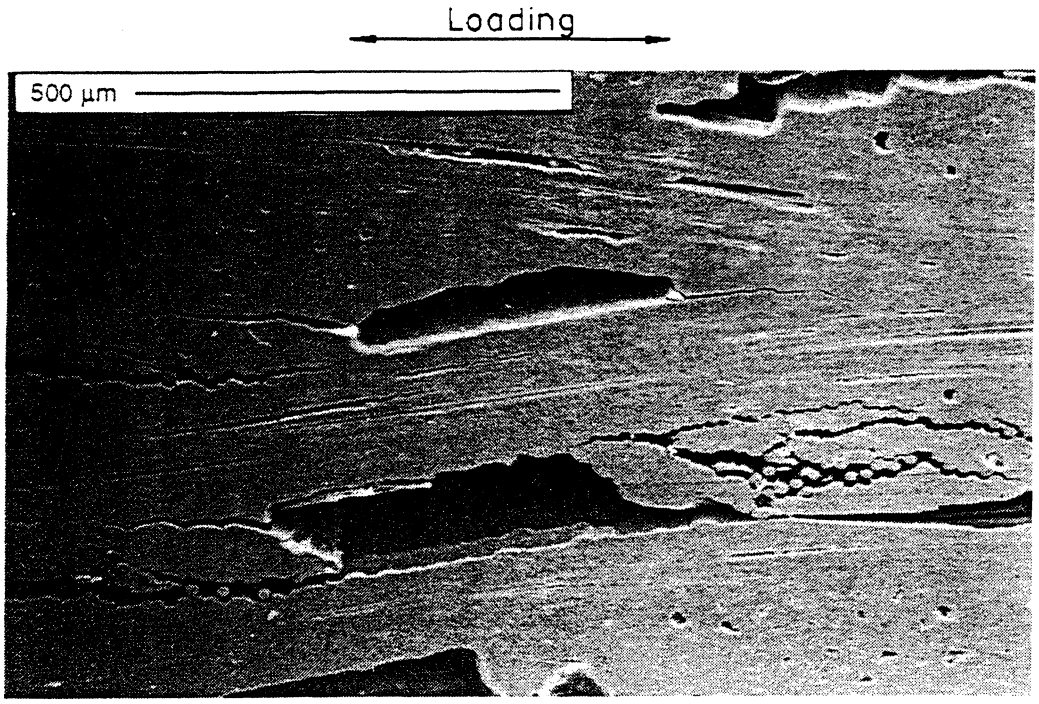

FIG. 7. Scanning Electron Microscope (SEM) micrograph of microcracking from pre-existing voids in SiC—SiC composite under compressive loading. The microcracks grow parallel to the loading direction. Taken from Kaute *et al.* (1996).

ite. This mechanism appears to be the same basic mode of failure as the fissuring of rocks (Nemat-Nasser and Horii, 1982; Sammis and Ashby, 1986; Ashby and Hallam, 1986). Briefly, the tensile microcracks grow stably from local stress-raisers under increasing remote compression; eventually, they interact and the body fails along a macroscopic shear band. This failure mode dominates when the stiffness of the matrix exceeds that of the fibers, and when the composite has a low toughness and high porosity. For SiC—SiC composite made by the chemical vapor infiltration route, the elastic modulus of the fibers (E = 200 GPa) is only half that of the matrix (E = 400 GPa); thus, the fibers act as compliant inclusions and help to induce the splitting mode of failure.

The compression strength is given roughly by the formula (Sammis and Ashby, 1986)

$$\sigma_c = \frac{C(f)K_{IC}}{\sqrt{\pi a}} \tag{2.4}$$

where K_{IC} is the mode I fracture toughness of the matrix, a is the average radius of the pores perpendicular to the direction of loading, and C is a coefficient which depends upon the porosity, f. The magnitude of C

ranges from 2 for 30% porosity to 15 for 0.3% porosity. For the case of the SiC—SiC composite investigated by Kaute *et al.* (1996), $f = 15\%$ and $C = 3$. On taking $K_{IC} = 3$ MPa $\sqrt{\text{m}}$, and $a = 100$ μm, the formula (2.4) gives $\sigma_c = 510$ MPa, which is of the same order as the observed range of 650–750 MPa. (We note in passing that the measured tensile strength is about 200 MPa, which is about one third of the compressive strength; for monolithic ceramics, the knockdown factor between tensile and compressive strength is typically an order of magnitude.)

E. Buckle Delamination

Splitting in a direction parallel to the main load-bearing fiber direction is encouraged when a surface layer is debonded over a finite length. Debonding may occur as a result of: (i) the manufacturing route, (ii) accidental surface impact or battle damage in defense applications, and (iii) out-of-plane loading induced by waviness of the fibers.

Whitcomb (1986) and Hutchinson and Suo (1991) have analyzed the case of buckle delamination of a straight-sided blister. They consider a semi-infinite solid with a pre-existing debond crack of length $2b$ lying parallel to the free surface and at a depth h below the surface. The crack is assumed to be of infinite extent in the direction transverse to the direction of uniaxial stressing σ, as shown in Figure 1e. Hence, plane strain conditions are assumed. For the case of the subsurface crack laying in an isotropic, homogeneous solid, the critical stress, σ_c, is set by the Euler buckling condition

$$\sigma_c = \frac{\pi^2}{12} E' \left(\frac{h}{b}\right)^2 \tag{2.5}$$

where E' is the plane strain value of Young's modulus. At this critical load, the crack tip stress intensity vanishes. Under increasing load, the crack opens and the strain energy release rate $\mathcal{G}$ increases according to (Hutchinson and Suo, 1991)

$$\frac{\mathcal{G}}{\mathcal{G}_o} = \left(1 - \frac{\sigma_c}{\sigma}\right)\left(1 + 3\frac{\sigma_c}{\sigma}\right) \tag{2.6}$$

where

$$\mathcal{G}_o \equiv [h/2E']\sigma^2. \tag{2.7}$$

The crack tip suffers mixed-mode loading, such that $|K_{II}/K_I| = 0.778$ at $\sigma = \sigma_c$; the mode II component increases under increasing remote load

such that for $\sigma \geq 7.55\sigma_c$, the delamination crack suffers pure mode II loading.

The precise sequence of events under increasing load depends somewhat on the relation between interfacial toughness $\mathcal{G}_c$ and mode mix. Here we consider the simplest case and assume that toughness $\mathcal{G}_c$ is independent of mode mix. Then, buckling begins at $\sigma = \sigma_c$, where σ_c is given by (2.5). Delamination crack growth begins at the value of σ which satisfies (2.6), with $\mathcal{G} = \mathcal{G}_c$: the delamination is immediately unstable under fixed load. An explicit expression for the maximum stress $\sigma_{\max}$ follows from (2.5–2.7) in the limiting case of small $E'\mathcal{G}_c/\sigma_c^2 h$:

$$\sigma_{\max} = \sigma_c\left[1 + \frac{1}{2}\left(\frac{E'\mathcal{G}_c}{\sigma_c^2 h}\right)\right] \tag{2.8}$$

Typically, for ceramic matrix composites the term $E'\mathcal{G}_c/\sigma_c^2 h$ is much less than unity so that the maximum load is approximated by (2.5). Also, we take E' to be the longitudinal modulus of the orthotropic composite parallel to the debond.

Buckle delamination has been observed by Kaute *et al.* (1996) for a satin-weave composite made from Nicalon™ SiC fibers in a Lanxide alumina matrix, as shown in Figure 8. They observed crack initiation and growth near the free surface at a location of intervening tows by splitting of a transverse tow, see Figures 8a and b. This was followed by catastrophic Euler buckling of the debonded layer, at a critical stress in the range 200 MPa to 680 MPa, depending on the precise details of the local geometry of initial defects and on the overall alignment of the specimen in the loading grips. From measured values of the composite axial modulus, $E = 120$ GPa, and an observed value of b/h of 10–15, the predicted compressive strength is in the range 440–990 MPa. These predicted values are somewhat higher than the measured values: the source of the error is partly due to the fact that the compressive strength is further knocked down by out-of-plane normal loading by the transverse plies (see Figure 8c), and partly due to the difficulty in measuring b/h accurately.

F. Shear-Band Formation

In polymer-matrix fiber composites with very low fiber volume fractions, *shear banding* can occur, see Figure 1f. Matrix yield and fracture occur in a band, oriented at about 45° with respect to the loading axis (Fried, 1963).

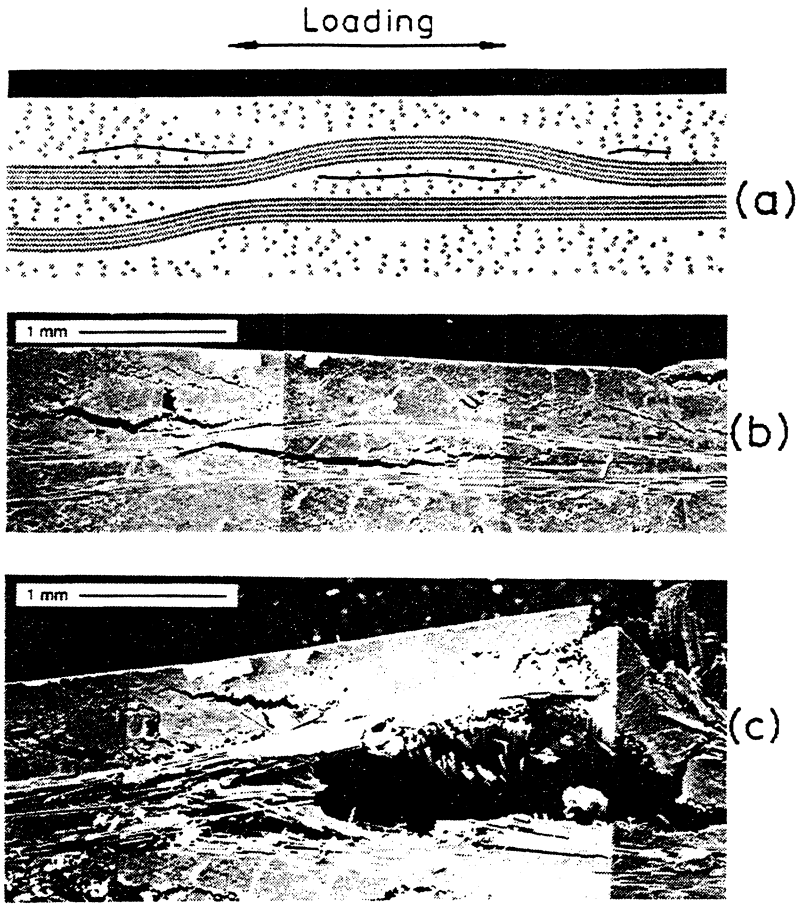

FIG. 8. Failure of SiC fiber-reinforced alumina under direct compression by buckle delamination. (a) Schematic of crack initiation from initial defects; (b) SEM micrograph of stable buckling under increasing remote load; (c) Post-buckling catastrophic failure. Taken from Kaute *et al.* (1996).

This failure mode is essentially identical to that which would occur in the unreinforced matrix material and is not expected to be significant at conventional fiber volume fractions.

G. FAILURE MAPS

The competition between the various compressive failure mechanisms can be displayed on a fracture mechanism map. The appropriate non-dimensional axes of the map are generated by considering the boundaries between each mechanism. For example:

(i) Plastic microbuckling dominates elastic microbuckling when $\bar{\phi}/\gamma_y > 0$ by comparison of (2.1) and (2.3).
(ii) Fiber crushing occurs in preference to buckle delamination when the compressive strength associated with fiber crushing, σ_{crush}, is

less than the compressive strength given by (2.5) for buckle delamination. On writing $\sigma_{crush} = E\varepsilon_{fc}$, where E is the longitudinal modulus of the composite and ε_c is the fiber-crushing strain, we deduce that fiber crushing occurs instead of buckle delamination when $b/h < \pi/(2\sqrt{3\varepsilon_{fc}})$. Typically, $\varepsilon_{fc} \approx 2\%$ and so fiber crushing dominates when $b/h < 6.4$. For most practical composites, the condition $b/h < 6.4$ is met and fiber crushing occurs in preference to buckle delamination.

(iii) Fiber crushing occurs instead of plastic microbuckling when

$$\frac{\varepsilon_{fc}E}{G} < \frac{1}{1 + \left(\bar{\phi}/\gamma_y\right)}$$

via (2.3) and (2.4).

(iv) Splitting occurs in preference to plastic microbuckling when

$$\frac{CK_{IC}}{G\sqrt{\pi a}} < \frac{1}{1 + \left(\bar{\phi}/\gamma_y\right)}$$

from relations (2.2) and (2.5).

The boundaries identified above suggest that we can construct a three-dimensional failure map with axes $(\varepsilon_{fc}E/G,\ CK_{IC}/G\sqrt{\pi a},\ \bar{\phi}/\gamma_y)$. The resulting map is shown in Figure 9a, and includes the main compressive failure mechanisms with the exception of buckle delamination. The map displays the dominant mechanism of compressive failure for a given set of composite properties. The domain of dominance of competing failure mechanisms is sketched in Figure 9a: the map may be used to predict the operative failure mechanism for any given set of material parameters given by the axes of the map. Note that the region of elastic microbuckling occupies part of the plane, $\bar{\phi}/\gamma_y = 0$. For long surface debonds $b/h > 6.4$, the domain of fiber crushing is replaced by buckle delamination; the resulting map is of identical shape to that shown in Figure 9a but the axis $\varepsilon_{fc}E/G$ is replaced by

$$\frac{\pi^2}{12}\left(\frac{h}{b}\right)^2 \frac{E}{G}.$$

The map shown in Figure 9b includes contour surfaces of constant σ_c/G. Each contour is composed of a set of orthogonal planes, as depicted in the figure. For example, in the region of plastic microbuckling contours

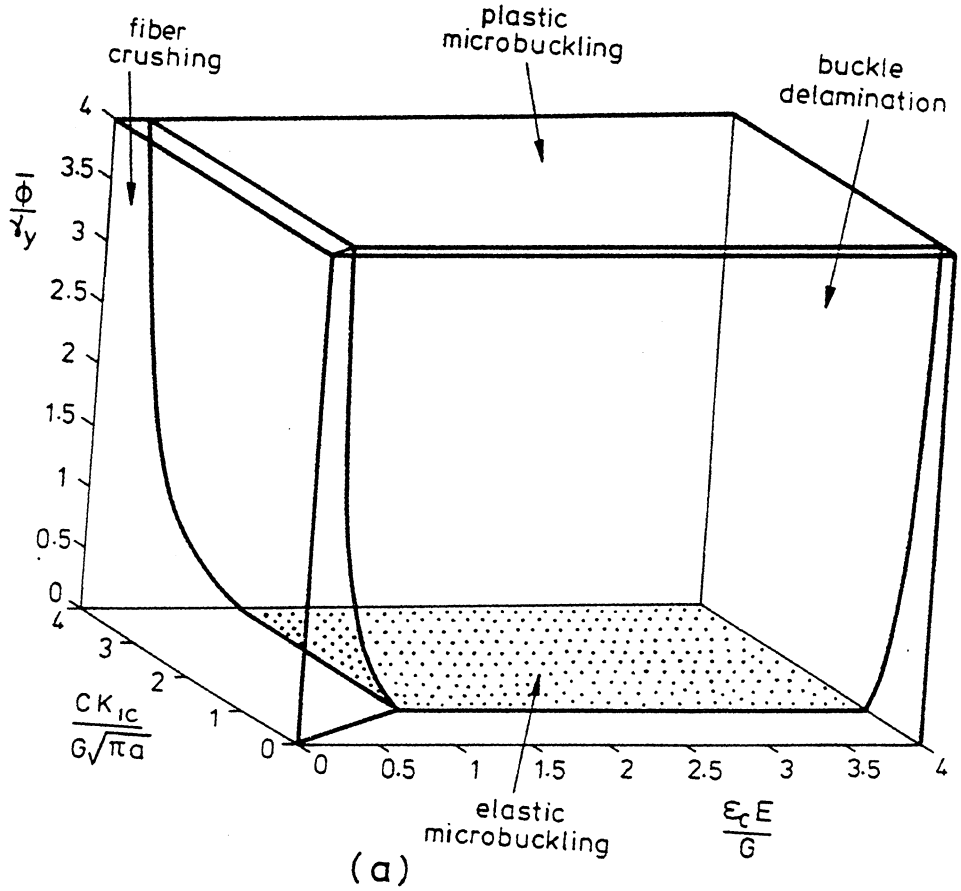

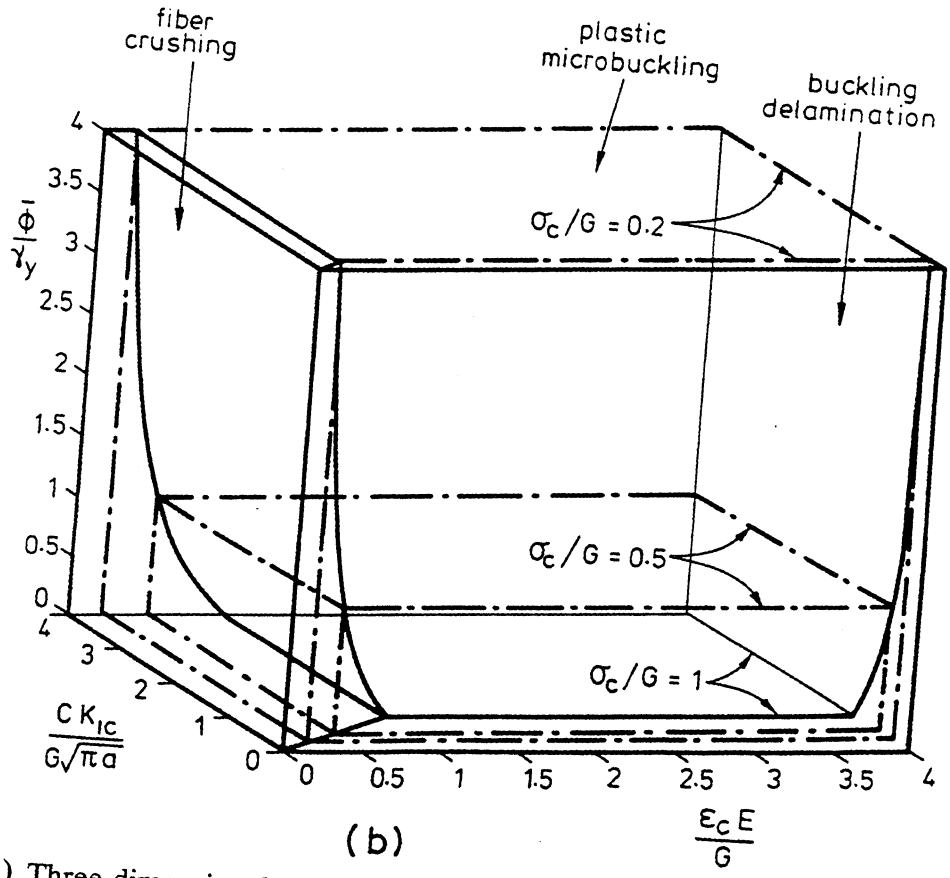

FIG. 9. (a) Three-dimensional failure map showing region of dominance of competing failure mechanisms; (b) Failure maps, with contours of strength added.

of constant σ_c/G exist as planes normal to the $\bar{\phi}/\gamma_y$-axis. The strength, σ_c/G, decreases with increasing $\bar{\phi}/\gamma_y$, as given by relation (2.3). The maximum possible strength shown on the map is $\sigma_c/G = 1$; this is achieved by elastic microbuckling, but, as already discussed above, other failure mechanisms usually intervene and give a lower strength than this maximum value.

A simpler two-dimensional version of the map is also instructive: it takes as axes the in-plane shear modulus of the composite G and the ratio of in-plane shear strength, τ_y, to fiber misalignment angle $\bar{\phi}$, see Figure 10. In other words, we take as axes the long-wavelength limit of the Rosen formula (2.1) for the elastic microbuckling strength, and the Argon expression (2.2) for the plastic microbuckling strength. Contours of compressive strength are straight lines with a plateau value given by the onset of fiber crushing. Material data for a number of carbon fiber composites are included in the figure: in all cases failure is by plastic microbuckling. It is clear that an increased compressive strength would be achieved by increasing τ_y and by decreasing $\bar{\phi}$, and that significant improvements in compressive strength may yet be made without the intervention of fiber crushing. The demand for improved toughness of composites has caused a progressive decrease in the shear strength of the matrix, so the only strategy available is to reduce the fiber misalignment $\bar{\phi}$ from a value of 2–3° to

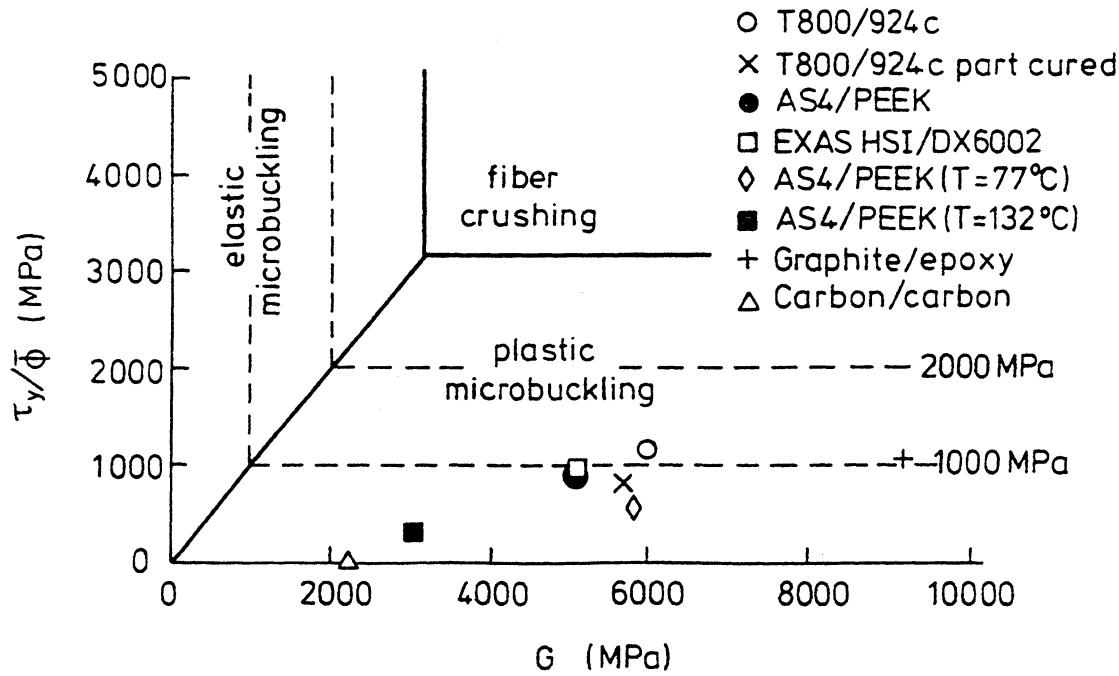

FIG. 10. Two-dimensional failure map, with test data added. Commercial polymer matrix composites fail by plastic microbuckling, as indicated.

much lower values. The use of pultrusion in composite manufacture (whereby the fibers and partially cured matrix are pulled through a die) has shown itself to be a practical processing route for highly aligned fiber composites.[1]

III. Compressive Strength of Unidirectional Composites Due to Microbuckling

In this section a number of theoretical and experimental studies are summarized in order to elucidate various aspects of the microbuckling phenomenon. In Section A, the simplest estimates of initiation strength for microbuckling in rate-independent composites are determined by *kinking theory*: the fibers are taken to be inextensional and fiber-bending resistance is neglected. The kinking theory is then used to estimate conditions for microbuckling for a variety of composite constitutive laws: elastic-plastic, creep, visco-elastic, and low-cycle fatigue.

In Section B, the effect of *fiber-bending resistance* on the infinite band-collapse response is determined through the use of *couple stress theory*. A small strain theory is adequate to predict the *initiation strength* and the width of a microbuckle: the width is set by fiber fracture in bending. Finite strain calculations are used in order to estimate the post-collapse response, particularly when fiber fracture is not an issue. The calculations show that the post-collapse strength settles to a *steady-state value*, σ_b, associated with *band broadening*; this steady-state value can be calculated directly by a work calculation from kinking theory. The infinite band-bending theory is also used to estimate the compressive strength associated with random fiber waviness. This calculation uses digital signal techniques in order to calculate the probability density function of failure associated with a given power spectral density of fiber waviness.

The compressive strength of the case of a finite region of initial fiber waviness is discussed in Section C. A two-dimensional finite element scheme is used, and couple stress theory is used to include the effects of finite fiber-bending resistance. Again, the fiber diameter sets the internal length scale of the microstructure. The main finding is that the compres-

[1] Neptco Inc. have recently introduced a carbon fiber-epoxy composite Graphlite™ with a fiber misalignment of less than 0.5°. The measured compressive strength is about 2.0 GPa (Neptco, 1994).

sive strength is given to a good approximation by kinking theory unless the region of initial waviness is small. The role of multi-axial loading in knocking down the axial compressive strength is addressed: the knockdown factors for a small region of fiber waviness are similar to those for an infinite band of initial waviness.

1. *Assumed Collapse Response from an Initial Imperfection in the Form of an Infinite Band*

We begin by summarizing the qualitative details of rate-independent microbuckling for a composite with a pre-existing infinite band of imperfection in the form of fiber misalignment. Quantitative details are covered in subsequent sections. Assume that the fibers are uniformly misaligned by a constant angle $\bar{\phi}$ within the band in the stress-free initial configuration as shown in Figure 3. The normal to the band is taken to be at an angle β to the fiber direction. The fibers are assumed to possess a finite-bending resistance so that the additional fiber rotation ϕ under load is continuous.

Consider the collapse response for the geometry given in Figure 3, under an axial stress σ^{∞}. The collapse response is presented in the form of remote axial stress versus maximum additional fiber rotation, ϕ_m, in Figure 11. The deformation mode within the band is a combination of in-plane shear parallel to the fiber direction and direct-straining transverse to the fibers. Fibers within the band attain large rotations (of up to about 60° for the case $\beta = 30°$) and so a non-linear constitutive response is appropriate for the smeared-out behavior of the composite within the band. Initially, fiber rotation occurs under an increasing remote stress, σ^{∞}, as indicated by a typical point A of Figure 11. Note that the fibers within the band rotate by a greater amount than material outside the band. The additional rotation leads to *geometric softening*, which more than offsets the *strain hardening* within the band. With continued fiber rotation the load goes through a maximum (point B) and then decreases to a lower steady-state value as shown in Figure 11. The maximum is attained after only a few degrees of fiber rotation. Beyond the maximum load point, fiber rotation continues and the band continues to broaden, see point C of Figure 11. Eventually, the matrix strain hardens sufficiently within the band for the material to "lock-up" and continued end shortening of the structure is due to broadening of the band in the axial direction at a constant value of remote stress, σ_p, point D. It is found experimentally that the lock-up state within the band is associated with a state of zero

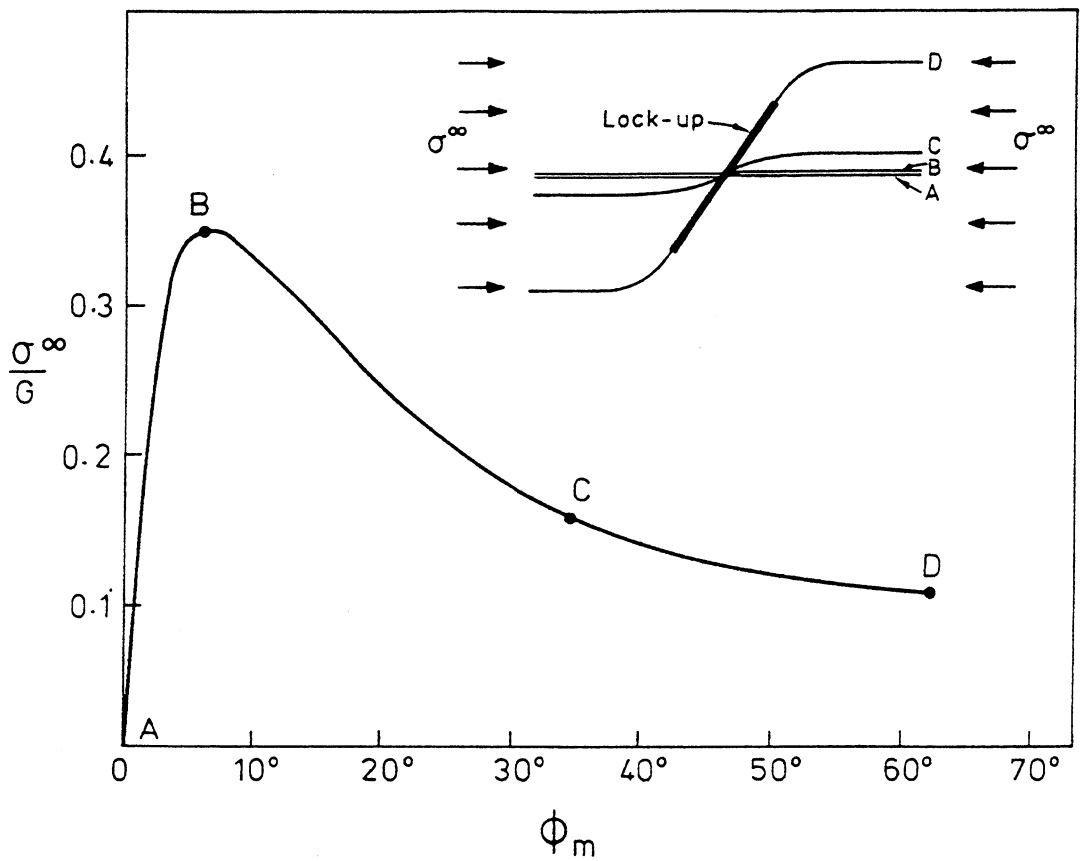

FIG. 11. Typical infinite band collapse response, with the role of fiber bending included. ϕ_m is the maximum value of fiber rotation in the composite, for any given remote stress σ^∞.

volumetric strain within the band: as the fibers rotate they first lead to dilation within the band, followed by compaction until lock-up occurs at vanishing volumetric strain (Chaplin, 1977; Evans and Adler, 1978; Sivashanker *et al.*, 1995). The overall buckling response is akin to tensile drawing of a polymer, whereby a neck forms by geometric softening; subsequently, orientation hardening occurs within the neck and leads to steady-state neck propagation known as drawing.

The total end shortening Δ_T of the composite of finite length h is the sum of *elastic shortening* Δ_E of the fibers and the end shortening Δ associated with fiber rotation; see Figures 12a and b. To an excellent approximation, the σ^∞ versus Δ collapse response may be considered to be the universal collapse curve, and the elastic end-shortening is given by $\Delta_E = \sigma^\infty h/E_L$, where E_L is the longitudinal elastic modulus of the composite. The σ^∞ versus Δ_T collapse response is sketched in Figure 12b for two different lengths h of composite: note that an increasingly strong *snap-back* behavior is predicted with increasing h. (Kyriakides *et al.*, 1995) have confirmed this using detailed finite element calculations where they treat the fibers and intervening matrix as a series of discrete layers.) The

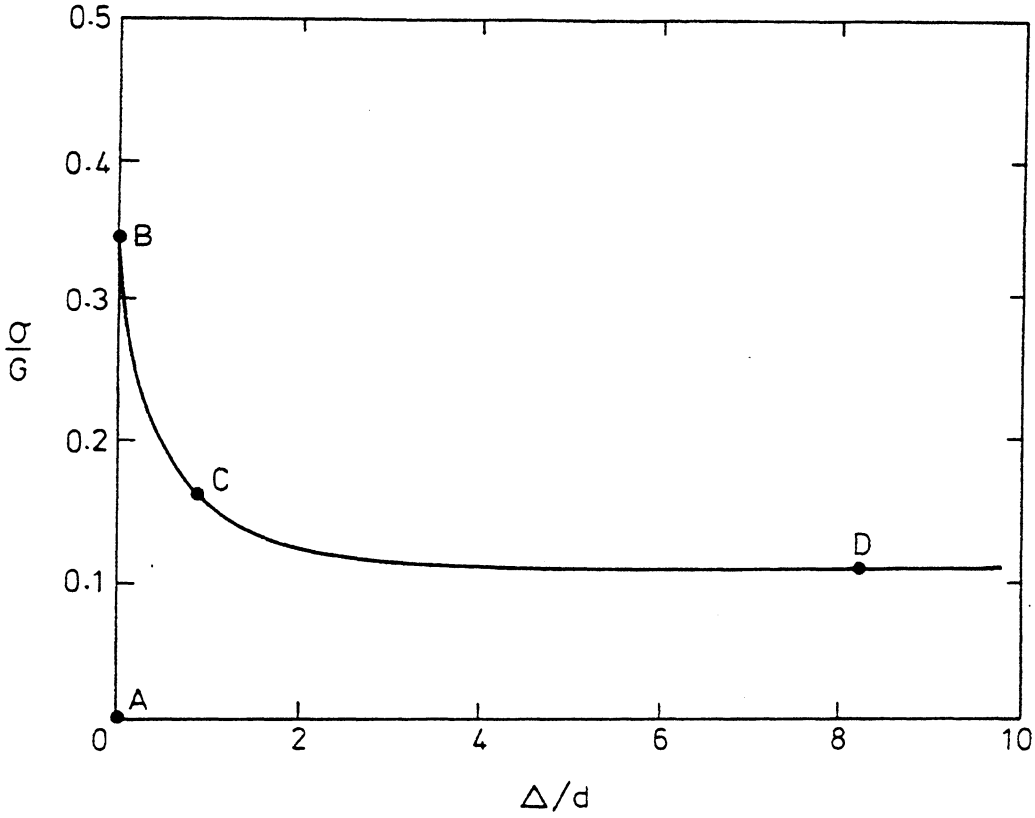

(a)

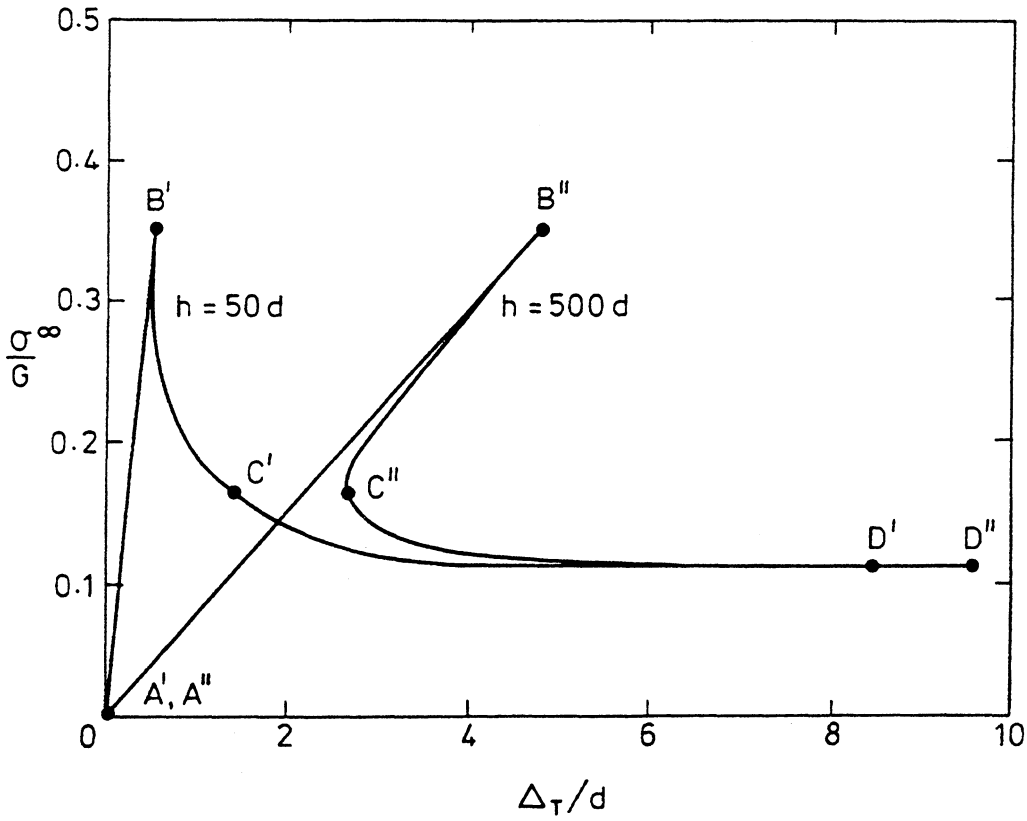

(b)

FIG. 12. Collapse response, presented in form of (a) σ^{∞} versus end shortening Δ associated with fiber rotation, and (b) σ^{∞} versus total end shortening Δ_T associated with both fiber rotation and elastic axial compliance of the composite of height h.

four representative stages of deformation A–D given in Figure 11 are also shown in Figures 12a and b.

The description above of the collapse process represents the consensus of opinion from the work of Shih and co-workers (Liu *et al.*, 1995; Moran *et al.*, 1995), Kyriakides and co-workers (Kyriakides *et al.*, 1995) and Fleck and co-workers (Sutcliffe and Fleck, 1994; Sivashanker *et al.*, 1995). Liu *et al.* (1995) were the first to observe steady-state band broadening by testing a composite of sufficiently high-failure strain for fiber fracture not to intervene (IM7 fibers in APC-2 PEEK matrix). Experimental observations (Sutcliffe and Fleck, 1994; Sivashanker *et al.*, 1995; Fleck *et al.*, 1996) have been made recently of band broadening in fiber composites which exhibit fiber fracture. It is observed that fiber fracture is intermittent along the length of a microbuckle band, and that the average traction carried by a microbuckle band is almost identical to that carried by a microbuckle band displaying no fiber fracture: the infinite band collapse response is hardly changed by the occurrence of fiber fracture.

A. Kinking Theory

As reviewed in Section II.B, the theoretical studies by Argon (1972) and Budiansky and Fleck (1993) have shown that microbuckling in polymer matrix composites is associated with a non-linear plastic response of the matrix. The analysis of Budiansky and Fleck (1993) for plastic microbuckling considers the effects of initial imperfections, plastic strain hardening, and combined remote shear stress and axial compression. Slaughter *et al.* (1992) extended the Budiansky and Fleck (1993) analysis to general multi-axial loading. We begin by summarizing the treatment of Slaughter *et al.* (1992).

The following kinking theory is an *infinite band* calculation in the spirit of one-dimensional shear localization analysis. A uniform imperfection in the form of a finite fiber misalignment angle $\overline{\phi}$ is assumed within a band (see Figure 3), and the evolution of fiber rotation within the band is deduced from algebraic equations for continuity of traction and displacement at the band boundary. The kinking analysis allows for the determination of analytical formulae for the critical stress for microbuckling. As in most treatments of compressive kinking, the fibers in these calculations are assumed to be inextensional. This has the effect of shielding the matrix

from axial stress, and therefore the actual effect of this stress on matrix plasticity is not taken into account.

Consider the collapse of a kink band inclined at an angle β to the main fiber direction, as shown in Figure 13. (It is observed experimentally that kink bands are inclined typically at $\beta = 20°–30°$.) It is assumed that the fibers are inextensible and that uniform straining within the kink band is associated with a fiber rotation, ϕ. It is further assumed that initial fiber misalignment within the composite is represented by the angle, $\bar{\phi}$.

Two Cartesian coordinate systems, $(\mathbf{e}_1, \mathbf{e}_2)$ and $(\boldsymbol{\varepsilon}_1, \boldsymbol{\varepsilon}_2)$, are defined such that $\mathbf{e}_1$ and $\mathbf{e}_2$ are parallel and normal to the fiber axes outside the kink band, and $\boldsymbol{\varepsilon}_1$ and $\boldsymbol{\varepsilon}_2$ are parallel and normal to the fiber axes inside the kink band. These two coordinate systems are related by

$$\begin{aligned} \mathbf{e}_1 &= \boldsymbol{\varepsilon}_1 \cos(\bar{\phi} + \phi) - \boldsymbol{\varepsilon}_2 \sin(\bar{\phi} + \phi) \\ \mathbf{e}_2 &= \boldsymbol{\varepsilon}_1 \sin(\bar{\phi} + \phi) + \boldsymbol{\varepsilon}_2 \cos(\bar{\phi} + \phi) \end{aligned} \tag{3.1}$$

The stress components outside the kink band are defined by

$$\boldsymbol{\sigma}^\infty = -\sigma_L^\infty \mathbf{e}_1\mathbf{e}_1 + \sigma_T^\infty \mathbf{e}_2\mathbf{e}_2 + \tau^\infty(\mathbf{e}_1\mathbf{e}_2 + \mathbf{e}_2\mathbf{e}_1) \tag{3.2}$$

and those within the kink band are defined by

$$\boldsymbol{\sigma} = \sigma_L \boldsymbol{\varepsilon}_1\boldsymbol{\varepsilon}_1 + \sigma_T \boldsymbol{\varepsilon}_2\boldsymbol{\varepsilon}_2 + \tau(\boldsymbol{\varepsilon}_1\boldsymbol{\varepsilon}_2 + \boldsymbol{\varepsilon}_2\boldsymbol{\varepsilon}_1) \tag{3.3}$$

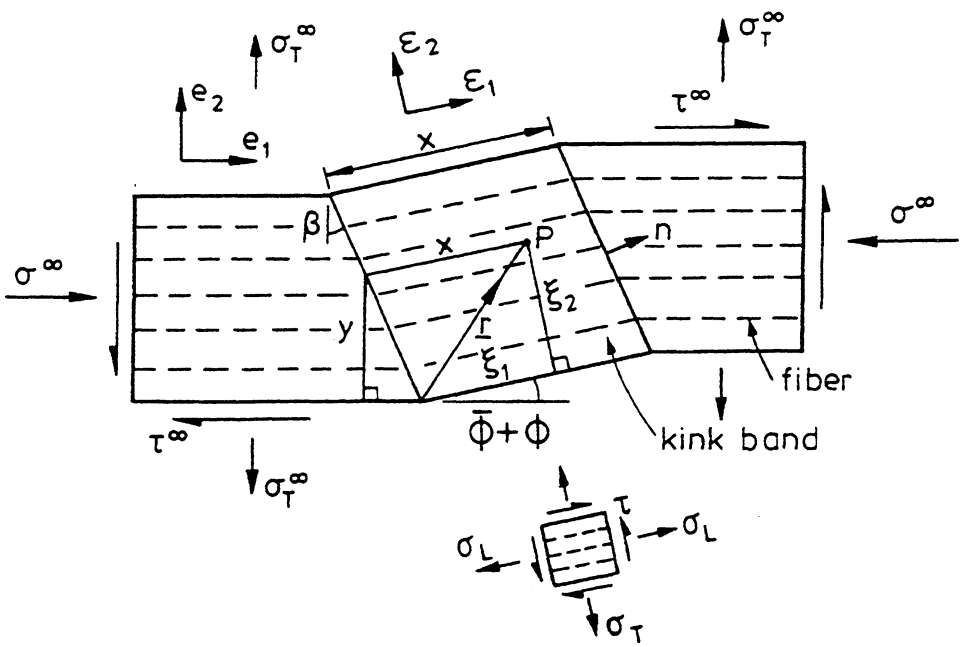

FIG. 13. Definition of coordinates within kink band. The fibers are taken to be inextensional.

Continuity of Tractions Continuity of tractions across the kink band interface can be expressed as

$$\mathbf{n} \cdot \boldsymbol{\sigma}^{\infty} = \mathbf{n} \cdot \boldsymbol{\sigma} \tag{3.4}$$

where $\mathbf{n} = \mathbf{e}_1 \cos\beta + \mathbf{e}_2 \sin\beta$ is the unit normal to the kink band interface. Equations (3.1)–(3.3) lead to the two scalar equations for continuity of tractions in the $\boldsymbol{\varepsilon}_1$ and $\boldsymbol{\varepsilon}_2$ directions, respectively,

$$\begin{aligned} &-\sigma_L^{\infty} \cos\beta \cos(\bar{\phi} + \phi) + \sigma_T^{\infty} \sin\beta \sin(\bar{\phi} + \phi) + \tau^{\infty} \sin(\beta + \bar{\phi} + \phi) \\ &\quad = \sigma_L \cos(\beta - \bar{\phi} - \phi) + \tau \sin(\beta - \bar{\phi} - \phi) \end{aligned} \tag{3.5}$$

$$\begin{aligned} &\sigma_L^{\infty} \cos\beta \sin(\bar{\phi} + \phi) + \sigma_T^{\infty} \sin\beta \cos(\bar{\phi} + \phi) \\ &\quad + \tau^{\infty} \cos(\beta + \bar{\phi} + \phi) \\ &\qquad = \sigma_T \sin(\beta - \bar{\phi} - \phi) + \tau \cos(\beta - \bar{\phi} - \phi) \end{aligned} \tag{3.6}$$

Because the fibers are assumed to be inextensible, the axial stress in the kink band, σ_L, is of no interest in the analysis to follow and eq. (3.5) need not be considered further.

It is assumed that the initial misalignment, $\bar{\phi}$, is small. Furthermore, it is anticipated that consideration of small deformation angles, ϕ, will be sufficient to examine the critical events associated with microbuckling. For small $\bar{\phi} + \phi$, linearization of eq. (3.6) provides

$$\begin{aligned} &(\bar{\phi} + \phi)(\sigma_L^{\infty} \cos\beta - 2\tau^{\infty} \sin\beta) \\ &\quad \approx (\sigma_T - \sigma_T^{\infty})\sin\beta - (\bar{\phi} + \phi)\sigma_T \cos\beta \\ &\qquad + (\tau - \tau^{\infty})[\cos\beta + (\bar{\phi} + \phi)\sin\beta] \end{aligned} \tag{3.7}$$

Equation (3.7) can be further approximated, when $(\pi/2) - \beta \gg 0$, by dropping the term $(\tau - \tau^{\infty})(\bar{\phi} + \phi)\sin\beta$ from the right-hand side, to give

$$\sigma_L^{\infty} - 2\tau^{\infty} \tan\beta \approx \frac{\tau - \tau^{\infty} + (\sigma_T - \sigma_T^{\infty})\tan\beta}{\bar{\phi} + \phi} - \sigma_T \tag{3.8}$$

This form of the approximation is chosen so that, when the composite behaves elastically, a proper account of the terms involving the remote stresses is maintained.

Kinematic Relations Kinematic conditions for kink-band deformation are now examined. Consider a material point P within the kink band, as shown in Figure 13. The position vector **r** to point P is

$$\mathbf{r} = \xi_1 \boldsymbol{\varepsilon}_1 + \xi_2 \boldsymbol{\varepsilon}_2 = y(-\mathbf{e}_1 \tan \beta + \mathbf{e}_2) + x\boldsymbol{\varepsilon}_1 \tag{3.9}$$

where the scalar lengths ξ_1, ξ_2, x, and y are defined as shown in Figure 13 and are related by

$$\left.\begin{aligned} x &= \xi_1 + \xi_2 \tan(\beta - \bar{\phi} - \phi) \\ y &= \xi_2 \cos \beta \sec(\beta - \bar{\phi} - \phi) \end{aligned}\right\} \tag{3.10}$$

The velocity of point P is

$$\boldsymbol{v} = y\dot{\gamma}^{\infty}\mathbf{e}_1 + y\dot{e}_T^{\infty}\mathbf{e}_2 + x\dot{\phi}\boldsymbol{\varepsilon}_2 \tag{3.11}$$

where $\dot{\gamma}^{\infty}$ and $\dot{e}_T^{\infty}$ are, respectively, the shear strain rate and transverse strain rate outside the kink band, and $\dot{f}(t) \equiv df(t)/dt$.

The strain rate tensor within the kink band is related to the velocity field by

$$\dot{\boldsymbol{\varepsilon}} = \frac{1}{2}[\nabla \boldsymbol{v} + (\nabla \boldsymbol{v})^T] \tag{3.12}$$

where the superscript T denotes the transpose, and the gradient operator ∇ is

$$\nabla = \boldsymbol{\varepsilon}_1 \frac{\partial}{\partial \xi_1} + \boldsymbol{\varepsilon}_2 \frac{\partial}{\partial \xi_2} \tag{3.13}$$

With the strain-rate components within the kink band defined by

$$\dot{\boldsymbol{\varepsilon}} = \dot{e}_T \boldsymbol{\varepsilon}_2\boldsymbol{\varepsilon}_2 + \frac{1}{2}\dot{\gamma}(\boldsymbol{\varepsilon}_1\boldsymbol{\varepsilon}_2 + \boldsymbol{\varepsilon}_2\boldsymbol{\varepsilon}_1) \tag{3.14}$$

eq. (3.12), along with eqs. (3.1) and (3.9–3.11), gives the kinematic relations

$$\left.\begin{aligned} \dot{e}_T &= \dot{\phi} \tan(\beta - \bar{\phi} - \phi) \\ &\quad + \left[\dot{e}_T^{\infty} \cos(\bar{\phi} + \phi) - \dot{\gamma}^{\infty} \sin(\bar{\phi} + \phi)\right] \cos \beta \sec(\beta - \bar{\phi} - \phi) \\ \dot{\gamma} &= \dot{\phi} + \left[\dot{\gamma}^{\infty} \cos(\bar{\phi} + \phi) + \dot{e}_T^{\infty} \sin(\bar{\phi} + \phi)\right] \cos \beta \sec(\beta - \bar{\phi} - \phi) \end{aligned}\right\} \tag{3.15}$$

Differentiating eq. (3.9), and noting that $\dot{\mathbf{r}} = \boldsymbol{\nu}$, $\dot{y} = y\dot{e}_T^\infty$, and $\dot{\boldsymbol{\varepsilon}}_1 = \dot{\phi}\boldsymbol{\varepsilon}_2$, it follows from eq. (3.11) that

$$\dot{\beta} = -(\dot{e}_T^\infty \sin\beta + \dot{\gamma}^\infty \cos\beta)\cos\beta \tag{3.16}$$

For $\bar{\phi} + \phi$, e_T^∞, and γ^∞ small, eqs. (3.15) and (3.16) reduce to the approximate kinematic equations

$$\left.\begin{aligned} e_T &\approx e_T^\infty + \phi\tan\beta \\ \gamma &\approx \gamma^\infty + \phi \\ \beta &\approx \beta_o \end{aligned}\right\} \tag{3.17a}$$

where β_o is the kink-band angle associated with zero remote straining. In the limiting case $\beta \to 0$, the analysis reduces to the case of pure shear deformation within the kind band, as outlined by Wisnom (1990). In the case of vanishing remote transverse strain and shear strain, the rate equations (3.15) can be integrated to give

$$\left.\begin{aligned} \gamma &= \phi \\ e_T &= \log\left[\frac{\cos(\beta - \bar{\phi} - \phi)}{\cos(\beta - \bar{\phi})}\right] \end{aligned}\right\} \tag{3.17b}$$

Note that (3.17b) implies that the volumetric strain in the band vanishes when the fibers have rotated to the point when $\phi = 2(\beta - \bar{\phi})$.

Constitutive Relations: Deformation and Flow Theory Versions of Plasticity
If the composite deforms elastically, then the stress components (σ_T, τ) in the band are related to the strain components (e_T, γ) in the band via

$$\sigma_T = E_T e_T \tag{3.18a}$$

$$\tau = G\gamma \tag{3.18b}$$

where E_T and G are the transverse and shear elastic moduli for the composite. Similarly, the components of remote stress $(\sigma_T^\infty, \tau^\infty)$ are related to the remote strain state $(e_T^\infty, \gamma^\infty)$ via $\sigma_T^\infty = E_T e_T^\infty$ and $\tau^\infty = G\gamma^\infty$. The state of stress within the band may be related to the rotation ϕ within the band via (3.17), to give

$$\left.\begin{aligned} \sigma_T &\approx \sigma_T^\infty + E_T\phi\tan\beta \\ \tau &\approx \tau^\infty + G\phi \end{aligned}\right\} \tag{3.19}$$

The exact equation for continuity of tractions, eq. (3.6), combined with this result and then linearized gives the approximate elastic kink-band response

$$\sigma_L^\infty + \sigma_T^\infty - 2\tau^\infty \tan\beta \approx \left[G + E_T \tan^2\beta\right] \frac{\phi}{\bar{\phi} + \phi} \tag{3.20}$$

An examination of eq. (3.8), the approximate equation for continuity of tractions, shows that it also reduces to the correct result for elastic kink-band response, eq. (3.20).

Flow-Theory Version The following constitutive equations for a flow-theory version of plasticity have been derived by Budiansky and Fleck (1993) and the derivation is only outlined here. A similar approach has been adopted by Sun and Chen (1989), Sun and Yoon (1991), and Schapery (1995).

The elastic component of the strain tensor is given by (3.18). Assume that the composite is characterized by the quadratic yield condition

$$\left(\frac{\tau_e}{\tau_y}\right)^2 = \left(\frac{\tau}{\tau_y}\right)^2 + \left(\frac{\sigma_T}{\sigma_{Ty}}\right)^2 \tag{3.21}$$

where τ_y and σ_{Ty} are the plane strain yield stresses in pure shear and pure transverse tension in the case of perfect plasticity (when $\tau_e = \tau_y$, a constant). The effective stress, τ_e, which can be rewritten as

$$\tau_e \equiv \sqrt{\tau^2 + (\sigma_T/R)^2} \tag{3.22}$$

is used as a plastic potential for the plastic strain rates, $\dot{\gamma}^p$ and $\dot{e}_T^p$. The parameter $R = \sigma_{Ty}/\tau_y$ defines the eccentricity of the yield ellipse, which expands homogeneously with increasing τ_e due to strain hardening.

Discounting the possibility of elastic unloading, the associated flow theory relations for plastic-strain rates, based on τ_e as a plastic potential, can be written as

$$\left.\begin{aligned} \dot{\gamma}^p &= F(\tau_e)\frac{\partial \tau_e}{\partial \tau}\,\dot{\tau}_e \\ \dot{e}_T^p &= F(\tau_e)\frac{\partial \tau_e}{\partial \sigma_T}\,\dot{\tau}_e \end{aligned}\right\} \tag{3.23}$$

where $F(\tau_e)$ is a measure of the rate of strain hardening. A work-equivalent effective plastic strain rate, $\dot{\gamma}_e^p$, is defined by

$$\tau\dot{\gamma}^p + \sigma_T \dot{e}_T^p = \tau_e \dot{\gamma}_e^p \tag{3.24}$$

and it follows that

$$\dot{\gamma}_e^p = F(\tau_e)\dot{\tau}_e = \sqrt{(\dot{\gamma}^p)^2 + R^2(\dot{e}_T^p)^2}\,. \tag{3.25}$$

Thus, we interpret $F(\tau_e)$ as the inverse of the tangent modulus of the τ versus γ^p response in pure shear.

Deformation Theory Version Next, we derive a deformation theory version which coincides with the above flow-theory version for the special case of proportional loading. Substituting eq. (3.24) into eq. (3.22) and assuming proportional loading leads to

$$\left.\begin{aligned} \gamma^p &= \left(\frac{\gamma_e^p}{\tau_e}\right)\tau \\ e_T^p &= \left(\frac{\gamma_e^p}{\tau_e}\right)\frac{\sigma_T}{R^2} \\ \gamma_e^p &= \sqrt{(\gamma^p)^2 + R^2(e_T^p)^2} \end{aligned}\right\} \tag{3.26}$$

Note that the functional dependence of γ_e^p on τ_e is taken to be the same as that of γ^p on τ for pure shear. Equations (3.26) have the form of a deformation theory of plasticity. The linear elastic portion of the strain state is related to the stress state via (3.18).

It is unclear whether deformation or flow theory is the more appropriate constitutive law for addressing fiber microbuckling. We shall see below that the maximum compressive stress is carried by the kink band at rather small values of fiber rotation (a few degrees). In this regime, relation (3.17a) indicates that straining is proportional within the kink band for the case of uniaxial compression: the distinction vanishes between deformation and flow theories. In the post-collapse regime of large fiber rotations within the kink band, straining is non-proportional and the flow theory prediction is stronger than the deformation theory prediction. There are strong theoretical arguments and convincing experimental evidence that deformation theory is more accurate in the prediction of plastic buckling loads in metallic structures; see for example the review by Hutchinson

(1974). Fleck and Jelf (1995) have performed non-proportional loading tests on hoop-wound carbon fiber-epoxy tubes; they found that the deformation theory description (3.26) is more accurate than the flow theory version (3.23). We shall continue with the deformation theory description and now derive the compressive strength of a kink band for a rigid-perfectly plastic solid, and then for a Ramberg-Osgood strain-hardening solid.

2. *Rigid-Perfectly Plastic Solid under Multi-Axial Loading*

Slaughter *et al.* (1992) have derived an algebraic expression for the axial collapse strength, σ_c, under multi-axial loading for the limiting case of a rigid-perfectly plastic solid of shear yield strength τ_y,

$$\sigma_c = \frac{\alpha\tau_y - \tau^\infty - \sigma_T^\infty \tan\beta}{(\bar{\phi} + \phi)} \tag{3.27}$$

where $\alpha \equiv \sqrt{1 + R^2 \tan^2 \beta}$. This relation indicates a large knockdown effect of both in-plane shear stress and transverse stress on the axial compressive strength. Jelf and Fleck (1994) have confirmed the accuracy of (3.27) for the case of combined axial and shear loading by performing compression-torsion tests on unidirectional carbon fiber-reinforced epoxy tubes.

3. *Effect of Strain Hardening on Compressive Strength*

The in-plane shear response of polymer matrix composites at small levels of strain may be adequately described by the Ramberg-Osgood description

$$\frac{\gamma}{\gamma_Y} = \frac{\tau}{\tau_Y} + \frac{3}{7}\left(\frac{\tau}{\tau_Y}\right)^n \tag{3.28}$$

in terms of the three-parameter fit (τ_Y, γ_Y, n). The shear modulus G follows as $G = \tau_Y/\gamma_Y$. For polymer matrix composites, τ_Y is in the range 40–60 MPa, γ_Y equals approximately 1%, and the strain-hardening exponent n is in the range 3–10, as collated by Fleck and Jelf (1995).

For the case of an inclined kink band, the strain state within the band is composed of both shear and transverse straining. The Ramberg-Osgood description (3.28) generalizes to

$$\frac{\gamma_e}{\gamma_Y} = \frac{\tau_e}{\tau_Y} + \frac{3}{7}\left(\frac{\tau_e}{\tau_Y}\right)^n \tag{3.29}$$

where τ_e is given by (3.22) and the effective strain γ_e is composed of an elastic part

$$\gamma_e = \frac{\tau_e \gamma_Y}{\tau_Y}$$

and a plastic part

$$\gamma_e^p = \frac{3\gamma_Y}{7}\left(\frac{\tau_e}{\tau_Y}\right)^n.$$

For the deformation theory solid, γ_e^p is given by (3.26), and for the flow theory solid, $\dot{\gamma}_e^p$ is defined by (3.25).

Budiansky and Fleck (1993) have developed the following analytical expression for the uniaxial compressive strength for the deformation theory solid,

$$\frac{\sigma_c}{G^*} = \frac{1}{1 + n\left(\frac{3}{7}\right)^{1/n}\left[\frac{\bar{\phi}/\gamma_Y^*}{n-1}\right]^{(n-1)/n}} \tag{3.30}$$

where $G^* \equiv [1 + R^2 \tan^2 \beta]G$ and $\gamma_Y^* \equiv \gamma_Y/\sqrt{1 + R^2 \tan^2 \beta}$. The critical stress σ_c is achieved in the regime of proportional straining at small values of fiber rotation ϕ, and so the above result also remains valid for flow theory. Figure 14 shows how σ_c varies with $\bar{\phi}/\gamma_Y^*$ for $n = 3, 5, 9$ and ∞: we note that strain hardening has little effect on the strength and so the elastic-perfectly plastic estimates of Section II.B remain valid. Typically, the measured compressive strength of polymer matrix composites is $\sigma_c/G \approx 0.2$ and the corresponding estimated value for fiber waviness is $\bar{\phi}/\gamma_Y^* \approx 4$ from Figure 13. With γ_Y^* taken as 1% this suggests a fiber misalignment angle of about 2.3°.

4. *Time-Dependent Kinking*

Many fiber composites are known to exhibit time-dependent deformation behavior, or *creep*. These include polymer matrix composites (Horoschenkoff *et al.*, 1988; Ha *et al.*, 1991) and woods (Dinwoodie, 1981).

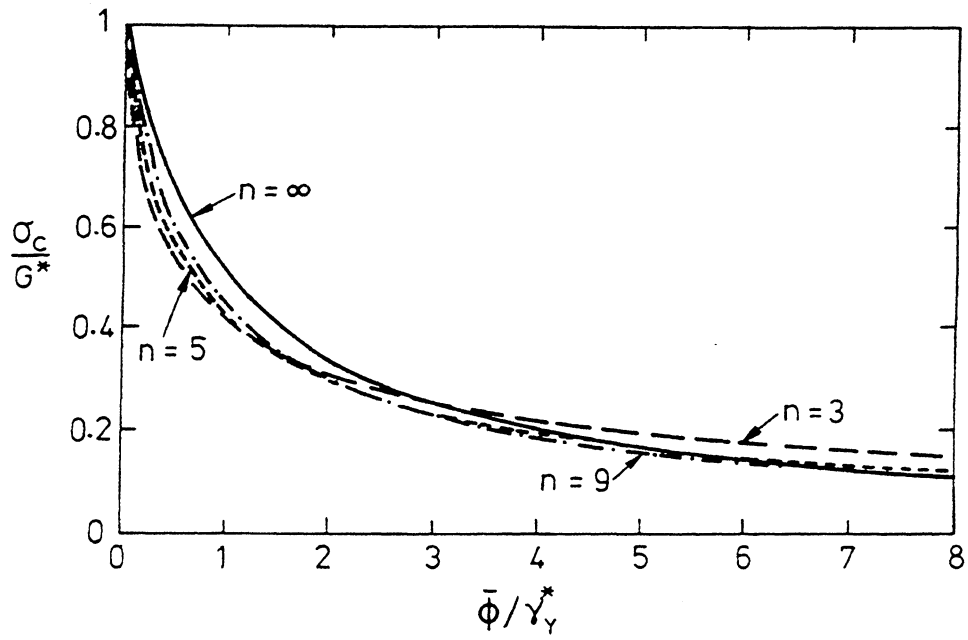

FIG. 14. Effect of fiber misalignment angle $\bar{\phi}$ upon the collapse strength σ_c for a range of values of strain-hardening exponent n. The results are taken from the kinking analysis of Budiansky and Fleck (1993).

The literature on visco-elastic buckling is extensive. Early analyses (e.g., Biot, 1957) performed a bifurcation analysis to predict the critical load for a perfect structure. More recently, the significance of initial imperfection and material non-linearity have been appreciated in governing time-dependent microbuckling (Schapery, 1993; Slaughter *et al.*, 1992; Slaughter and Fleck, 1994a). In each case, the above equilibrium and kinematic relations hold for the kink band and the lifetime is calculated by time-integrating the rate of fiber rotation in the band, for a range of assumed constitutive laws. Unfortunately, there remains a lack of experimental data on visco-elastic microbuckling, and the critical event dictating the failure life, t_f, has not been resolved. There are several possibilities which remain to be explored:

(i) a critical value of fiber rotation ϕ_f can be assigned, corresponding to tensile fracture at the fiber-matrix interface.
(ii) failure occurs by static plastic kinking when $\bar{\phi} + \phi$ reaches a value of misalignment that, together with $\sigma = \sigma_c$, satisfies the static criterion (3.30); or
(iii) we simply say that an upper bound to t_f corresponds to $\phi = \infty$.

At elevated temperatures, metal matrix and ceramic matrix composites undergo creep. Slaughter *et al.* (1993) have performed a theoretical analy-

sis of creep microbuckling, based on power-law viscous behavior within the kink band. The composite is assumed to creep under in-plane shear by a shear-strain rate $\dot{\gamma}$ related to a shear stress τ via

$$\frac{\dot{\gamma}}{\dot{\gamma}_o} = \left(\frac{\tau}{\tau_o}\right)^m \tag{3.31}$$

where $(\tau_o, \dot{\gamma}_o)$ and the creep exponent m are material constants. The amount of fiber rotation ϕ as a function of time t for kinking under a fixed-axial stress σ is deduced by substituting the constitutive law (3.31) into the equilibrium and kinematic statements given above to obtain (Slaughter *et al.*, 1992),

$$t = \left(\frac{1}{m-1}\right)\frac{1}{\dot{\gamma}_o^*}\left(\frac{\tau_o^*}{\sigma}\right)^m\left[\frac{1}{\bar{\phi}^{m-1}} - \frac{1}{(\bar{\phi}+\phi)^{m-1}}\right] \tag{3.32}$$

Here, the inclination β of the kink band is taken into account through the definitions

$$\dot{\gamma}_o^* = \dot{\gamma}_o/\alpha, \qquad \tau_o^* = \alpha\tau_o, \qquad \alpha = \sqrt{1 + R^2\tan^2\beta} \tag{3.33}$$

where (see eq. (3.22)) R can be regarded as a parameter equal to the ratio of transverse creep strength to shear creep strength. The creep lifetime depends upon the particular criterion chosen to define failure. If we adopt the assumption (iii) given above that the creep lifetime, t_f, is set by the time for $\phi \to \infty$, then (3.32) reduces to

$$t_f = \left[(m-1)\dot{\gamma}_o^*\ \bar{\phi}^{m-1}(\sigma/\tau_o^*)^m\right]^{-1} \tag{3.34}$$

It is of some interest to estimate whether creep kinking might be an issue in ceramic fiber/metal matrix composites, under conditions of moderately elevated temperature and sustained high load. Assuming the plausible values $\tau_o = 100$ MPa, $\dot{\gamma}_o = 10^7\ \mathrm{s}^{-1}$, $\sigma = 1500$ MPa, $\bar{\phi} = 3°$, and $m = 5$, gives $t_f = 120$ hours, which suggests that creep kinking may indeed have to be considered in the design of metal-matrix composites.

5. *Kinking Fatigue*

Slaughter and Fleck (1992) have analyzed fatigue kinking from two viewpoints: (i) fatigue failure by low-cycle fatigue of the matrix within the kink band, and (ii) failure by cyclic ratchetting of the material within the

kink band until the plastic strain accumulation is sufficient to trigger the plastic microbuckling instability. Little experimental data are available on compressive fatigue failure of fiber composites. Soutis *et al.* (1991a) observed fatigue kink growth from a circular hole in a carbon fiber epoxy composite, and Huang and Wang (1989) measured the stress-life fatigue curve for un-notched specimens made from alumina fibers in an aluminum alloy matrix. Slaughter and Fleck (1992) found that the predictions of their ratchetting fatigue model were in better agreement with the experimental results of Huang and Wang than the predictions of the low-cycle fatigue model. Further work is clearly required in order to elucidate the fatigue failure mechanisms as a function of material composition.

B. The Role of Fiber Bending: Infinite-Band Analysis

The infinite-band analyses described above suffer from two main limitations:

(i) they are unable to predict the width of the microbuckle band, as the constitutive law contains no length scale, and
(ii) they assume that the initial imperfection exists as an infinite band with an assumed orientation β rather than as a finite region.

In the current section the first assumption is relaxed by including the role of fiber bending in an infinite-band analysis. In the following Section, III.C, the compressive strength is calculated for a two-dimensional initial region of waviness, relaxing the second assumption.

Commonly, the fiber-bending strength is sufficiently small for fully-developed kink bands to be bounded by fiber breaks. The onset of fiber fracture during collapse sets the kink-band width, defined as the fiber length w within the kink band. An early analysis (Budiansky, 1983), based on the simplifying assumptions of perfectly aligned fibers and rigid-ideally plastic behavior of the composite in shear and transverse tension, together with incorporation of the effects of couple stresses provided by fiber bending, gave

$$\frac{w}{d} = \frac{\pi}{4}\left(\frac{E_L}{2\tau_Y^*}\right)^{1/3} \tag{3.35}$$

for the ratio of the final kink width to the fiber diameter d, in terms of the longitudinal composite modulus E_L and the β-modified shear yield strength $\tau_Y^* = \alpha\tau_Y$. This formula was based on the additional assumption that the fibers were perfectly brittle in tension. Measurements of kink-band widths by Jelf and Fleck (1992) were in good agreement with (3.35) over a wide range of parameters.

1. *Summary of the Couple Stress Analysis of Fleck et al. (1995b)*

In this analysis, the individual responses of the fibers and matrix are smeared out, and the composite is considered to behave as a homogeneous, anisotropic solid. A couple-stress formulation is used to take fiber-bending resistance into account. Descriptions of kinematics and equilibrium are now outlined, followed by constitutive laws and a criterion for fiber fracture.

Kinematics In the initial stress-free configuration, the fibers are assumed to possess a small, initial angular misalignment, $\bar{\phi}$, which is perfectly correlated along a direction inclined at an angle β to the transverse direction. Thus, $\bar{\phi}$ depends on the single variable $x + y \tan \beta$, where the Cartesian coordinates (x, y) are parallel and transverse to the ideal fiber direction, respectively, as shown in Figure 15a. For $y = 0$, it is assumed that $\bar{\phi}$ is an even function of x.

Equilibrium Consider equilibrium of a representative material element in the deformed configuration (see Figure 15b). The element is subjected to a longitudinal compressive stress σ aligned with the fiber direction, a sliding shear stress τ_S, a transverse shear stress τ_T, and a transverse tensile stress, σ_T. The fibers embedded in the material offer bending resistance; thus, the representative material element carries a bending moment per unit area, or couple stress, m.

Moment equilibrium gives

$$\frac{\partial m}{\partial x} = \tau_s - \tau_T \tag{3.36}$$

The presence of couple stresses makes the stress tensor unsymmetric, with $\tau_S \neq \tau_T$.

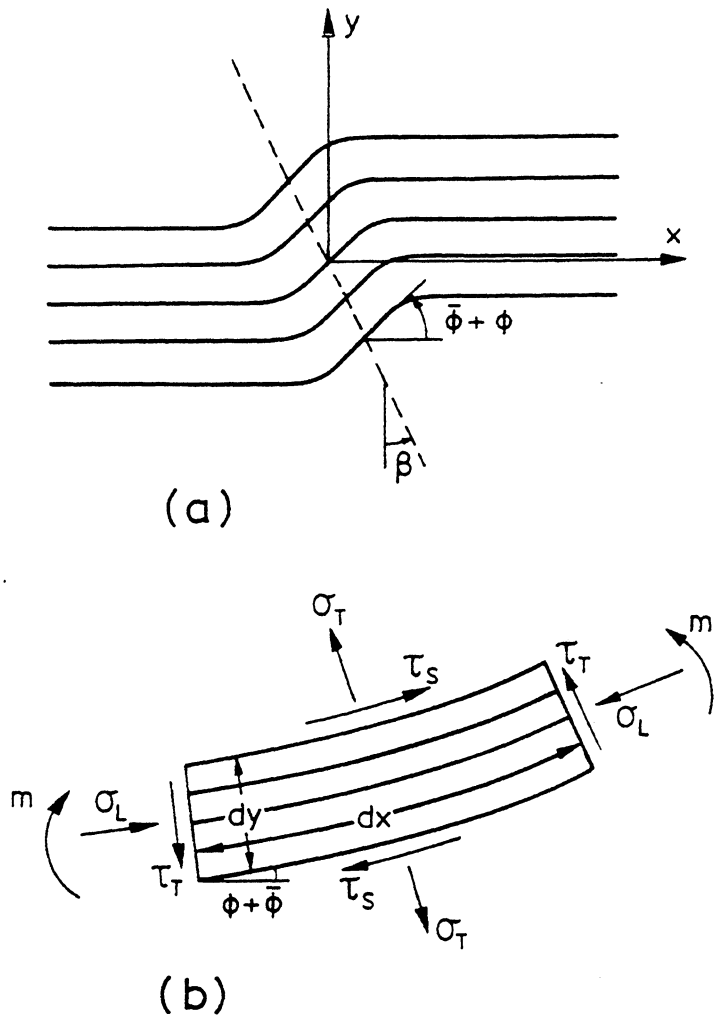

FIG. 15. (a) Deformed shape of infinite band. Under load, the fibers bend and rotate from an initial inclination $\bar{\phi}(x)$ to a deformed inclination $\bar{\phi}(x) + \phi(x)$. (b) Stresses on a representative element of solid. The fibers and matrix have been smeared out to a continuum.

As explained by Fleck *et al.*, (1995b), considerations of equilibrium and the kinematics of Figure 3 provides the governing differential equation of equilibrium

$$\frac{dm}{dx} + \sigma(\phi + \bar{\phi}) = \tau_S + \sigma_T \tan \beta \tag{3.37}$$

In order to proceed, we need a constitutive law in order to relate the generalized stress components (m, τ_S, σ_T) to the fiber rotation, ϕ.

Constitutive Law The fibers are treated as linear elastic beams undergoing inextensible bending, and the matrix contributions to couple stresses are neglected. Simple beam theory for circular fibers of diameter d,

Young's modulus E_f, and volume fraction c gives the relation between the couple stress m on the composite and the associated curvature $d\phi/dx$ as

$$m = \frac{cE_f d^2}{16} \frac{d\phi}{dx} \tag{3.38}$$

The shear and transverse responses of the composite are taken to be those of a non-linear deformation theory solid, as suggested by (3.18), (3.26), and (3.28).

Fiber Fracture Criterion It is found experimentally (see for example Soutis and Fleck, 1990) that the width of the kink band is set by fiber fracture in tension due to local fiber bending. The strain in the fibers is the sum of the bending strain and the compressive strain associated with the axial stress σ. We equate the maximum tensile strain in each fiber with the tensile fracture strain of the fiber ε_F to obtain the fracture criterion

$$\varepsilon_F = \left(\frac{d}{2}\right)\left|\frac{d\phi}{dx}\right|_{\max} - \frac{\sigma}{E} \tag{3.39}$$

where $|d\phi/dx|_{\max}$ is the maximum absolute value of curvature along each fiber, and E is the longitudinal Young's modulus of the composite. This fracture condition will be satisfied at two locations, $x = \pm x_F$, and the width of the kink band is defined as the distance $2\,|x_F|$ along the fibers between the points of fiber fracture.

It is noted that the assumption of inextensible fibers was made in the kinematics and equilibrium relations, but axial straining of the fibers is implicit here in the fiber fracture condition. Budiansky and Fleck (1993) have included fiber extensibility in the kinematic and equilibrium relations of a particular version of their kinking analysis, and found that for typical polymer-matrix composites, fiber extensibility has little effect on the collapse response.

Solution Method The equilibrium equation (3.37) may be reduced to a differential equation in ϕ by eliminating m, τ_S, and σ_T via (3.26) and (3.38) to give

$$\frac{Ed^2}{16}\frac{d^2\phi}{dx^2} + \sigma(\phi + \bar{\phi}) = \tau_e\sqrt{1 + R^2\tan^2\beta} \tag{3.40}$$

where the composite modulus E has been used as an approximation for cE_f. The effective stress τ_e is related to the effective strain γ_e by the

non-linear Ramberg-Osgood relation (3.28), and in turn, γ_e may be written in terms of ϕ as

$$\gamma_e = \phi\sqrt{1 + R^2 \tan^2 \beta} \tag{3.41}$$

We treat (3.40) as the governing non-linear differential equation for the rotation $\phi(x)$ to be solved, together with (3.41) and the Ramberg-Osgood relation (3.28).

The imperfection in fiber alignment $\bar{\phi}(x)$ is assumed to take the form

$$\left.\begin{aligned} \bar{\phi}(x) &= \bar{\phi}_0 \cos\left(\frac{\pi x}{\bar{w}}\right) \qquad |x| < \frac{\bar{w}}{2} \\ \bar{\phi}(x) &= 0 \qquad\qquad\qquad\quad |x| > \frac{\bar{w}}{2} \end{aligned}\right\} \tag{3.42}$$

where the magnitude of the fiber waviness $\bar{\phi}_0$ and the wavelength $\bar{w}$ characterize the imperfection.

Using the above analysis, Fleck *et al.* (1995b) generalized the result (3.35) for an elastic-ideally plastic composite, with finite fiber failure strain ε_F, and obtained the implicit equation for the kink width w as

$$4(\tau_Y^*/E)^2\left[\left(\frac{4w}{\pi d}\right)^2 - \frac{\gamma_Y^* E}{\tau_Y^*}\right] = \left[\varepsilon_F + \left(\frac{4w}{\pi d}\right)^{-2}\right]^2 \tag{3.43}$$

For $\varepsilon_F = \gamma_Y^* = 0$, this reduces to Budiansky's previous result (3.35). Typically, for polymer matrix composites, τ_Y^*/E is in the range 0.005–0.015, and w/d is in the range 10–20 for a wide range in value of $\varepsilon_F = 0$–2% and $\gamma_Y^* = 0$–2%. Fleck *et al.* (1995b) further showed that w/d is rather insensitive to the value of strain-hardening exponent, n, for the case of a composite which strain hardens in accordance with (3.28). The inclination of the kink band, β, and the width and magnitude of the initial waviness also have little effect on w/d.

The typical collapse response is shown in Figure 11 for the strain-hardening case ($n = 3$) with a small initial imperfection ($\bar{\phi}/\gamma_Y^* = 4$, width of imperfection $\bar{w}/d = 20$). With increasing fiber rotation, plastic deformation spreads along the fiber direction and the compressive stress attains a maximum value σ_c. Fleck *et al.* (1995b) showed that the value of σ_c exceeds the kinking strength (3.30) by less than 10%, provided $\bar{w}/d$ exceeds about 20. In other words, kinking theory suffices in order to predict compressive strength unless the physical size of the imperfection is

less than about 20 fiber diameters. During collapse the fibers rotate within the microbuckle band, leading to an end shortening of the composite, as shown in Figure 12a. Eventually, at a fiber rotation of $\phi_m = 2(\beta - \bar{\phi})$, volumetric lock-up occurs and continued end shortening of the composite is associated with broadening of the locked-up central region, as depicted in Figures 11 and 12. A steady state is achieved, with the remote stress equal to the band-broadening stress, σ_b.

2. *Calculation of the Band-Broadening Stress, σ_b*

The band-broadening stress can be calculated by a work calculation, along similar lines to that given by Moran *et al.* (1995). In steady state, remote material outside the microbuckle band is convected into a state of simple shear within the locked-up band; the stored elastic-bending energy within the band of locked-up material vanishes. Finite strain-kinking theory is adequate in order to calculate the associated energy change, provided we assume the composite behaves as a deformation theory solid. Consider the steady-state limit of broadening of a band of locked-up fibers under a constant remote stress, σ_b. We neglect the effect of fiber fracture and examine the work done when a strip of width δw is convected into the locked-up state $\phi = 2\beta$ within the microbuckle band from a remote state of uniaxial compression. The end shortening is $\delta w(1 - \cos(2\beta))$ and the external work done W^E is given by

$$W^E = \sigma_b \, \delta w(1 - \cos(2\beta)) \tag{3.44}$$

The internal work done W^I in rotating fibers within a band of fiber length δw from $\phi = 0$ to $\phi = 2\beta$ is given by

$$W^I = \delta w \int_{\phi=0}^{\phi=2\beta} \left[\frac{\cos(\beta - \phi)}{\cos\beta} \, \tau_e \, \frac{d\gamma_e}{d\phi} \right] d\phi \tag{3.45}$$

by making use of the kinematic relations (3.17b) and the constitutive law (3.26). The band-propagation stress is calculated by equating the internal work and the external work; typical results are shown in Figure 16 for a Ramberg-Osgood strain-hardening curve, as specified by (3.29). In order to interpret Figure 16, we assume that the propagation direction β of the microbuckle is set by the details of the propagation process (elucidated in Section IV), and is therefore an assumed parameter rather than a prediction from the band-broadening analysis. Typically, β is in the range

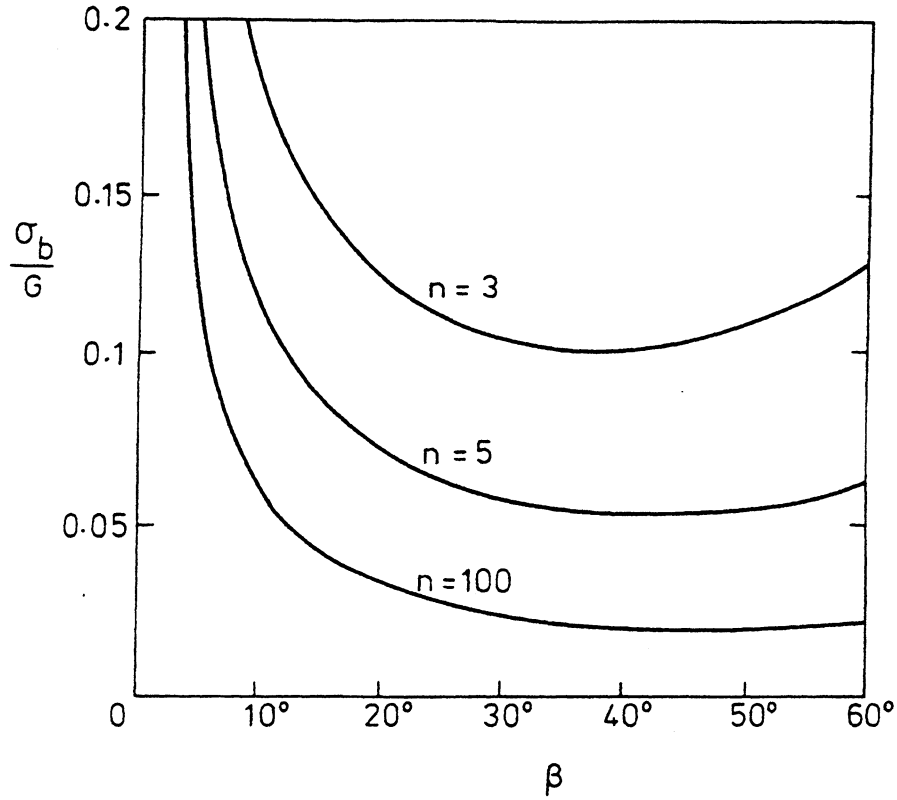

FIG. 16. The steady state band-broadening stress, σ_b, for a Ramberg-Osgood deformation theory composite, under uniaxial stress. The magnitude of σ_b depends upon the assumed inclination β of the microbuckle band.

20–30°, giving a value for σ_b/G in the range 0.03–0.12, depending on the assumed value for the strain-hardening exponent n. We note that the band-broadening stress is significantly less than the typical collapse strength of $\sigma_c/G = 0.2$: initiation of microbuckling from the initial imperfection determines the load-carrying capacity of the structure. In contrast to the initiation strength σ_c, which is relatively insensitive to the strain-hardening exponent n, the band-broadening stress σ_b increases substantially with increasing n. The band-broadening stress will be used later in Section IV as one ingredient in a crack model of microbuckle propagation.

3. *Knockdown in Strength under Multi-Axial Loading*

The knockdown in compressive strength due to the presence of in-plane shear and transverse stress has already been discussed in Section III.A.6, for the case of kinking theory. For the rigid-ideally plastic solid, the knockdown in compressive strength follows from (3.27) as

$$\frac{\sigma_c}{\sigma_{co}} = 1 - \frac{\tau^\infty}{\alpha\tau_Y} - \frac{\sigma_T^\infty}{\alpha\tau_Y}\tan\beta \tag{3.46}$$

where σ_{co} is the uniaxial compressive strength and $\alpha \equiv \sqrt{1 + R^2 \tan^2 \beta}$. Slaughter *et al.* (1992) and Shu and Fleck (1996) have shown that (3.46) remains reasonably accurate when strain-hardening and fiber-bending resistance are taken into account.

4. *Infinite-Band Strength in Case of Random Waviness*

In practice, the fiber misalignment angle $\bar{\phi}$ varies throughout the composite in a three-dimensional random manner. The underlying relationship between fiber waviness and processing conditions remains unexplored. Although Yurgatis (1987) has shown that the distribution in misalignment angle is roughly Gaussian in nature, little information is available on the statistical nature of random fiber waviness. Significant progress has been made on this difficult experimental task: Clarke *et al.* (1996) have measured the power spectral density of a glass fiber-reinforced epoxy by confocal laser-scanning microscopy. In a related study, Slaughter and Fleck (1994b) determined the relation between the power spectral density of fiber waviness and the observed Weibull distribution of compressive strength. Briefly, they assumed a flat-power spectral density for the misalignment angle as a function of distance along the fiber direction. The fiber shape is taken to be invariant along lines inclined at an angle $(\pi/2 - \beta)$ to the fiber direction. Slaughter and Fleck further assumed the power spectral density was characterized by a given value for the mean-square spectral slope, with a lower cut-off for the spectral wavelength. Monte-Carlo realizations for the fiber waviness were generated, and the compressive strength for each realization was determined by the couple-stress formulation of Fleck *et al.* (1995b) in order to take fiber bending resistance into account. The ensemble of results was then used to compute a probability density for compressive strength, and a Weibull fit was conducted to extract the Weibull parameters. Good agreement was observed between the predicted Weibull parameters and the values measured independently by Jelf and Fleck (1992). Thus, the underlying relationship between the statistics of fiber waviness and the resulting distribution of compression strength was determined. Further work is required in order to measure imperfection spectra and the corresponding distribution of compressive strength for a range of composites. Additional micromechanical calculations are needed in order to establish the relationship between the two.

C. Initiation Strength for a Finite Imperfection

So far, we have idealized the initial fiber misalignment as an infinite band, so that the response can be calculated in a one-dimensional framework. Recently, this assumption has been relaxed and the compressive strength has been estimated for a *two-dimensional* distribution of initial fiber misalignment. Two alternative strategies have been adopted:

1. The composite is treated as distinct, perfectly-bonded layers of fibers and matrix.
2. The effect of the individual fibers is "smeared-out" by treating the composite as a Cosserat continuum capable of bearing couple stresses.

Kyriakides *et al.* (1995) used the first strategy to study the early stages of microbuckling from a small region of waviness. In similar fashion, Sutcliffe *et al.* (1996) used this method to calculate microbuckle initiation and early growth from a sharp, open notch under remote compressive loading. This approach is useful when the initial region of fiber waviness extends over only a small number of fibers, but becomes prohibitively expensive in computer time when a large number of fibers are considered.

Fleck and Shu (1995) and Shu and Fleck (1996) have adopted the alternative strategy of smearing out the effects of each individual fiber and developed a finite strain, finite element code based on couple-stress theory. Thus, it is conceived that each element contains many embedded fibers. Here, we summarize the two-dimensional theory and then collect the main results found to date. In order to obtain the constitutive law, the fibers are assumed to behave as elastic Timoshenko beams embedded within a non-linear dilitant plastic matrix. A virtual work expression is obtained for a two-dimensional unit cell consisting of a fiber of volume fraction c adhered to matrix of volume fraction $(1 - c)$. Macroscopic stress and strain quantities are thereby derived for the smeared-out homogeneous composite. It is found that the governing equations are identical to those of Cosserat couple stress theory (Cosserat and Cosserat, 1909). The significance of the unit cell analysis is that the *independent micro rotation angle* θ in the general couple stress theory is shown to be the *independent rotation angle* θ_f of the fiber cross section. The bending resistance of the fibers is set by the fiber diameter, d, and so the constitutive law involves the fiber diameter as the internal length scale. Deformation and flow theory versions of a dilitant plasticity law for the composite are proposed along the lines of (3.21–3.29).

The finite element procedure is based upon a Lagrangian formulation of the general finite deformation of the composite, and can deal with both geometrical and material non-linearities (see Fleck and Shu, 1995, for details). A version of the modified Riks algorithm (Crisfield, 1991) is adopted to handle snap-back behavior associated with the microbuckling response. Imperfections in the form of fiber waviness are included in the formulation.

The finite element code has been used to determine the effect of a finite region of initial waviness upon the compressive strength of the composite. The main results to date are summarized below.

1. *Effect of Imperfection Size on Compressive Strength*

Shu and Fleck (1996) have explored the effect of a finite region of initial fiber misalignment on the collapse response of the composite. Again, a uniform remote compressive stress σ^∞ is applied in the x_1-direction, as shown in Figure 17. Consider the case where the initial fiber misalignment is confined to an ellipse of length ℓ and width w in the (x_1, x_2) plane, as

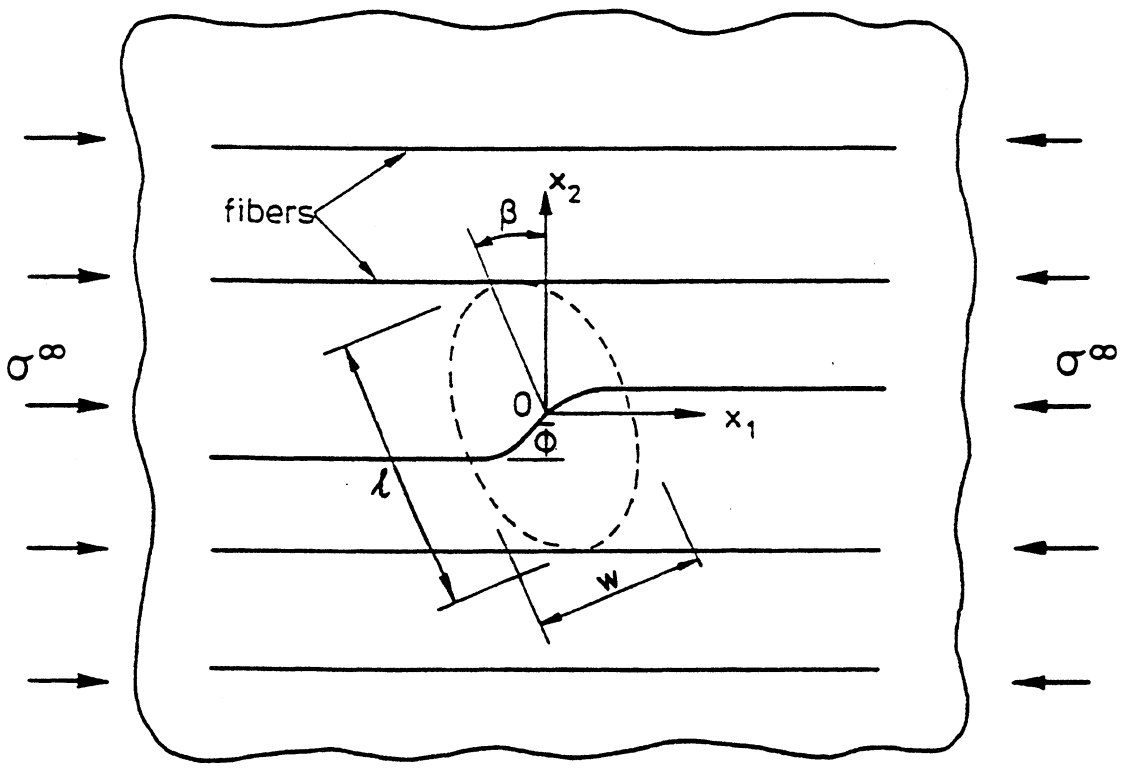

FIG. 17. Sketch of initial imperfection. Fiber misalignment $\bar{\phi}$ is confined to an ellipse of length ℓ and width w.

shown in Figure 17. The axes of the ellipse, (x_1', x_2'), are rotated through an angle, β, about the x_3 axis with respect to (x_1, x_2) axes, such that

$$x_1' = x_1 \cos\beta + x_2 \sin\beta \qquad \text{and} \qquad x_2' = -x_1 \sin\beta + x_2 \cos\beta. \quad (3.47)$$

In the region outside the ellipse, the fibers are straight and perfectly aligned in the x_1-direction. The fiber misalignment follows a cosine distribution within the elliptical region, as specified by

$$\bar{\phi} = \begin{cases} \bar{\phi}_o \cos\dfrac{\pi}{2}\rho, & \text{if } \rho < 1; \\ 0, & \text{if } \rho \geq 1. \end{cases} \quad (3.48)$$

Where

$$\rho \equiv \left\{ \left(\frac{2x_1'}{w} \right)^2 + \left(\frac{2x_2'}{\ell} \right)^2 \right\}^{1/2}. \quad (3.49)$$

As the band length $\ell \to \infty$, the imperfection tends to an infinite band as described in the previous section. At the other limit of $\ell \to 0$, the fiber misalignment vanishes and the compressive strength σ_c approaches the Rosen value of $\sigma_c = G$, where G is the in-plane shear modulus of the composite. These limits provide a useful check to our finite element calculations.

A finite element mesh of the unidirectional composite was constructed of six-noded triangular elements with three degrees of freedom at each node (two in-plane displacements and one rotation along the normal to the plane of deformation). Full details can be found in Fleck and Shu (1995). The mesh was loaded parallel to the fiber direction by applying uniform end displacements u_1^∞, and the finite element calculation gives the corresponding remote stress σ^∞.

A typical plot of the average remote stress σ^∞ versus the end shortening u_1^∞ is given in Figure 18 for the inclination $\beta = 0°$ ($n = 3$, $\bar{\phi}_o/\gamma_y = 4$, $w/d = 20$, $\ell/d = 50$). The response is almost linear with a sharp snap-back behavior at maximum load. Since we focus our attention on the initiation and early propagation of a microbuckle, the calculation of the post-buckling response was stopped when the load dropped to about 75%

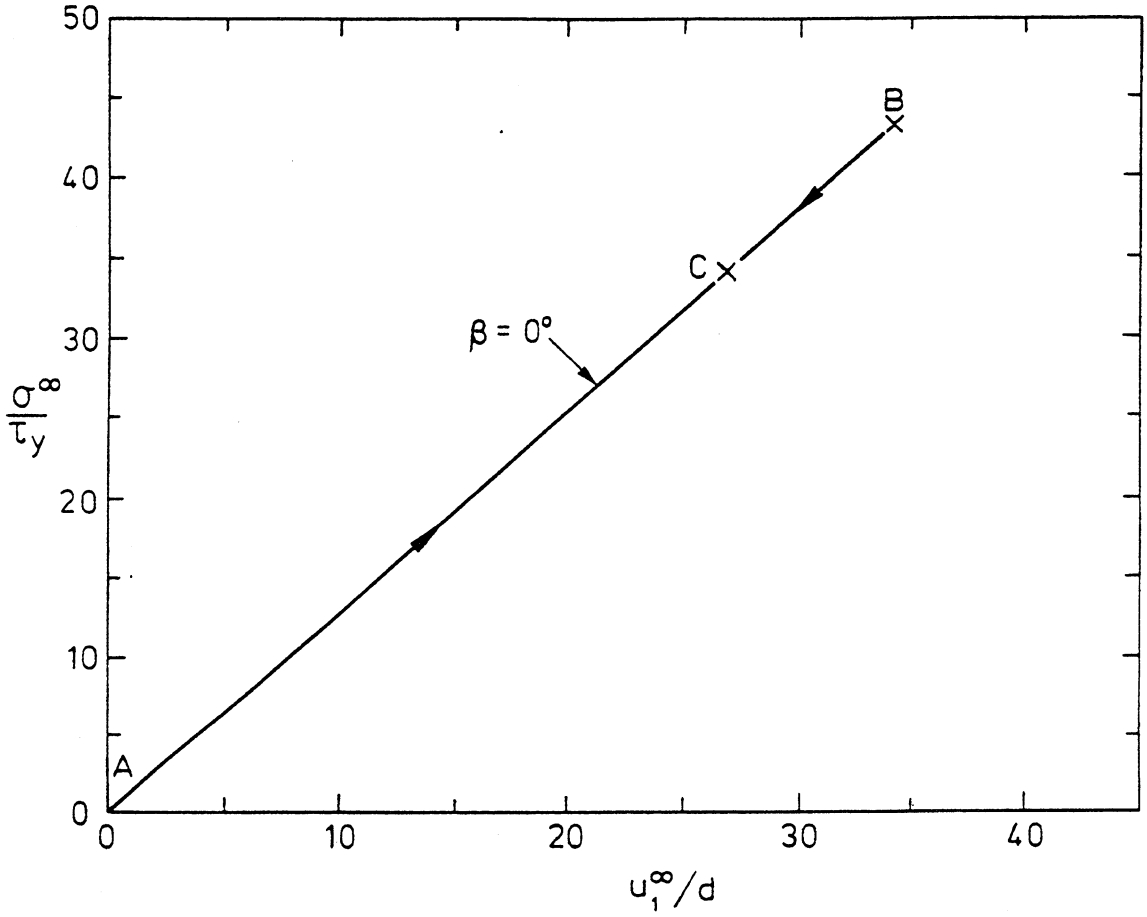

FIG. 18. Remote stress σ^∞ versus end displacement u_1^∞ response for a finite imperfection of $\beta = 0°$, $\ell/d = 50$, $n = 3$ and $\bar{\phi}_o/\gamma_y = 4$.

of the maximum load. The severe snap-back response of Figure 18 is due to the fact that the mesh is long in the fiber direction ($4000d$). The snap back is more severe than in the infinite band case, as the fibers surrounding the finite imperfection remain almost straight at maximum load. Numerical experimentation showed that the weakest orientation is $\beta = 0°$, as found previously for the infinite band limit by Budiansky and Fleck (1993) employing kinking theory, and by Fleck *et al.* (1995b) employing couple stress theory.

The progressive nature of the collapse is exhibited in Figure 19 in the form of contours of total fiber rotation ϕ_t, for the three stages of loading A–C shown in Figure 18. State A is the initial unloaded configuration with $\phi = 0$ and $\phi_t = \bar{\phi}$; state B is immediately post-maximum load (99.7% of maximum load); and state C is at 78% of maximum load. We note that state B, at just past maximum load, displays:

(i) a relatively small maximum value of fiber rotation $\phi = \phi_t - \bar{\phi}$. The maximum fiber rotation is $\phi = 4.4°$ for the case $\beta = 0°$.

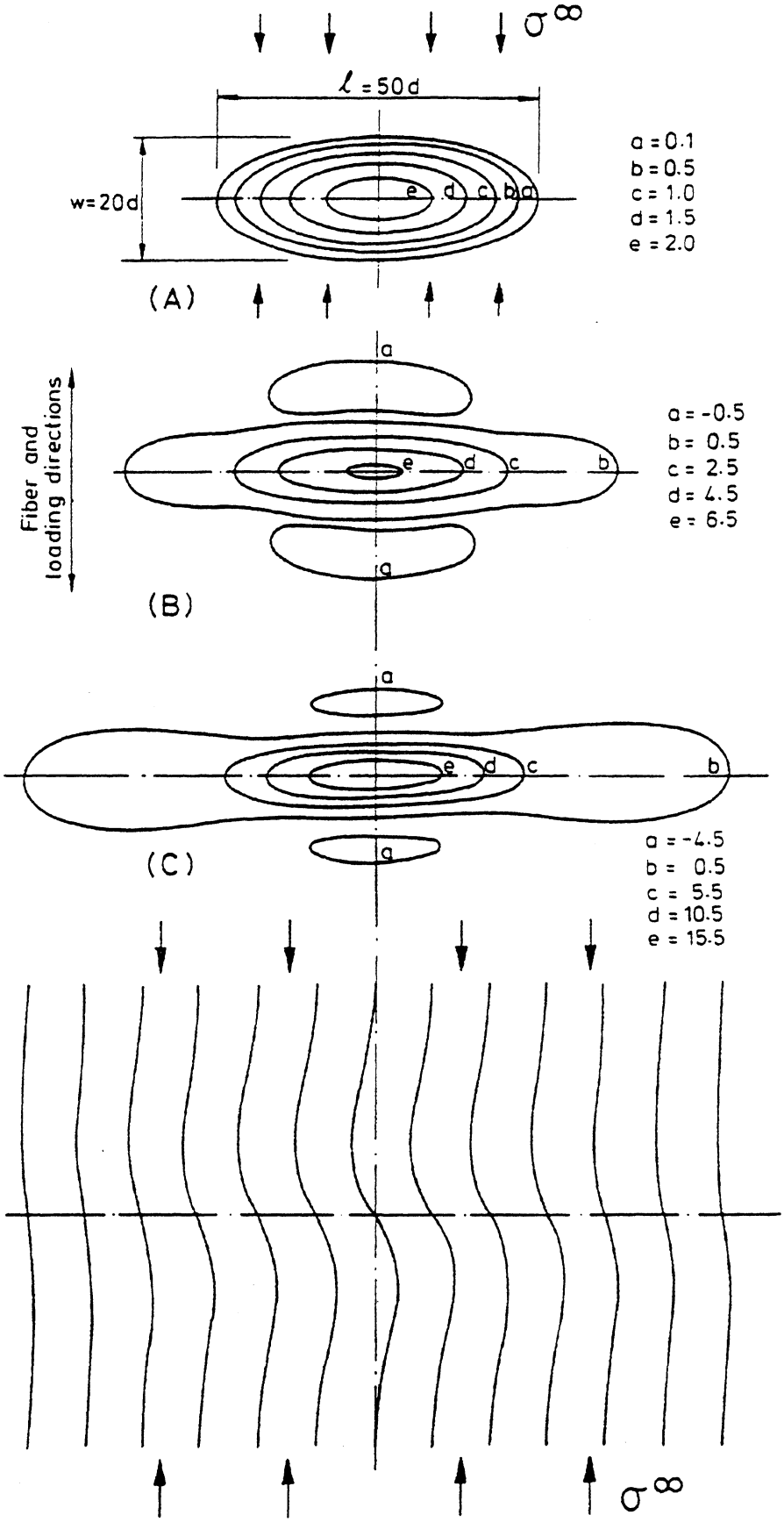

FIG. 19. Contours of total fiber rotation ϕ_t (in degrees) at the three stages marked A, B and C in Fig. 18 for $\beta = 0°$. Remote stresses at stages B and C are respectively 99.7% and 78.2% of the maximum load. The shape of the deformed fibers at state C is included at the bottom of the figure.

(ii) a spatially small region of fiber rotation. At maximum load the region over which the total fiber rotation exceeds 0.5° is only $70d$, i.e. 2.3% of the width of the mesh.

Two versions of the finite element code were written: in version I the phenomenon of "fiber lock-up" was neglected and large compressive transverse strains were allowed to accumulate within the microbuckle band. Experimental observations of microbuckle bands suggests that volumetric lock-up occurs such that the transverse strain does not become strongly negative. (A useful indicator of the magnitude of the transverse strain is given by (3.17a), from the infinite band calculation.) In version II of the finite element program, fiber lock-up is included, and the constitutive response is taken to be elastic when the transverse strain becomes negative. Both versions of the finite element code revealed that the microbuckle grew initially at an orientation $\beta \approx 0°$: the microbuckle band initially propagates in the transverse x_2 direction. In version I of the code, large, compressive transverse strains (of order 5%) accompanied transverse propagation of the microbuckle. In version II, fiber lock-up occurred and the direction of propagation of the microbuckle increased to realistic values of order 20°. Typical results for the orientation of a growing microbuckle from an initial small-defect oriented one at $\beta = 0°$ is shown in Figure 20, by using the "fiber lock-up" version II of the finite element code. In parallel studies, Kyriakides *et al.* (1995) and Sutcliffe and Fleck (1996) modelled the tip region of a propagating microbuckle by alternating layers of fibers and matrix. The microbuckle was observed to propagate in a similar manner to that of an inclined mode II crack at an inclined angle $\beta = 5–30°$, depending upon the strain-hardening exponent n and the shear-yield strain γ_Y of the composite.

The effect upon the collapse strength σ_c of the initial length ℓ and orientation β of the imperfection, is shown in Figure 21 (page 92). As the length ℓ increases from zero to infinity, the collapse strength decreases from the elastic bifurcation strength $\sigma_c = G$ given by Rosen (1965) to the infinite band result given by Fleck *et al.* (1995b). The collapse strength is mid-way between the elastic bifurcation value and the infinite band value at a "transition length" $\ell/d \approx 20$. For $\ell > 0$, the strength decreases with increasing magnitude of initial misalignment $\bar{\phi}_o$ and with increasing strain-hardening index n.

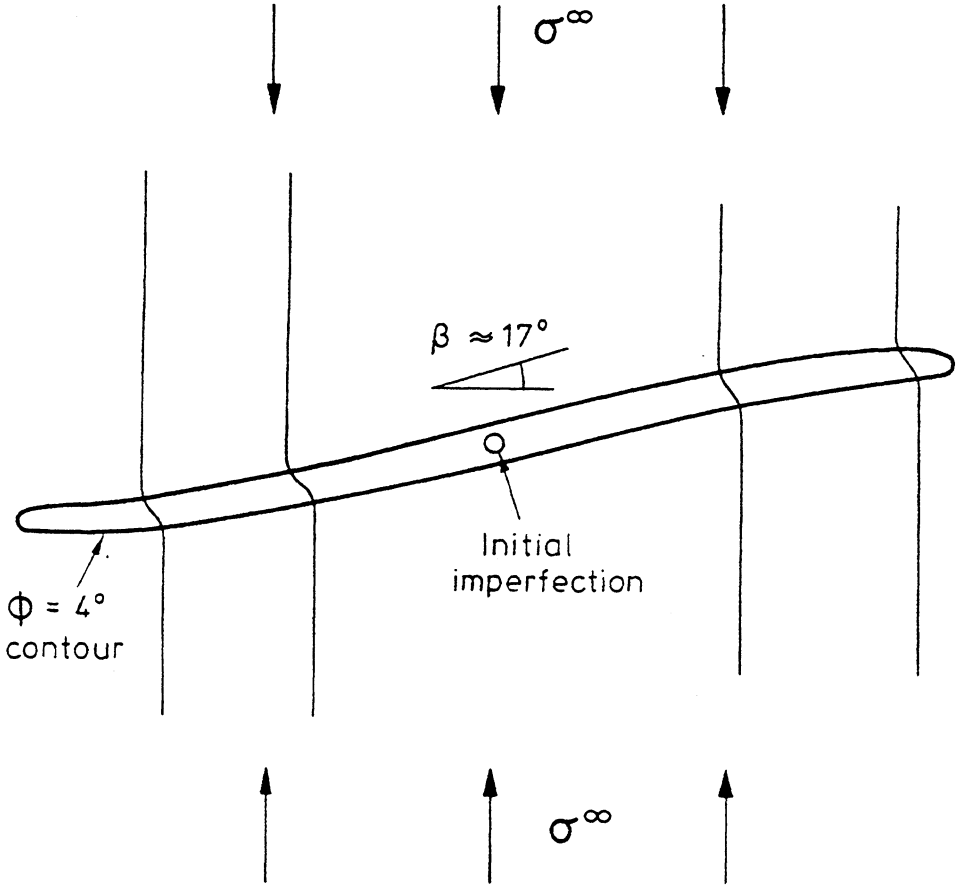

FIG. 20. Evolution of an in-plane microbuckle from an initial circular imperfection of diameter $10d$, and $\phi_o = 5°$. The effect of volumetric lock-up is included in the constitutive law from the composite. Note that the microbuckle grows to a steady-state orientation of about 17°.

2. *Effect of Imperfection Shape on Compressive Strength*

The effect of the shape of the region of fiber waviness on compressive strength has been explored by Shu and Fleck (1996). They considered three types of initial imperfection, as shown in the insert of Figure 22:

1. Infinite band of width L inclined at $\beta = 0$.
2. Circle of diameter L.
3. Ellipse of width $20d$ and length L, oriented at $\beta = 0$.

All three shapes of imperfection are described by (3.47)–(3.49), with $\bar{\phi}_o/\gamma_Y = 4$ (we take $\gamma_Y = 1\%$, giving $\bar{\phi}_o = 2.3°$). The compressive strength as a function of imperfection size of each of the three shapes is shown in Figure 22, for $n = 3$. We note that the infinite band prediction is signifi-

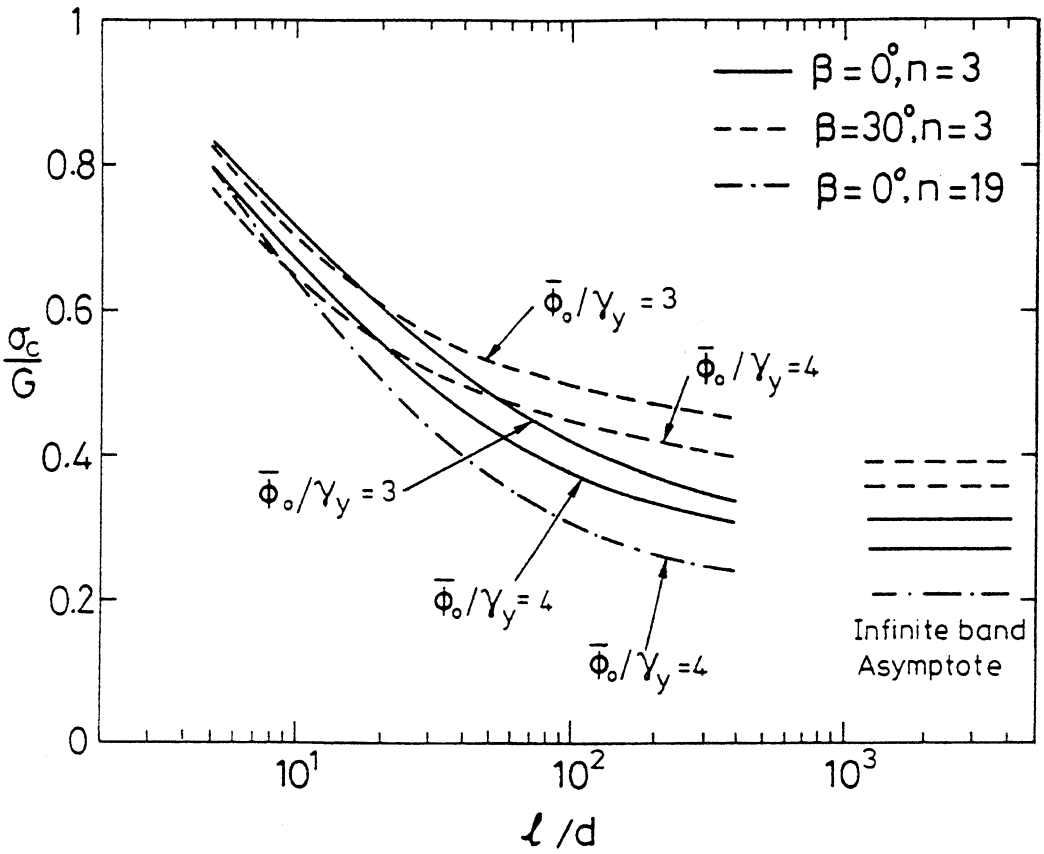

FIG. 21. Compressive strength as a function of the length ℓ of the elliptical region of fiber misalignment. $w/d = 20$. The infinite band results are taken from Fleck, Deng, and Budiansky (1995).

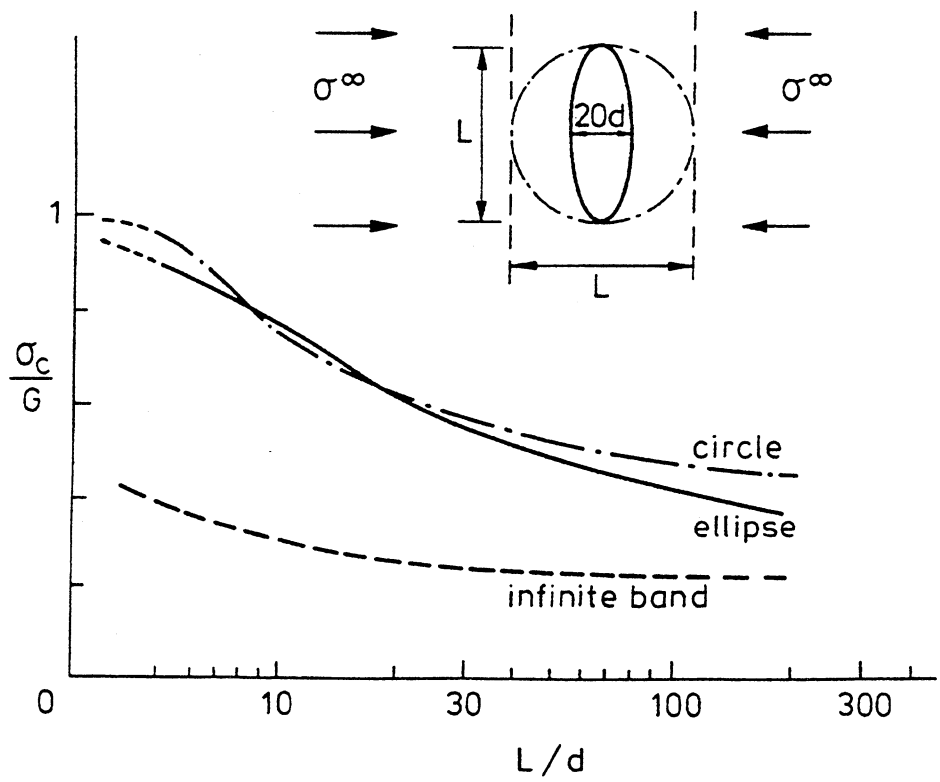

FIG. 22. Effect of imperfection size and shape upon compressive strength. $n = 3$, $\bar{\phi}_o/\gamma_Y = 4$.

cantly weaker than the other shapes for the L/d values considered. In the limit of large L/d (greater than about 30 for the infinite band, and greater than about 300 for the circle and the ellipse) the strengths converge to the asymptote given by the kinking solution (3.30). It is instructive to compare the strengths for the ellipse and for the circle at $L/d > 20$. Then, the circle circumscribes the ellipse; the circular patch has the larger physical size but gives less of a stress-concentrating effect than the ellipse. These two factors compete, and result in the circle being slightly stronger than the ellipse, for the same value of L/d. The main practical conclusion to draw from Figure 22 is that compressive strength is significantly influenced by both the shape of the imperfection, and by the size in relation to the fiber diameter d.

3. *Effect of Multi-Axial Loading upon the Knockdown in Strength for a Finite Imperfection*

The knockdown in compressive strength due to in-plane shear and transverse tension has been calculated by Shu and Fleck (1996) for the case of a circular patch of waviness, of diameter $L = 20d$. Contours of compressive strength are plotted in Figure 23 for the case $n = 100$. The contours are approximately straight lines of constant spacing, suggesting that the knockdown in strength can be given by the following analytical formula:

$$\frac{\sigma_c}{\sigma_{co}} \approx 1 - 0.8\frac{\tau^\infty}{\tau_Y} - 0.1\frac{\sigma_T^\infty}{\tau_Y} \tag{3.50}$$

where σ_{co} is the compressive strength in the absence of in-plane shear stress and transverse stress. The knockdown in strength for an infinite band is given by (3.46). For the case $\beta = 20°$ and $R = 2$ we have $\alpha = 1.24$ and (3.46) becomes

$$\frac{\sigma_c}{\sigma_{co}} = 1 - 0.8\frac{\tau^\infty}{\tau_Y} - 0.3\frac{\sigma_T^\infty}{\tau_Y} \tag{3.51}$$

We conclude that the knockdown effect of shear stress on compressive strength is the same for the infinite-band case and for the case of a circular imperfection. The presence of transverse stress causes a greater reduction in strength for the infinite-band imperfection than for the circular imperfection.

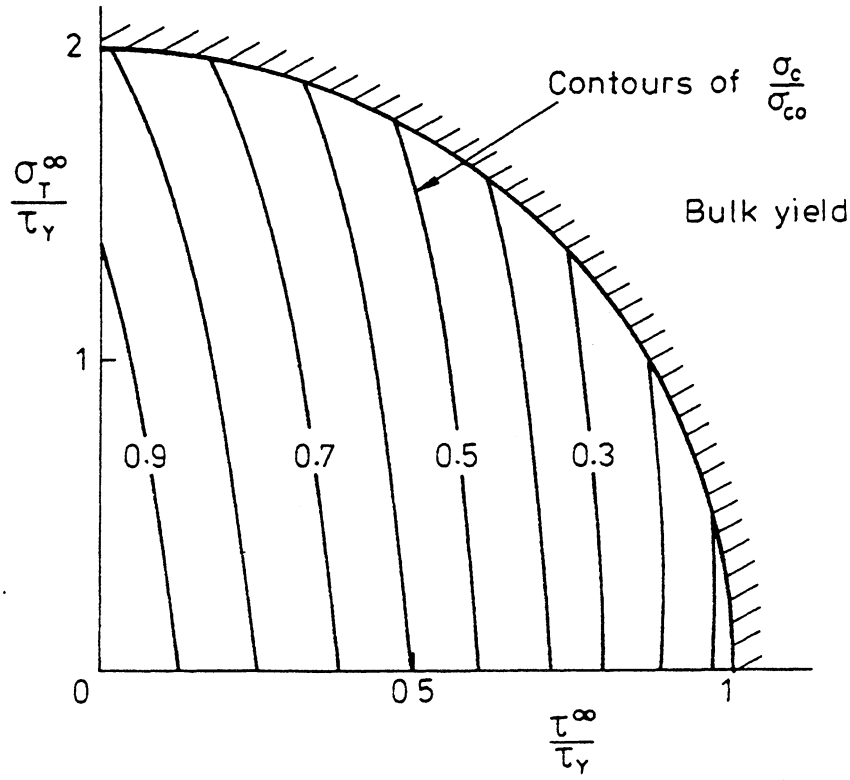

FIG. 23. Contour plot of normalized compressive strength of a circular imperfection region of diameter $20d$, under general in-plane loading.

IV. Propagation of a Microbuckle in a Unidirectional Composite

So far, we have been concerned primarily with the compressive strength associated with the initiation of a microbuckle from a region of pre-existing fiber waviness. In this section we examine the growth of a microbuckle in unidirectional material. First, recent experimental findings are reported on the stable propagation of a microbuckle, and then a mode I crack propagation model is described in order to model the propagation response.

A. Experimental Observations

The investigation of kink-band propagation in fibrous polymer composites is difficult, since unstable propagation usually occurs as soon as kinking has initiated. Notched unidirectional carbon-fiber epoxy composites typically split at the notch ends when loaded along the fiber direction. Fleck and co-workers (Sivashanker *et al.*, 1995; Fleck *et al.*, 1996) overcame this problem for edge-notched plates of unidirectional composite by first nucleating a microbuckle at the root of a starter notch by an

indentation technique. The specimen was then loaded in axial compression and stable microbuckle growth was observed in a consistent, repeatable manner for microbuckle lengths limited only by the ligament width of the specimen (35 mm for the geometry employed). The specimen geometry is shown in Figure 24.

Typical plots of remote axial stress versus microbuckle extension are shown in Figure 25 for three representative carbon fiber composites:

(i) Toray T800 medium strength fibers in a toughened epoxy matrix, Ciba Geigy 924c.
(ii) Medium strength AS4 fibers in a thermoplastic PEEK matrix, ICI APC-2, and
(iii) High strength Hercules IM8 fibers in a PEEK matrix.

It is clear from Figure 25 (page 97) that there is little effect of composition upon the collapse response. In each case, out-of-plane microbuckle propagation occurred, as sketched in Figure 26 (page 98). Examination of the side face of the specimens after the microbuckle had grown about 15 mm revealed that the microbuckle grew in a crack-like manner: the width of the microbuckle increased roughly as the square root of distance back from the microbuckle tip, see Figure 27 (page 99). A typical view of the microbuckle tip in the T800-924c material is given in Figure 28 (page 99): the SEM micrograph shows progressive broadening of the flanks of the microbuckle with increasing distance back from the microbuckle tip. If the microbuckle growth were to occur in a dislocation-like fashion, then one would expect the width of the microbuckle band to be constant. For the case of IM8-PEEK, the fibers are sufficiently strong for no fiber fracture to accompany microbuckling, Moran *et al.* (1995) and Fleck *et al.* (1996). The T800 and AS4 fibers are weaker and undergo fiber fracture within the microbuckle band. Figure 28 shows that the number of microbuckles increases with increasing distance back from the tip of the microbuckle, but the average width w of each individual kink band is constant at $15-25d$. The phenomenon of multiple kinking in the wake of a growing microbuckle is the same phenomenon as steady-state band broadening for an infinite microbuckle band. Strain gauges were placed along the trajectory of microbuckle propagation in the edge-notch tests and were used to measure the compressive stress across the flanks of the microbuckle. The results are summarized in Figure 29 (page 100). For all three materials, band broadening is observed to occur at a constant value of bridging stress of about 100 MPa across the flanks of the microbuckle.

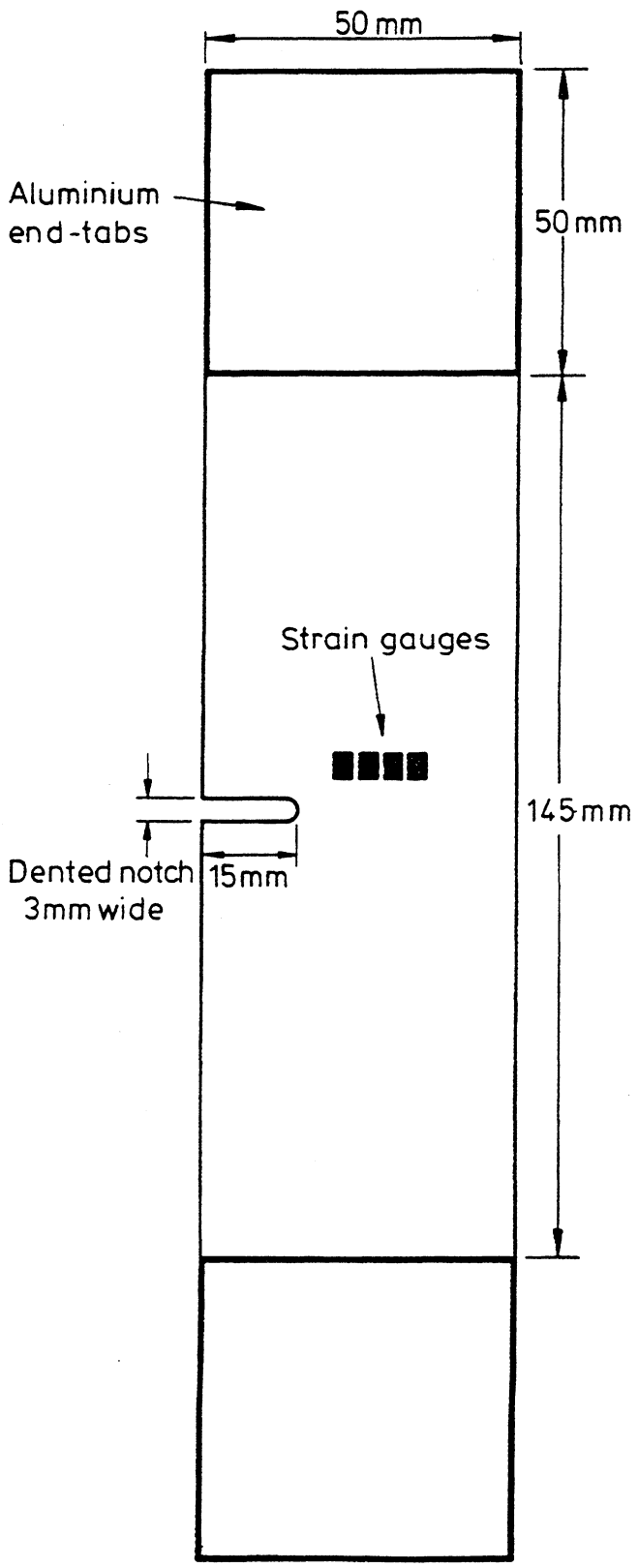

FIG. 24. 3 mm thick edge-notched unidirectional specimens for measurement of microbuckle propagation. The 15 mm notch is indented in order to nucleate a microbuckle of length about 2 mm. Anti-buckling guides, lubricated with PTFE spray, prevent Euler macrobuckling of the specimen.

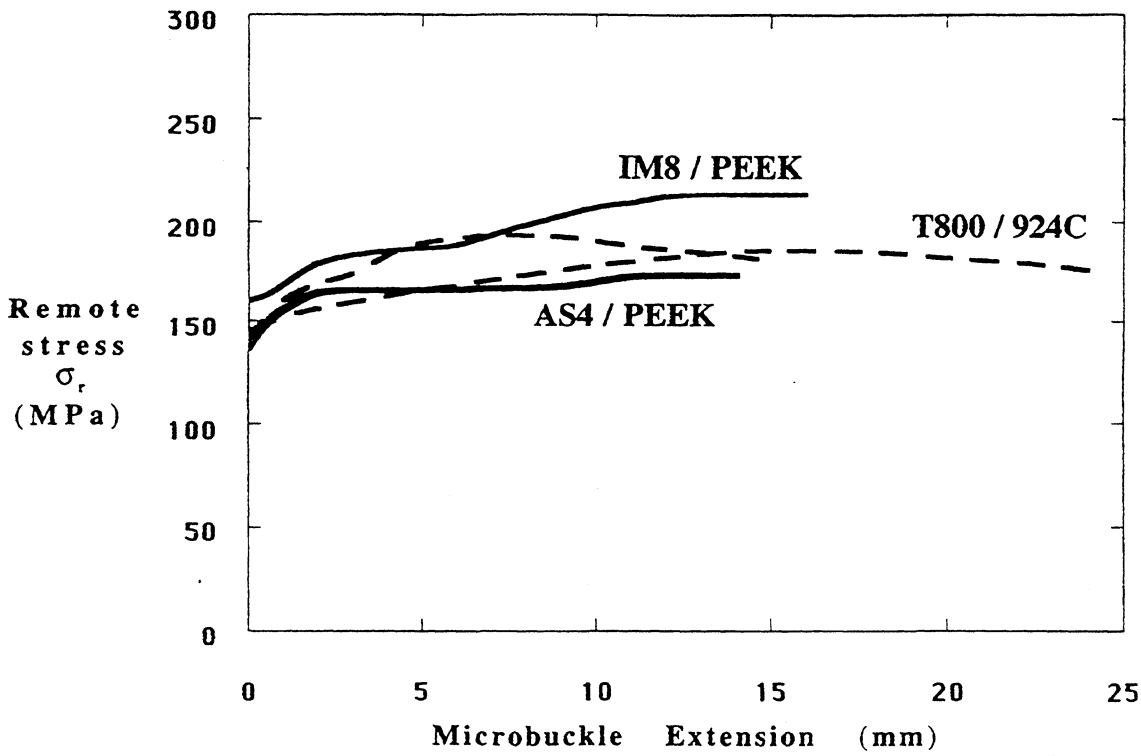

FIG. 25. Typical plots of remote axial stress versus microbuckle extension for unidirectional composites.

Note that the magnitude of the steady-state bridging stress in the wake of the microbuckle is approximately equal to twice the shear yield strength of the materials ($\tau_Y \approx 60$ MPa), in agreement with the estimate for the band-broadening stress at high n and $\beta = 20 - 30°$, as shown in Figure 16.

B. Theoretical Predictions

The observation that a microbuckle propagates in a crack-like manner rather than in a dislocation-like manner suggests that a crack-bridging line model can be used to estimate the relation between applied stress and microbuckle length. The out-of-plane microbuckle development in the thin composite plate is reminiscent of the cracking behavior of thin metallic plates under mode I tension: an inclined crack forms with out-of-plane displacements close to the crack tip and a mode I displacement field forms farther from the crack tip. A pragmatic approach for the microbuckling problem is to treat the microbuckle as an *overlapping mode I crack*. The infinite band response of remote stress σ^∞ versus shortening Δ can be used to provide the crack-traction versus crack-overlap displacement law in

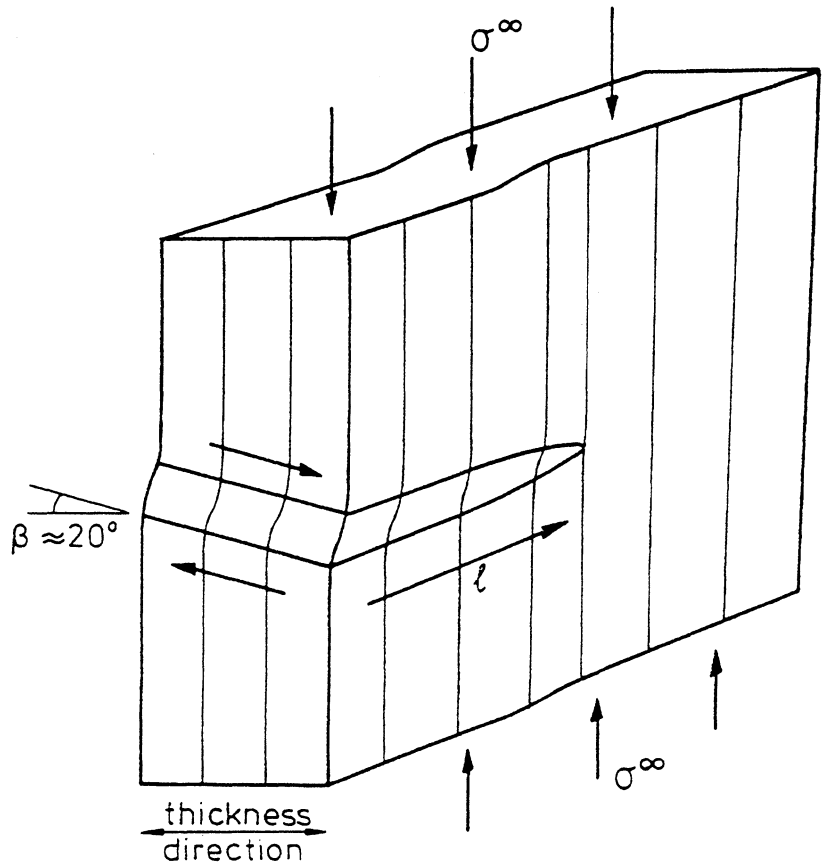

FIG. 26. Sketch showing out-of-plane microbuckle growth in unidirectional carbon fiber composite specimens (cf Fig. 24) under axial loading.

a mode I cohesive zone at the crack tip. Outside the cohesive zone, the cracked structure is treated as a linear, elastic orthotropic solid. A typical plot of σ^∞ versus Δ is repeated in Figure 30 (page 101): the stress peaks at the Rosen value $\sigma^\infty = G$ for the case of vanishing initial imperfection, and σ^∞ rapidly falls to the steady-state band-broadening stress σ_b, as discussed in Section III. We use the infinite band σ^∞ versus Δ response as the non-linear spring law for the cohesive zone at the crack tip. The analysis is simplified considerably by partitioning the area under the σ^∞ versus Δ curve into two parts: (i) the area below the line $\sigma^\infty = \sigma_b$, and (ii) a finite remainder, termed G_{tip}. This partitioning allows us to treat the propagating microbuckle as a crack carrying a constant bridging stress σ_b along its flanks, with a mode I tip toughness G_{tip}, as depicted in the insert of Figure 31 (page 102). (A similar strategy has been adopted by Palmer and Rice (1973) in the study of mode II shear faults in soils and rocks).

The tip toughness G_{tip} has been calculated using the finite strain couple-stress code of Fleck and Shu (1995), which has already been outlined in Section III.C. Numerical experimentation shows that the non-

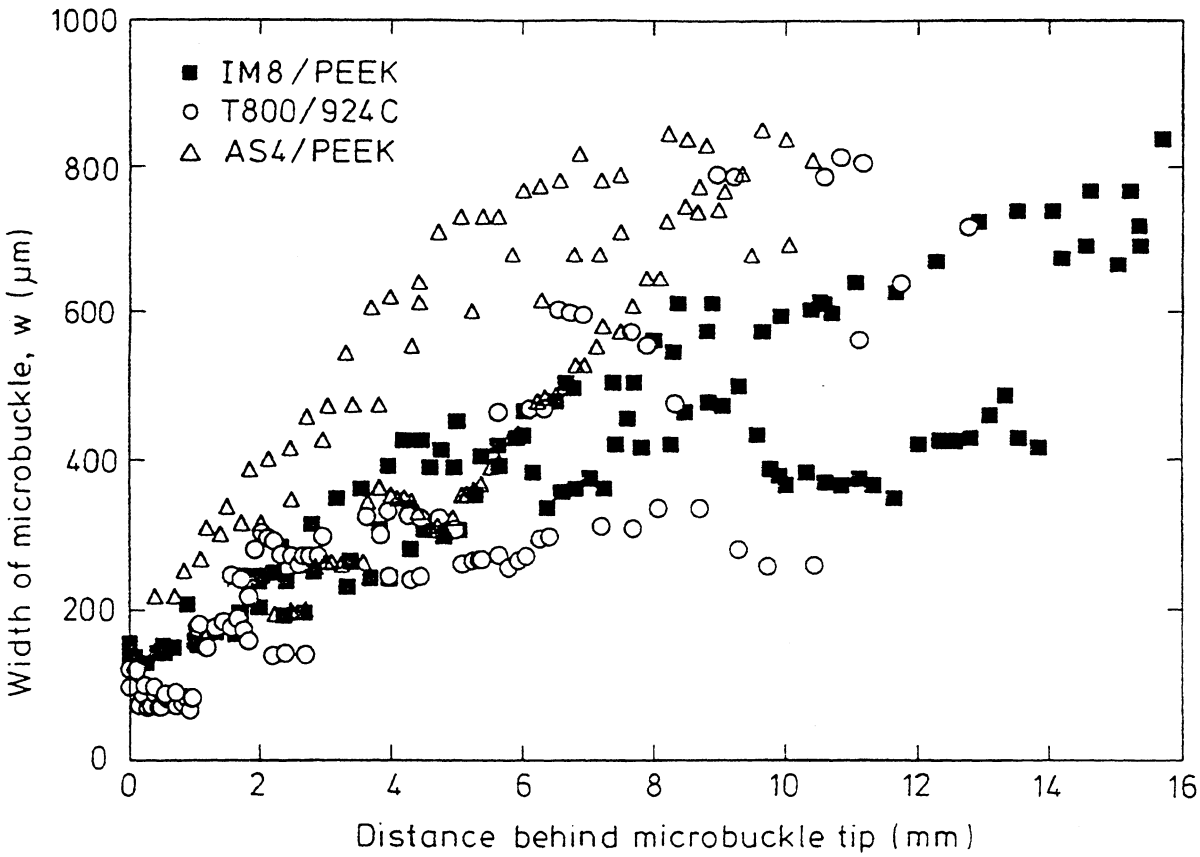

FIG. 27. The crack-like nature of microbuckle growth in carbon fiber composites. The width of the microbuckle band increases with increasing distance back from the microbuckle tip.

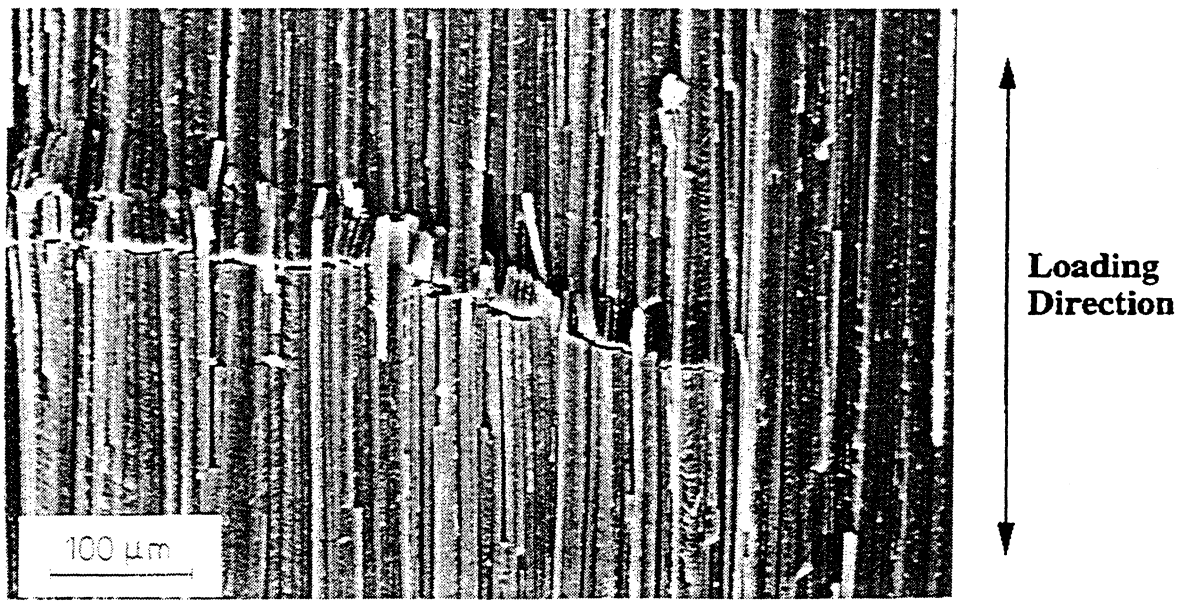

FIG. 28. Side view of microbuckle tip region of T800-924c composite. Near the tip of the microbuckle, two planes of fiber fracture are evident and a single kink band is formed. With increasing distance back from the microbuckle tip, the number of parallel fracture planes increases: multiple kink bands are formed.

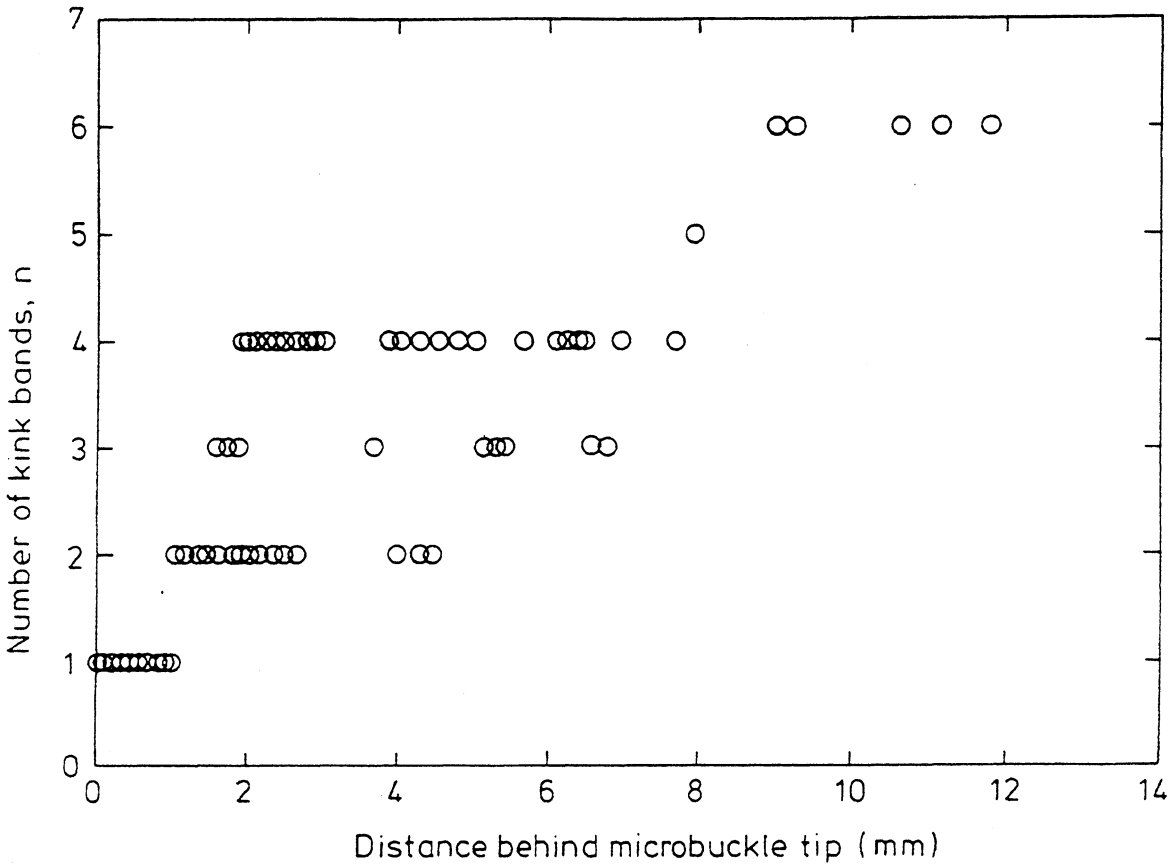

FIG. 29. The number of individual kink bands within the overall microbuckle band as a function of distance from the tip of the microbuckle. Unidirectional composite made from T800 carbon fibers in a 924c epoxy matrix.

dimensional group $G_{tip}/d\sqrt{\tau_Y E_L}$ is only weakly dependent on the value of the strain-hardening exponent n and to the ratio of longitudinal modulus E_L to shear yield strength τ_Y. Typical results are shown in Figure 32 (page 103) for $\beta = 30°$. For rough design calculations we may state that $G_{tip}/d\sqrt{\tau_Y E_L} = 0.3 - 0.5$.

1. *Comparison of Mode I Model with Experimental Data*

Sivashanker *et al.* (1995) and Fleck *et al.* (1996) have implemented the above fracture mechanics model in order to compare the predicted response of microbuckle length in terms of applied stress with the observed behavior for their edge-notched panels, described in Section IV.A above. They made use of existing calibrations for the mode I stress intensity factor and crack-opening profile for an orthotropic edge-cracked strip as laid down by Bao *et al.* (1992) and Wu and Carlsson (1991). Representative results for the AS4-PEEK material are presented in Figure 33a, page 104. The value of the applied stress at the onset of microbuckle growth was

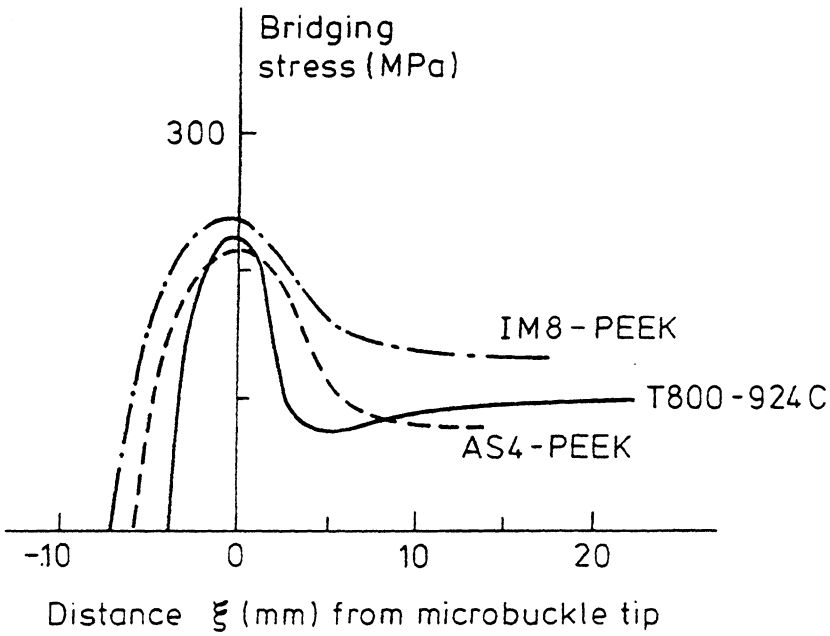

FIG. 30. Estimate of the bridging stresses across a propagating microbuckle in three carbon fiber composites. Wire resistance strain gauges were placed about 1.5 mm from the plane of trajectory of the microbuckle, and the strain was recorded with increasing microbuckle extension past the gauge. The gauge stress was estimated by multiplying the axial strain detected by the gauge by the longitudinal modulus of the composite (thereby neglecting the small Poisson ratio effect).

used to estimate the tip toughness $G_{tip} = 20.0\ \mathrm{kJm}^{-2}$ (corresponding to a compressive mode I stress intensity of 30.3 MPa $\sqrt{\mathrm{m}}$). Strain gauge measurements of the bridging stress across the flanks of the microbuckle indicated $\sigma_b = 100$ MPa. With these assumed values for G_{tip} and for σ_b, the crack model gave good agreement with the observed dependence of microbuckle length upon applied stress; see Figure 33a. An additional comparison can be made between model and experiment, by comparing the predicted width of microbuckle band with the observed profile. Kinking theory suggests that the crack overlap displacement δ due to fiber rotation to lock-up of $\phi = 2\beta$ within a band of width w and inclination β is given by

$$\delta = w(1 - \cos 2\beta) \tag{4.1}$$

Thus, the width of the microbuckle band may be estimated from the predicted mode I displacement profile δ behind the crack tip of the crack model, and by converting these values to a profile in w via (4.1). The comparison is shown in Figure 33b. Again, good agreement is observed in firm support of the simple mode I crack model of microbuckle propagation in preference to a dislocation model. Similar agreement is observed for the

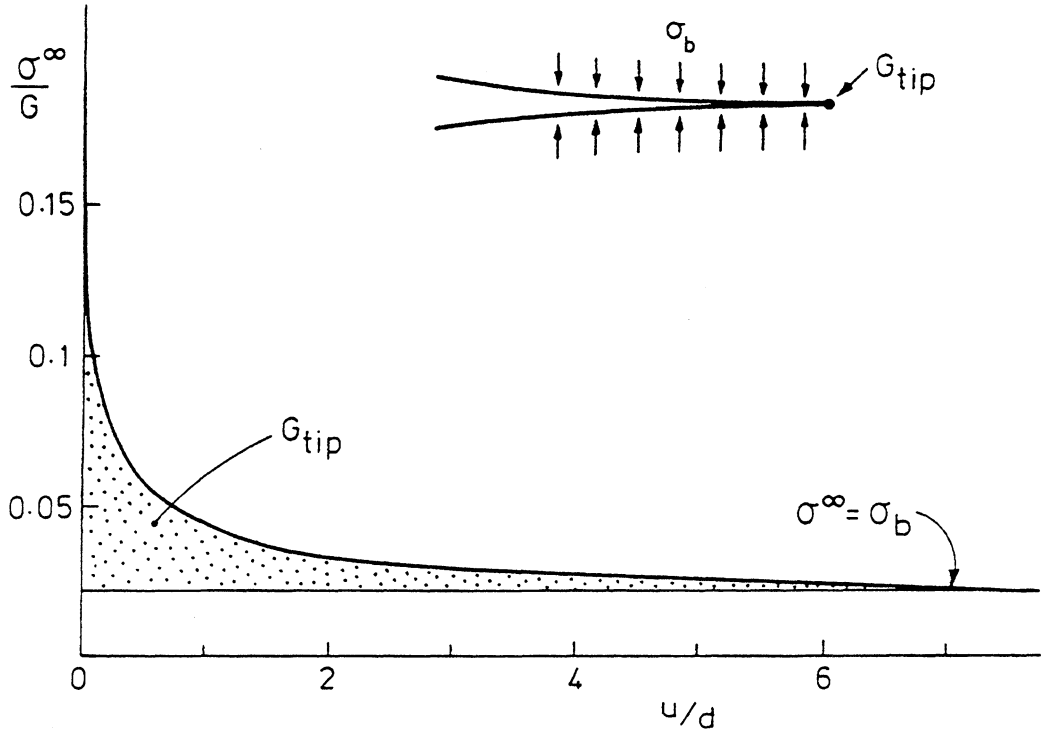

FIG. 31. Sketch of the infinite band collapse response, assuming zero initial imperfection. The collapse response is calculated by couple stress theory. The area under the curve is split into a rectangular region under the line $\sigma^{\infty} = \sigma_b$ and a remaining area designated G_{tip}. This suggests a mode I crack model, with a constant bridging stress of σ_b and a tip toughness G_{tip}, as shown in the insert of the figure.

other two materials tested by Fleck *et al.* (1996): T800-924c and IM8-PEEK unidirectional composites.

Fleck *et al.* (1996) and Sutcliffe and Fleck (1996) have measured G_{tip} for the T800-924c, AS4-Peek, and IM8-PEEK unidirectional composites using the experimental procedure described above. They find that $G_{tip}/d\sqrt{\tau_Y E_L}$ lies in the range 0.5–1.1, which exceeds the predicted values by a factor of about two. The discrepancy between the predictions of the elastic crack-line model and experimental data has been discussed by Sutcliffe and Fleck (1996). In brief, the microbuckle tip is surrounded by a plastic zone and the coupling of shear tractions to normal tractions on the microbuckle is significantly different from that predicted by the crack model. We conclude that the cohesive zone approach, based on the infinite band response, provides a useful but approximate estimate of the manner by which a microbuckle propagates in unidirectional material. A two-dimensional analysis of microbuckle propagation is more satisfactory but more cumbersome (Sutcliffe and Fleck, 1996).

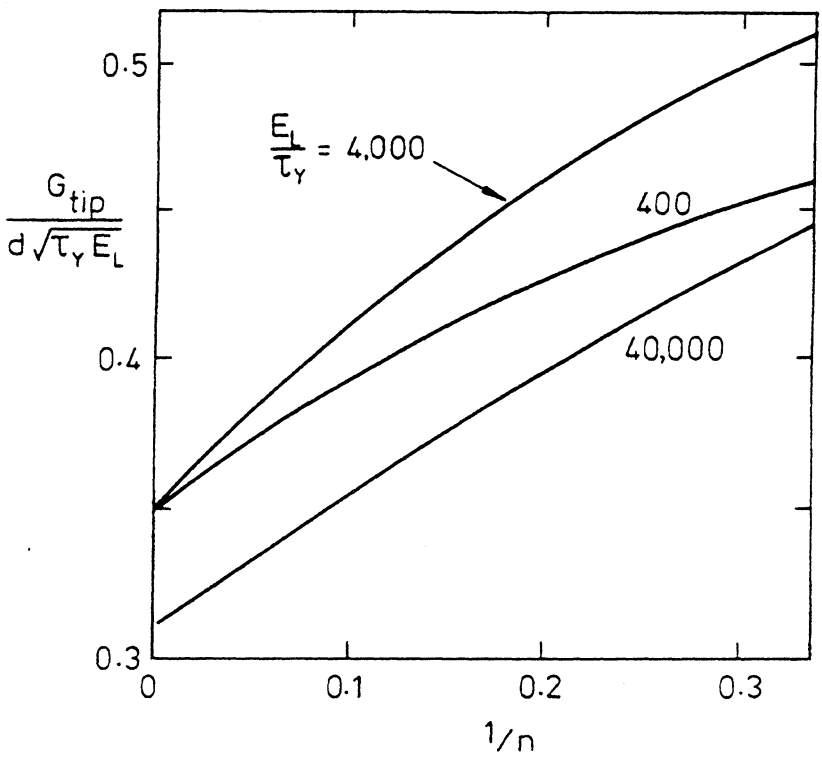

FIG. 32. Calculated tip toughness G_{tip} from the infinite-band couple stress theory. $\beta = 30°$.

V. The Notched Strength of Multi-Axial Composites

Microbuckle initiation and growth in multi-directional composites is much less understood than microbuckle development in unidirectional material. Failure is dominated by microbuckle initiation and growth in the load bearing 0° plies. To a first approximation, the compressive failure strain of unnotched multi-directional laminates is the same as for unidirectional material, and so laminate plate theory can be used to estimate the compressive strength (Soutis *et al.*, 1993). This is consistent with the observation that the compressive strength is set by microbuckle initiation from a local region of fiber misalignment in the 0° plies. Further work is required to explore experimentally and theoretically the effect of fiber lay-up on the initiation strength.

A more difficult but highly practical problem is the prediction of compressive strength for multi-directional panels containing notches, such as holes. Composite panels contain holes, either by design (holes for fasteners, inspection holes, etc.) or by accident (service or battle damage). The effect of transverse impact on a composite plate is to induce a region of extensive damage in the form of fiber fracture, microbuckling, and

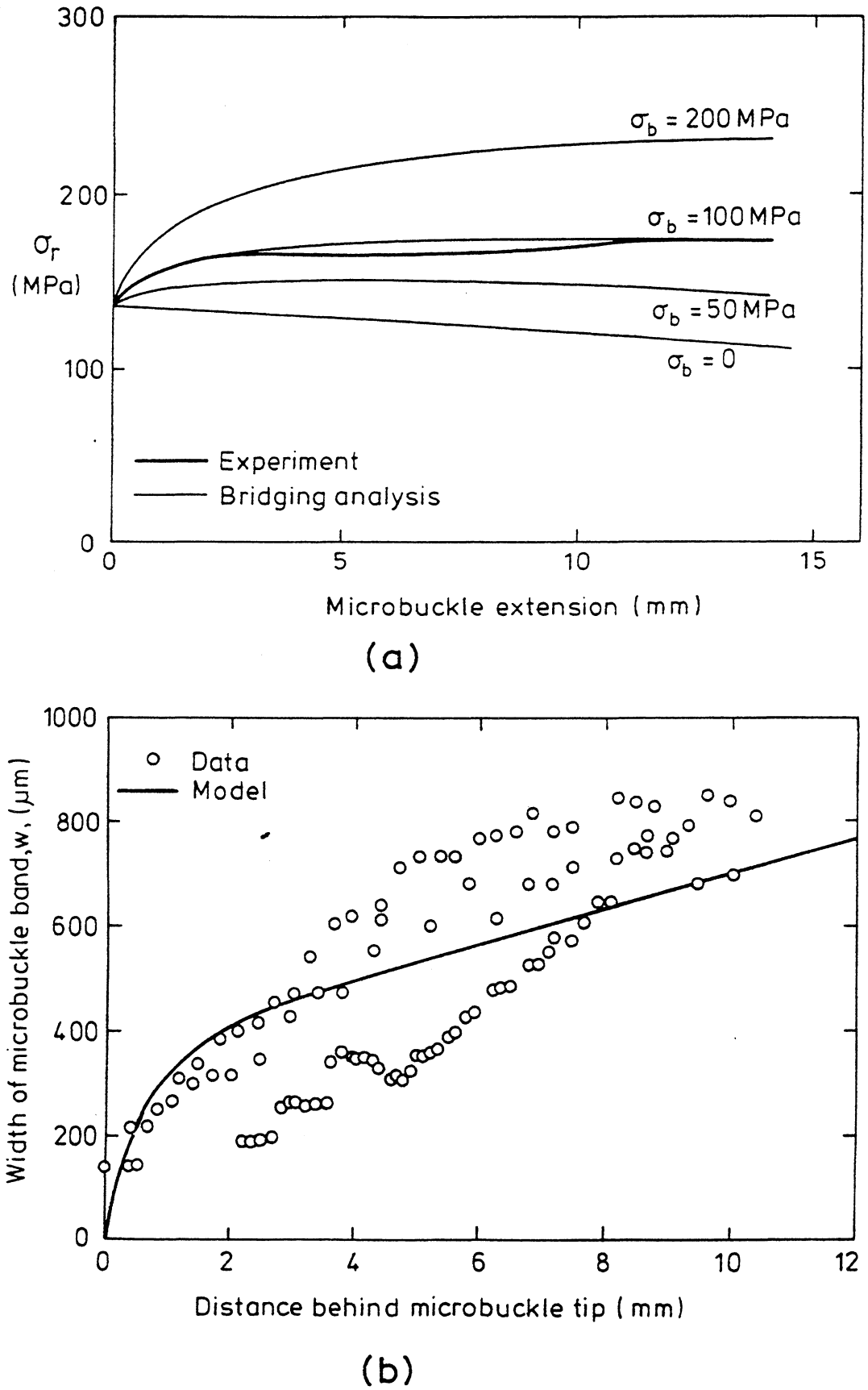

FIG. 33. Comparison of measured and predicted microbuckle growth in AS4-PEEK material. (a) Remote stress versus microbuckle length. (b) Measured width of microbuckle band for a microbuckle which has grown 14 mm from the notch root.

delamination. One approach is to neglect the load-carrying capacity of this damage region and to treat it as a hole in the panel.

It is observed experimentally that failure from a hole in a multi-directional composite plate under compression is by microbuckle nucleation at the edge of the hole (Soutis *et al.*, 1993). The *local* axial stress at the hole edge for microbuckle nucleation is found to be approximately equal to the compressive strength of an unnotched multi-directional specimen. This suggests that a cohesive zone model may be used to predict microbuckle initiation, with a peak value of bridging stress equal to the unnotched strength of the multi-directional material. With increasing remote load, the microbuckle grows from the hole edge, first in a stable manner and then unstable at peak load. A crack-bridging model has been developed as a useful engineering tool for prediction of notched compressive strength. The model is described in the following section, and representative predictions are summarized. The model has been incorporated in PC-driven software to predict notched strength for a wide range of geometries and fiber architectures (Xin *et al.*, 1995).

A. Large-Scale Crack-Bridging Model

Soutis *et al.* (1991b) have developed a crack-bridging model for the initiation and growth of compressive damage from the edge of a blunt notch such as a hole. The damage zone is simulated by a compressive mode I crack with a cohesive zone ahead of its tip.

Consider compressive failure of a finite width, multi-directional composite panel, which contains a central circular hole. It is assumed that microbuckling initiates when the local compressive stress parallel to the 0° fibers at the hole edge equals the un-notched strength of the laminate σ_{un}, that is

$$k_t \sigma^{\infty} = \sigma_{un}, \tag{4.2}$$

where k_t is the stress concentration factor and σ^{∞} is the remote axial stress.

Damage development by microbuckling of the 0° plies, delamination, and damage by plastic deformation in the off-axis plies is represented by a crack with a cohesive zone at its tip; see Figure 34. For the sake of simplicity, a linearly softening spring law is taken for the cohesive zone: the crack-bridging normal traction T assumed to decrease linearly with

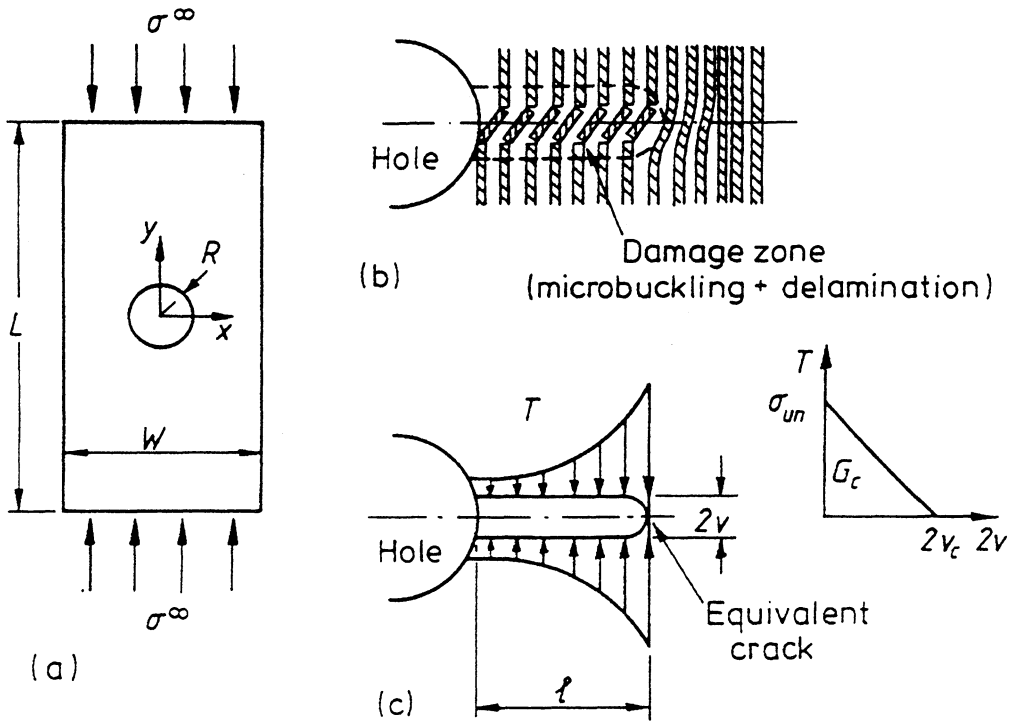

FIG. 34. Cohesive zone model for microbuckling of multi-directional composites.

increasing crack-face overlap 2ν from a maximum value (equal to the un-notched compressive strength σ_{un} of the composite) to zero at a critical crack-face overlap of $2\nu_c$. The cohesive zone is assumed to remove any singularity from the crack tip and stresses remain bounded everywhere. It is assumed that the length ℓ of the equivalent crack represents the length of the microbuckle. When the remote load is increased, the equivalent crack grows in length, thus representing microbuckle growth. The evolution of microbuckling is determined by requiring that the total stress intensity factor at the tip of the equivalent crack K_{tot} equals zero,

$$K_{tot} = K^{\infty} + K_T = 0, \tag{4.3}$$

where K^{∞} is the stress intensity factor due to the remote stress σ^{∞}, and K_T is the stress intensity factor due to the local bridging traction T across the faces of the equivalent crack. When this condition is satisfied, stresses remain finite everywhere.

The equivalent crack length ℓ from the circular hole is deduced as a function of remote stress σ^{∞} using the following algorithm. For an assumed length of equivalent crack ℓ, we solve for σ^{∞} and for the crack-bridging tractions by matching the crack-opening profile from the crack-bridging law to the crack profile deduced from the elastic solution for a cracked body. The cracked body is subjected to a remote stress σ^{∞}

and crack-face tractions T. At a critical length of equivalent crack, ℓ_{cr}, the remote stress σ^{∞} attains a maximum value, σ_n, and catastrophic failure occurs.

1. *Input Parameters for the Model*

The model contains two parameters which are measured independently from specimens made from the *same material and same lay-up*: the un-notched strength σ_{un} and the area G_c under the assumed linear traction-crack displacement curve. σ_{un} is measured from a compression test on the un-notched multi-directional laminate, and G_c is measured from a compressive fracture toughness test. The concept of *compressive fracture toughness* may be explained as follows. Consider a finite specimen containing a single crack, with a cohesive zone at the crack tip. The cohesive zone is assumed to be much smaller than other in-plane dimensions. Then, stresses decay remotely with radius r from the crack tip as $r^{-1/2}$, characterized by the remote mode I stress intensity factor, K. A cohesive zone exists at the crack tip such that the total stress intensity factor at the tip of the cohesive zone vanishes. Rice (1968) has shown that the work done to advance the crack by unit area G_c equals the area under the crack traction versus crack-opening displacement curve,

$$G_c = 2\int_0^{v_c} \sigma(v)\, dv = \sigma_{un} v_c, \tag{4.4}$$

where $2v_c$ is the critical crack-closing displacement on the crack traction—crack displacement curve, as shown in Figure 34. For an orthotropic plate in plane stress, the fracture energy G_c is related to K_c by (Paris and Sih, 1969)

$$G_c = \frac{1}{\sqrt{2E_{xx}E_{yy}}}\left[\sqrt{\frac{E_{xx}}{E_{yy}}} + \frac{E_{xx}}{2G_{xy}} - \nu_{xy}\right]^{1/2} K_c^2 \tag{4.5}$$

where E and G are the laminate in-plane extensional and shear moduli, respectively, and ν is Poisson's ratio in the reference system shown in Figure 34. This is analogous to the fracture mechanics relationship for an isotropic elastic plate in plane stress, $G_c = K_c^2/E$.

We assume that the toughness G_c represents the total energy dissipated by fiber microbuckling, matrix plasticity in the off-axis plies, and by delamination. The compressive toughness G_c of a laminate may be mea-

sured by performing a compressive fracture toughness test to measure K_c, and then by using (4.5). The compressive fracture toughness concept is meaningful provided the damage zone at the onset of crack advance is much smaller than other specimen dimensions. Also, the crack faces much not interfere at distances remote from the crack tip.

2. *Application of the Model*

The approach has been applied to a wide range of specimen geometries (Sutcliffe and Fleck, 1993), and has been used to examine the effect of fiber architecture upon notched strength of carbon fiber laminates (Soutis *et al.*, 1993). Additional tests have been performed on 2-D- and 3-D-woven composites, on woods, and on plywood. In each of these cases, the model adequately predicts the compressive strength and the corresponding microbuckle length at maximum load. As an example, results are presented for $[(\pm 45, O_2)_3]_S$ panels made from T800-924C and AS4-PEEK carbon fiber composites. The typical damage state immediately prior to failure is shown in Figure 35a for an AS4-PEEK specimen. (The T800-924c failed in a qualitatively similar manner.) Microbuckles initiate from the edge of the hole in both the 0° and 45° plies; some splitting of the 0° plies and delamination between the 0° plies and the 45° plies are also apparent.

The evolution of microbuckle length with remote, applied stress was monitored periodically by interrupting a test and X-raying the specimen: a typical response showing initial stable microbuckle development prior to catastrophic failure is given in Figure 35b. The predicted response by the Soutis *et al.* (1991b) model is included in the figure and is in good agreement with the observed initiation and growth of a microbuckle. The model slightly underestimates the stress for initiation of a microbuckle but accurately predicts both the maximum load and the associated microbuckle length.

The notched strength σ_n of the T800-924C material is compared with that of the AS4-PEEK material in Figure 35c. Again, predictions of the

*FIG. 35. (a) Dye penetrant enhanced X-ray micrograph of $[(\pm 45, O_2)_3]_S$ AS4-PEEK laminate, with 10 mm diameter central hole. (b) Comparison of the predictions of the Soutis *et al.* (1993) model with the observed growth of a microbuckle from a 5 mm central hole in a $([45, O_2)_3]_S$ AS4-PEEK laminate. (c) Comparison of the measured and predicted compressive strengths σ_n for $[(\pm 45, O_2)_3]_S$ AS4-PEEK and T800-924c laminates. The panels are of width $w = 50$ mm wide, and the notch strength is plotted as a function of hole radius R. The theoretical predictions—are given by the Soutis *et al.* (1993) model.

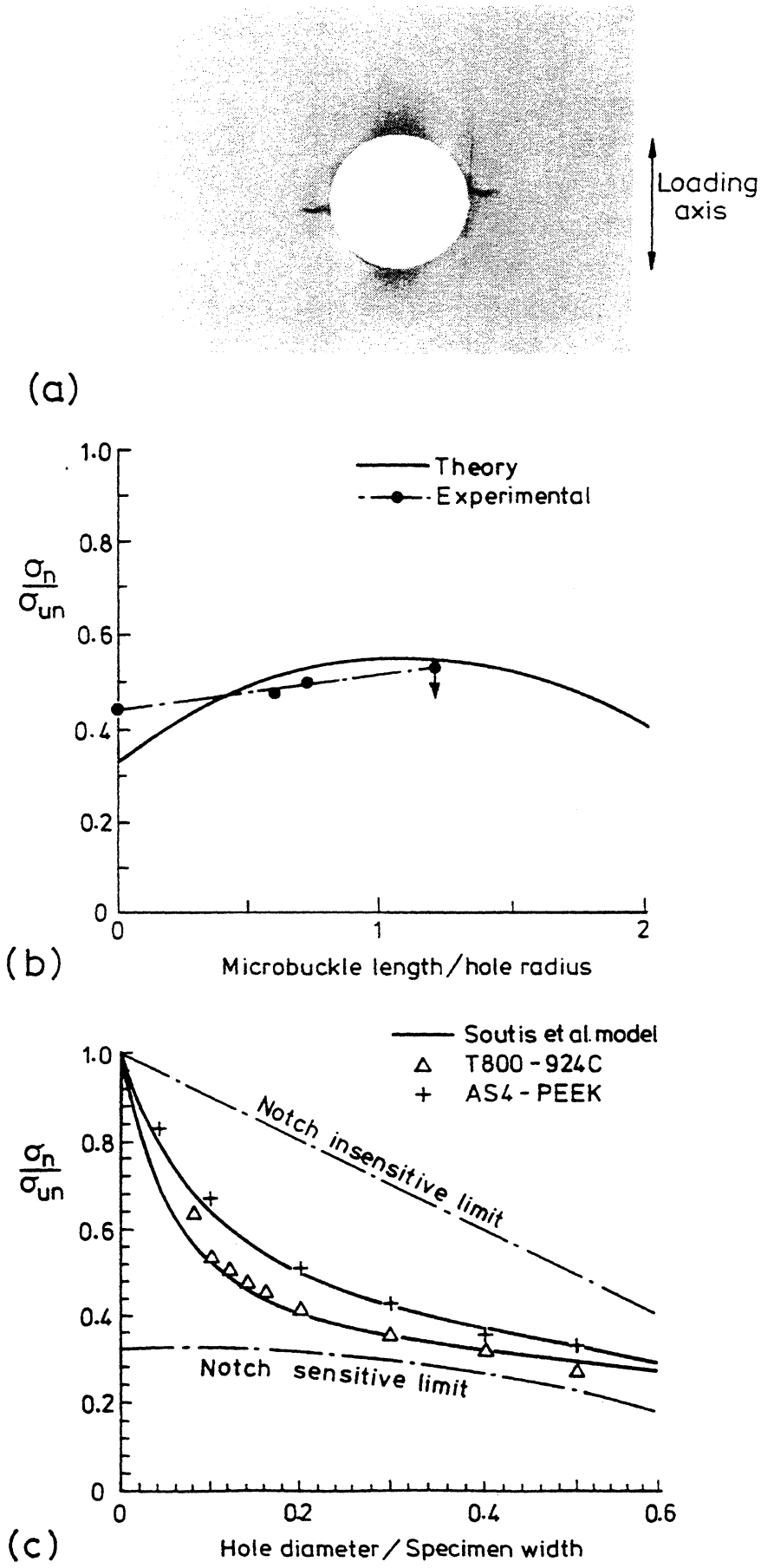
Loading axis
(a)
Theory
Experimental
σ_n / σ_{un}
1.0
0.8
0.6
0.4
0.2
0
0
1
2
(b)
Microbuckle length/hole radius
Soutis et al. model
T800 - 924C
AS4 - PEEK
Notch insensitive limit
Notch sensitive limit
σ_n / σ_{un}
1.0
0.8
0.6
0.4
0.2
0
0
0.2
0.4
0.6
(c)
Hole diameter / Specimen width

FIG. 35. *

Soutis *et al.* (1993) theory are included in the figure: excellent agreement is found between theory and experiment for both materials. The AS4-PEEK material has a higher compressive fracture toughness (K_c = 55 MPa $\sqrt{\text{m}}$) than the T800-924C laminate (K_c = 46 MPa $\sqrt{\text{m}}$) and is less notch sensitive. The notched strengths of both materials lie between the limits of notch insensitivity (where the net-section failure stress equals the un-notched strength) and the perfectly brittle limit (where the local stress at the root of the notch equals the un-notched strength).

The cohesive zone model of Soutis *et al.* (1991b) has proved to be a useful engineering approach to compressive failure of notched, multi-directional laminates. However, further work is required in order to relate the failure toughness of a multi-directional laminate to that of unidirectional material, as described in Section IV.B.

VI. Directions for Future Research

A number of important problems remain in order to complete our understanding of the compressive failure of fiber composites. Some of these topics are listed below.

1. *Dynamic Microbuckling*

Lankford (1989, 1991, 1994) has measured the compressive strength of a range of ceramic matrix and polymer matrix composites, and has observed a sharp increase in strength with increasing strain rate, at strain rates above about 300 s^{-1}. Slaughter *et al.* (1996) have analyzed the response of a fiber composite to a suddenly applied stress pulse; they include the effects of material inertia and initial imperfection, and perform a one-dimensional infinite band calculation using couple-stress theory. The more realistic calculation of a suddenly applied pulse in velocity to the end of the specimen, remains to be addressed. Dynamic kinking is an important topic as structural composites are commonly subjected to shock loading, particularly in military and sports applications.

2. *Microbuckling from Random Waviness*

In practice, fiber misalignment exists as a random three-dimensional distribution throughout the composite. The compressive strength is determined by some combination of the magnitude of the fiber misalignment

and its physical size. Work remains to be done on the statistical characterization of waviness and its implications for the distribution in compressive strength for an ensemble of composite parts. A similar strategy of reliability analysis exists for the imperfection-sensitive buckling of shell structures, for the tensile failure of ceramics using Weibull statistics, and for the fracture of brittle solids using probabilistic fracture mechanics. It is envisaged that a defect assessment can be made of composite parts in terms of the measured distribution of imperfections such as fiber misalignment.

3. *Microbuckling from Defects Such As Voids*

Compressive failure of fiber composites occurs from holes and voids, as well as from regions of fiber waviness. The presence of matrix voids is difficult to avoid in composite manufacture. A large cylindrical hole reduced the compressive strength by a factor of about three, depending on the degree of orthotropy. In the other limit of vanishing hole size in relation to fiber diameter d, no reduction in strength occurs. Thus, a significant hole size effect is expected for small holes. Preliminary data showing the effect is presented in Figure 36: tests were performed on unidirectional specimens of T800-924c carbon fiber–epoxy composite containing holes of diameter in the range 0.3–2 mm. Microbuckling occurred from the hole and led to failure in some of the cases. In other, nominally identical specimens, splitting occurred from the edge of the hole, thereby reducing the stress-concentrating effect of the hole. In general, the specimens which displayed splitting were stronger than the specimens for which splitting is absent; see Figure 36. Further experimental and theoretical work is needed to determine the relation between hole and void size and compressive strength.

4. *Tunnelling of Microbuckles in Multi-Directional Composites*

Recent observations of microbuckle propagation in multi-directional laminates (Fleck *et al.*, 1996) suggested that microbuckles grow in the 0° plies of thick composites by a tunnelling mechanism, as sketched in Figure 37. When the microbuckle is sufficiently long, it advances under constant applied stress, termed the "tunnelling stress." The phenomenon of crack tunnelling has been described in detail by Hutchinson and Suo (1992). For the case of tunnel microbuckling, the tunnelling process involves the combination of microbuckling of the 0° plies and mixed-mode

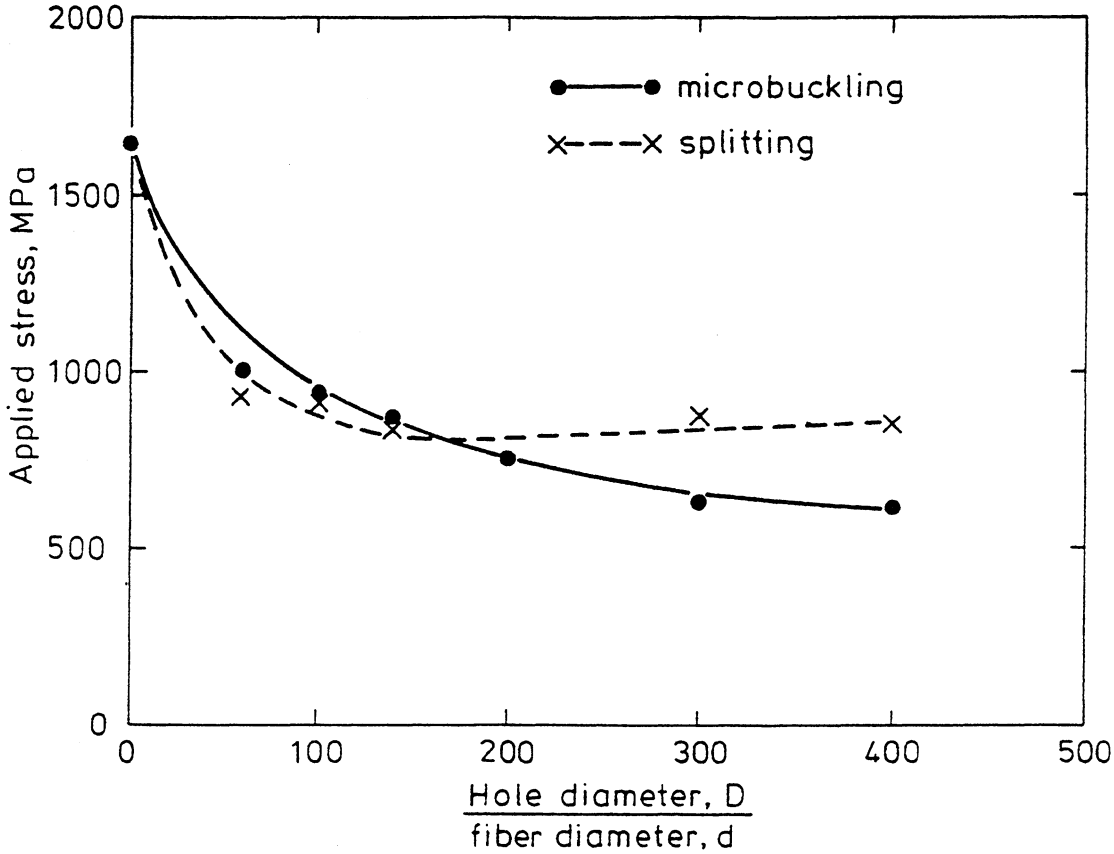

FIG. 36. Effect of hole diameter D in unidirectional T800-924c carbon fiber-epoxy composite upon the measured compressive strength. A size effect is noted, whereby the strength is greater for holes of diminishing diameter. Failure is by microbuckling from the hole edge.

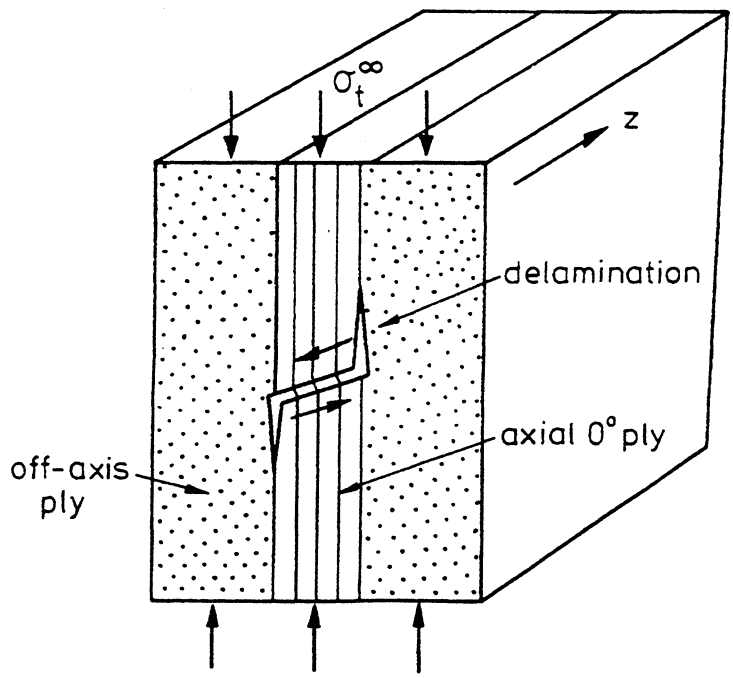

FIG. 37. Tunnelling of a microbuckle in a thick multi-directional composite, under a tunnelling stress σ_t^∞.

delamination between 0° plies and adjacent off-axis plies. Calculations remain to be done on the magnitude of the tunnelling stress as a function of layer thickness and the delamination toughness.

Acknowledgments

The author is most grateful for the extensive collaboration with B. Budiansky and M. P. F. Sutcliffe, and for the research support given by C. Soutis, P. M. Jelf, J. H. Shu, S. Sivashanker, and X. J. Xin. Financial support is gratefully acknowledged from the EPSRC, from the Defence Procurement Executive, and from the U.S. Office of Naval Research (contract number 0014-91-J-1916, directed by Y. D. S. Rajapakse).

References

Argon, A. S. (1972). Fracture of composites. *Treatise Mater. Sci. Technol.* **1**, 79–114.

Ashby, M. F., and Hallam, S. D. (1986). *Acta Metall.* **34**(3), 497–510.

Bao, G., Ho, S., Suo, Z., and Fan, B. (1992). The role of material orthotropy in fracture specimens for composites. *Int. J. Solids Struct.* **29**(9), 1105–1116.

Barker, A. J., and Balasundaram, V. (1987). Compression testing of carbon fibre-reinforced plastic exposed to humid environments. *Composites* **18**(3), 217–226.

Biot, M. A. (1957). Folding instability of a layered viscoelastic medium under compression. *Proc. R. Soc. London* **A242**, 444–454.

Biot, M. A. (1967). Rheological stability with couple stresses and its application to geological folding. *Proc. R. Soc. London* **A298**, 402–423.

Budiansky, B. (1979). Remarks on kink formation in axially compressed fibre bundles. *In* Preliminary Reports, Memoranda and Technical Notes on the Materials Research Council Summer Conference, La Jolla, California, July 1979, Sponsored by DARPA.

Budiansky, B. (1983). Micromechanics. *Comput. Struct.* **16**, 3–12.

Budiansky, B., and Fleck, N. A. (1993). Compressive failure of fiber composites. *J. Mechanics Phys. Solids* **41**(1), 183–211.

Chaplin, C. R. (1977). Compressive fracture in unidirectional glass-reinforced plastics, *J. Mater. Sci.* **12**, 347–352.

Chatterjee, S. N., and McLaughlin, P. V. (1979). Inelastic shear instability in composite materials under compression. Proc. 3rd Engineering Mechanics Div. Specialty Conf., Sept. 17–19, 1979, University of Texas at Austin, ASCE, pp. 649–652.

Clarke, A. R., and Archenhold, G., Davidson, N., Slaughter, W. S., and Fleck, N. A. (1996). Determining the power spectral density of the waviness of unidirectional glass fibres in polymer composites. *Applied Composite Materials* **2**, 233–243.

Cosserat, E., and Cosserat, F. (1909). "Theorie des Corps Deformables." Herman et fils, Paris.

Cox, B. N., Carter, W. C., and Fleck, N. A. (1994). A binary model of textile composites. I. Formulation. *Acta Metall. Mater.* **42**(10), 3463–3479.

Crisfield, M. A. (1991). "Non-Linear Finite Element Analysis of Solids and Structures," Vol. 1, Chapter 9, Wiley, London.

Curtis, P. T. (1986). An investigation of the mechanical properties of improved carbon fibre composite materials. *RAE Tech. Rep.* 86021 DRA Farnborough, Hants., England.

deTeresa, S. J., Porter, R. S., and Farris, R. J. (1988). Experimental verification of a microbuckling model for the axial compressive failure of high performance polymer fibres. *J. Mater. Sci.* 1886–1894.

Dinwoodie, J. M. (1981). "Timber, Its Nature and Behaviour," Van Nostrand-Reinhold, Berkshire, England.

Evans, A. G., and Adler, W. F. (1978). Kinking as a mode of structural degradation in carbon fiber composites. *Acta Metall.* **26**, 725–738.

Ewins, P. D., and Potter, R. T. (1980). Some observations on the nature of fibre reinforced plastics and the implications for structural design. *Philos. Trans. R. Soc. London* **A294**, 507–517.

Fleck, N. A., and Jelf, P. M. (1995). Deformation and failure of a carbon fibre composite under combined shear and transverse loading. *Acta. Metall. Mater.* **43**(8), 3001–3007.

Fleck, N. A., and Shu, J. Y. (1995). Microbuckle initiation in fibre composites: A finite element study. *J. Mech. Phys. Solids* **43**(12), 1887–1918.

Fleck, N. A., Jelf, M., and Curtis, P. T. (1995a). Compressive failure of laminated and woven composites. *J. Compos.: Technol. Res.* 212–220, July 1995.

Fleck, N. A., Deng, L., and Budiansky, B. (1995b). Prediction of kink width in compressed fiber composites. *J. Appl. Mech.* **62**, 329–337.

Fleck, N. A., Sivashanker, S., and Sutcliffe, M. P. F. (1996). The propagation of a microbuckle in unidirectional and multidirectional composites. *Acta Metall. Mater.* submitted.

Fried, N. (1963). The compressive strength of parallel filament reinforced plastics—the role of the resin. Proc. 18th annual meeting of the Reinforced Plastics Division, Society of Plastics Industry, Section 9-A, 1–10.

Gibson, L. J., and Ashby, M. F. (1988). "Cellular Solids: Structure and Properties." Pergamon, New York.

Greszczuk, L. B. (1972). Failure mechanisms of composites subjected to compressive loading. AFML-TR-72107, U.S. Air Force.

Greszczuk, L. B. (1975). Microbuckling failure of circular fibre-reinforced composites. *AIAA J.* **13**(10), 1311–1318.

Grossman, P. U. A., and Wold, M. B. (1971). Compressive fracture of wood parallel to the grain. *Wood Sci. Technol.* **5**, 147–156.

Gupta, V., Anand, K., and Kryska, M. (1994). Failure mechanisms of laminated carbon-carbon composites—I. Under uniaxial compression, *Acta Metall. Mater.* **42**(3), 781–795.

Ha, S. K., Wang, Q., and Chang, F. (1991). Modelling the viscoplastic behavior of fiber-reinforced thermoplastic matrix composites at elevated temperatures. *J. Compos. Mater.* **25**, 335–373.

Hahn, H. T., and Williams, J. G. (1986). Compression failure mechanisms in unidirectional composites, "Composite Materials: Testing, and Design (Seventh Conference), ASTM STP 893," (J. M. Whitney, ed.), pp. 115–139. American Society for Testing and Materials, Philadelphia, Pennsylvania.

Hahn, H. T., Sohi, M., and Moon, S. (1986). Compression failure mechanisms of composite structures. NASA CR 3988.

Harte, A.-M., and Fleck, N. A. (1996). Unpublished research.

Horoschenkoff, A., Brandt, J., Warnecke, J., and Bruller, O. S. (1988). Creep behaviour of carbon fibre reinforced polyetheretherketone and epoxy resin. "New Generation Materials and Processes" (F. Saporiti, W. Merati, and L. Peroni, eds.), pp. 339–349. Milan.

Huang, Y. H., and Wang. S. S. (1989). Compressive fatigue damage and associated property degradation of aluminium-matrix composite. Proc. 4th Japan–U.S. Conf. on Composite Materials, 27–29 June, 1988, Washington, D.C., pp. 602–632. Technomic, Westport, Connecticut.

Hutchinson, J. W. (1974). Plastic buckling. *Adv. Appl. Mechanics* **14**, 67–144.

Hutchinson, J. W., and Suo, Z. (1991). Mixed mode cracking in layered materials. *Adv. Appl. Mechanics* **29**, 63–191.

Jelf, P. M., and Fleck, N. A. (1992). Compression failure mechanisms in unidirectional composites. *J. Compos. Mater.* **26**(18), 2706–2726.

Jelf, P. M., and Fleck, N. A. (1994). The failure of composite tubes due to combined compression and torsion. *J. Mater. Sci.* **29**, 3080–3084.

Jelf, P. M., Soutis, C., and Fleck, N. A. (1990). Notched compression failure of carbon fibre PEEK laminates. Presented at 3rd. Int. Symp. on Composites, Patras, Greece, Sept. 1990.

Johnson, A. M. and Ellen, S. D. (1974). A theory of concentric, kink, and sinusoidal folding and of monoclinal flexuring of compressible, elastic multilayers. I. Introduction. *Tectonophysics* **21**, 301–339.

Johnson, A. M., and Ellen, S. D. (1975a). A theory of concentric kink, and sinusoidal folding and of monoclinal flexuring of compressible, elastic multilayers. II. Initial stress and nonlinear equations of equilibrium. *Tectonophysics* **25**, 261–280.

Johnson, A. M., and Ellen, S. D. (1975b). A theory of concentric kink, and sinusoidal folding and of monoclinal flexuring of compressible, elastic multilayers. III. Transition from sinusoidal to concentric-like chevron folds. *Tectonophysics* **27**, 1–38.

Johnson, A. M., and Ellen, S. D. (1976). A theory of concentric, kink, and sinusoidal folding and of monoclinal flexuring of compressible, elastic multilayers. IV. Development of sinusoidal and kink folds in multilayers confined by rigid boundaries. *Tectonophysics* **30**, 197–239.

Johnson, N. J., and Hergenrother, P. M. (1987). High temperature thermoplastics: A review of neat resin and composite properties. 32nd Intl. SAMPE Symposium, April 6–9, 1987.

Kaute, D., Ashby, M. F., and Fleck, N. A. (1996). Compressive failure in ceramic matrix composites. Manuscript in preparation.

Kumar, S., Adams, W. W., and Helminiak, T. E. (1988). Uniaxial compressive strength of high modulus fibers for composites. *J. Reinf. Plast. Compos.* **7** (March 1988), 108–119.

Kyriakides, S., Arseculeratne, R., Perry, E. J., and Liechti, K. M. (1995). On the compressive failure of fiber reinforced composites. *Int. J. Solids Struct.* **32**(6/7), 689–738.

Lager, J. B., and June, R. R. (1969). Compressive strength of boron/epoxy composites. *J. Compos. Mater.* **3**(1), 48–56.

Lankford, J. (1989). Dynamic compressive fracture in fiber reinforced ceramic matrix composites. *Mater. Sci. Eng.* **A107**, 261–268.

Lankford, J. (1991). Compressive damage and failure at high loading rates in graphite fiber-reinforced polymeric matrix composites. *Ceram. Trans.* **19**, pp. 553–563.

Lankford, J. (1994). Shear versus dilatational damage mechanisms in the compressive failure of fiber-reinforced composites, to appear in *Composites*.

Liu, X. H., Moran, P. M., and Shih, C. F. (1995). The mechanics of compressive kinking in ductile matrix fiber composites. To appear in a special issue of *Composites Engineering on Thick Composites*.

Moncunill de Ferran E., and Harris, B. (1970). Compression of polyester resin reinforced with steel wires. *J. Compos. Mater.* **4**, 62–72.

Moran, P. M., Liu, X. H., and Shih, C. F. (1995). Kink band formation and band broadening in fiber composites under compressive loading. *Acta Metall. Mater.* **43**(8), 2943–2958.

Nemat-Nasser, S., and Horii, H. (1982). *J. Geophys. Res.* **87**(B8), 6805-6821.

Neptco Inc. (1994). Product information sheet on Graphlite. Box 2323, 30 Hamlet St., Pawtucket, Rhode Island, 02861–0323.

Palmer, A. C., and Rice, J. R. (1973). The growth of slip surfaces in the progressive failure of over-consolidated clay. *Proc. R. Soc. London*, **A332**, 527–548.

Paris, P. C., and Sih, G. C. (1969). Stress analysis of cracks. *Fracture Toughness and Applications* **ASTM STP 381**, 30–83.

Parry, T. V., and Wronski, A. S. (1981). Kinking and tensile, compressive and interlaminar shear failure in carbon fibre reinforced plastic beams tested in flexure. *J. Mater. Sci.* **16**, 439–450.

Piggott, M. R. (1981). A theoretical framework for the compressive failure of aligned fibre composites. *J. Mater. Sci.* **16**, 2837–2845.

Piggott, M. R., and Harris, B. (1980). Compression strength of carbon, glass and Kevlar-49 fibre reinforced polyester resins. *J. Mater. Sci.* **15**, 2523–2538.

Piggott, M. R., and Wilde, P. (1980). Compressive strength of aligned steel reinforced epoxy resin. *J. Mater. Sci.* **15**, 2811–2815.

Prandy, J. M., and Hahn, H. T. (1990). Compressive strength of carbon fibers. Proc. 35th International SAMPE Symposium, April 2–5 1990, pp. 1657–1670.

Rhodes, M. D., Mikulas, M. M., and McGowan, P. E. (1984). Effects of orthotropy and width on the compression strength of graphite-epoxy panels with holes. *AIAA J.* **22**(9), 1283–1292.

Rice, J. R. (1968). Mathematical analysis in the mechanics of fracture. *In* "Fracture" (H. Liebowitz, ed.), Vol 2, Chapter 3. Academic Press, New York.

Rosen, B. W. (1965). Mechanics of composite strengthening. "Fiber Composite Materials." pp. 37–75. Chapter 3, American Society of Metals.

Sammis, C. B., and Ashby, M. F. (1986). *Acta Metall* **34**(3), 511–526.

Schapery, R. A. (1993). Nonlinear viscoelastic effects in the compressive behavior of fiber composites. "Mechanics of Thick Composites, **AMD-162**." (Y. D. S. Rajapakse, ed.), pp. 81–90. American Society of Mechanical Engineers.

Schapery, R. A. (1995). Prediction of compressive strength and kink bands in composites using a work potential. *Int. J. Solids Struct.* **32**(6/7), 739–765.

Schulte, K., and Minoshima, K. (1991). Mechanisms of fracture and failure in metal matrix composites. 12th Riso Int. Symp. on Materials Science: Metal Matrix Composites Processing, Microstructure and Properties (N. Hansen *et al.*, eds.), pp. 123–147.

Shu, J. Y., and Fleck, N. A. (1996). Microbuckle initiation in fibre composites under multiaxial loading. *Proc. R. Soc. London*, to appear.

Sivashanker, S., Fleck, N. A., and Sutcliffe, M. P. F. (1995). Microbuckle propagation in a unidirectional carbon fibre–epoxy matrix composite. To appear in *Acta Metall. Mater.*

Slaughter, W. S., and Fleck, N. A. (1993). Compressive fatigue of fibre composites. *J. Mech. Phys. Solids* **41**(8), 1265–1284.

Slaughter, W. S., and Fleck, N. A. (1994a). Viscoelastic microbuckling of fibre composites. *J. Appl. Mech.* **60**(4), 802–806.

Slaughter, W. S., and Fleck, N. A. (1994b). Microbuckling of fiber composites with random initial fiber waviness. *J. Mech. Phys. Solids* **42**(11), 1743–1766.

Slaughter, W. S., Fleck, N. A., and Budiansky, B. (1992). Microbuckling of fibre composites: The roles of multi-axial loading and creep. *J. Eng. Mater. Technol.* **115**(3), 308–313.

Slaughter, W. S., Fan. J., and Fleck, N. A. (1996). Dynamic compressive failure of fiber composites. *J. Mech. Phys. Solids* **44**(11), 1867–1890.

Soutis, C., and Fleck, N. A. (1990). Static compression failure of carbon fibre T800/924C composite plate with single hole. *J. Compos. Mater.* **24**, 536–558.

Soutis, C., Fleck, N. A., and Smith, P. A. (1991a). Compression fatigue behaviour of notched carbon fibre–epoxy laminates. *Int. J. Fatigue* **13**(4), 303–312.

Soutis, C., Fleck, N. A., and Smith, P. A. (1991b). Failure prediction technique for compression loaded carbon fibre-epoxy laminate with open holes. *J. Compos. Mater.* **25**(11), 1476–1498.

Soutis, C., Curtis, P. T., and Fleck, N. A. (1993). Compressive failure of notched carbon fibre composites. *Proc. R. Soc. London* **440**, 241–256.

Sun, C. T., and Chen, J. L. (1989). A simple flow rule for characterizing nonlinear behavior of fiber composites. *J. Composite Mater.* **23**, 1009–1020.

Sun, C. T., and Yoon, K. J. (1991). Characterization of elastic–plastic behavior of AS4/PEEK thermoplastic composite for temperature variation. *J. Compos. Mater* **25**, 1297–1313.

Sutcliffe, M. P. F., and Fleck, N. A. (1993). Effect of geometry upon compressive failure of notched composites. *Int. J. Fract.* **59**, 115–132.

Sutcliffe, M. P. F., and Fleck, N. A. (1994). Microbuckle propagation in carbon fibre–epoxy composites. *Acta Metall. Mater.* **42**(7), 2219–2231.

Sutcliffe, M. P. F., and Fleck, N. A. (1996). Micobuckle propagation in fibre composites. *Acta Metall. Mater.* to appear.

Sutcliffe, M. P. F., Fleck, N. A., and Xin, X. J. (1995). Prediction of compressive R-curve for long fibre composites. To appear in *Proc. R. Soc. London.*

U.S. Polymeric (1990). Data sheets on properties of carbon fibre epoxy composites, 700E Dyer Rd., Santa Ana, California, 92707.

Whitcomb, J. D. (1986). Parametric analytical study of instability-related delamination growth. *Composite Science and Technology* **25**, 19–48.

Wilkinson, E., Parry, T. V., and Wronski, A. S. (1986). Compressive failure in two types of carbon fibre-epoxide laminates. *Composite Science and Technology* **26**, 17–29.

Wisnom, M. R. (1990). The effect of fibre misalignment on the compressive strength of unidirectional carbon fibre/epoxy. *Composites* **21**(5), September 1990, 403–408.

Wu, X. R. and Carlsson, A. J. (1991). "Weight Functions and Stress Intensity Factor Solutions." Pergamon, New York.

Xin, X. J., Sutcliffe, M. P. F., Fleck, N. A., and Curtis, P. T. (1995). "Cambridge Composite Designer: A User Manual." CUED/C-MATS/TR.226, August 1995.

Young, R. J., and Young, R. (1990). Strain measurement in fibres and composites using Raman spectroscopy. Proc. Fourth European Conference on Composite Materials, September 25–28 Stuttgart, pp. 685–690. Elsevier, Amsterdam.

Yurgatis, S. W. (1987). Measurement of small angle misalignments in continuous fibre composites. *Composites Science and Technology* **30**, 279–293.